Research Programme of the Research Fund for Coal and Steel

FIre and Seismic performances of Hybrid fire WALLs in case of single-storey industrial and commercial steel buildings (FISHWALL)

Parametric numerical analyses

Sara Pasquali, Nicola Tondini, Gabriele Zanon

University of Trento

WP4: Seismic behaviour of a hybrid fire wall solution with "fusible" links

Deliverable: D4.3

Contributing partners		
	CTICM	France

Grant agreement No: 101034083

Version	Issue	Purpose	Author	Reviewer	Approved
A	D4.3	20/06/2025	S. Pasquali N. Tondini G. Zanon	All partners	
B	D4.3	29/06/2025 (Comments from partners considered)	S. Pasquali N. Tondini G. Zanon	C. Renaud	C. Renaud
C	D4.3	Revised version following comments from EU experts (01/10/2025)	S. Pasquali N. Tondini G. Zanon	C. Renaud	C. Renaud

TABLE OF CONTENTS

ABSTRACT

It is well known that the intrinsic fire resistance of single-storey unprotected steel-framed buildings is largely sufficient to guarantee the evacuation of occupants in the event of fire. In consequence, for this type of building, the main concern of national fire regulations in Europe is how to prevent the spread of fire to the whole building. To achieve this objective, two performances shall be usually satisfied, namely, the appropriateness of constructive systems to ensure that there is no progressive collapse between fire compartments, and the efficiency of firewalls to stop the fire inside the initial compartment regardless of the state of structures exposed to fire. In practice, many constructional solutions can be implemented in order to preserve the integrity of the firewalls, while accepting that the fire exposed part of the structure may collapse. One of the most common solutions is to place a non-load bearing wall between two independent steel structures and to connect it to them by means of "fusible" links. In fire situation, these fusible links have to allow the wall to be disconnected from the structure affected by fire without endangering the separating function of the wall, which shall remain fixed to the steel structure on the other side of the wall and therefore not exposed to fire. However, due to the lack of corresponding scientific evidence, questions are being very often raised about the real efficiency of such systems in fire situation, which, in certain cases, have also to provide an adequate seismic resistance, if they are used in seismic areas.

Today, concrete or masonry wall solutions are frequently used for the compartmentation of buildings, predominately for low-rise commercial and industrial steel buildings. However, as an alternative, lightweight sandwich panels (comprising two thin flat metal faces and an insulated core) could become an appropriate steel firewall solution, offering numerous benefits in comparison to other solutions, including fire resistance, durability, flexibility, fast construction times and easy dismounting. Nonetheless, there is an evident lack of technical information about the adequate fire performance of such type of wall solutions when they are implemented in single-storey buildings with unprotected steel structure, which constitutes a major obstacle for their large use.

In this context, the overall goal of the FISHWALL project is to develop a design guidance and recommendations for an innovative hybrid firewall solution based on lightweight steel-faced sandwich panels associated with unprotected steel structure under both fire and seismic actions considered individually. This will be achieved through the following specific tasks: i) establishing of a full range of experimental evidence about the fire and seismic behaviour of the investigated hybrid firewall solution by carrying out a number of tests; ii) investigating intensively the fire and seismic performances of the above hybrid firewall solution in combination with unprotected single-storey steel structures through a variety of parametric numerical studies by means of validated FE numerical models; iii) developing both cost-effective and innovative “fusible” connection systems for firewalls to be used in combination with unprotected steel structures of single-storey buildings; and iv) developing a design guidance and practical recommendations for the studied hybrid firewall and fusible links solutions, on the basis of above studies, from which engineers can carry out very efficient design.

The present report aims at summarising the parametric analyses performed on global numerical models developed considering three relevant case studies of those presented in Deliverable 1.3. The main objective of the work is to study the global seismic response of the structures, the differential displacement between the steel structures separated by the firewalls and the seismic forces acting in the fusible links subjected to sets of spectrum-compatible accelerograms, modelled as shown in Deliverable 4.2. In addition, seismic fragility functions to be used either in a seismic risk assessment or in a fully probabilistic performance-based earthquake-engineering framework were developed for two of the six details presented in Deliverable 4.2, analysed in both wall configuration, parallel and perpendicular, and at two levels of seismicity, low and moderate, characterised by PGA values of 0.04g and 0.12g . Then, the results of a parametric study investigating the resistance of the fusible link solution consisting of a steel profile assembled with aluminium bolts to a steel channel spanning between the columns of the building steel structure. is also provided.

1 INTRODUCTION

This deliverable is divided into three parts. The first part reports on a parametric study investigating the resistance of the fusible link solution consisting of a steel profile assembled with aluminium bolts to a steel channel spanning between the columns of the building steel structure. This investigation was conducted using a detailed 3D FE model based on those developed during the project and presented in deliverable D4.2 [2]. The second part reports on the results of parametric nonlinear dynamic analyses performed using global numerical modelling on three case studies relevant to those presented in deliverable D1.3 [1]. The third part presents fragility functions developed for two of the six details presented in deliverable D4.2, which characterise their maximum capacity. As extensively presented in Deliverable D1.3, the design PGA values of the case studies correspond to two levels: 0.04g and 0.12g.

Global numerical models of different single-storey steel buildings were developed using Opensees software [3]. Each building is characterized by two main resisting system, portal frames in one direction and a bracing system in the other one. These elements were modelled as nonlinear elements with distributed plasticity using different definitions proposed by Mazzoni et al. [4] in accordance with the specific characteristics of the Case study. In general, the secondary elements were modelled as linear *elastic Beam-Column* elements. For the two levels of seismicity considered characterised by design PGA = 0.04g and design PGA = 0.12g, respectively , a series of spectrum-compatible accelerograms were selected from both the European and the Italian databases. In accordance with the Eurocode 8 [5], three accelerograms were selected for each seismicity level and the maximum value obtained from the three nonlinear dynamic analyses conducted, was selected for evaluating the detailed response of the fusible link systems. The parametric numerical analyses were carried out by defining several building configurations and varying many parameters when selecting the accelerograms. These parameters included the soil classification of the selected ground motions, the range of magnitude of the events and their distance. These differences will be presented in greater detail. In particular, 3 buildings were considered and for each building symmetric and asymmetric plan configurations were analysed; 2 levels of seismic intensity; 2 orientations of the fire wall (perpendicular and parallel), as well as all 6 fusible link details were considered for a total number of 108 analyses.

Finally, in order to provide fragility functions, one case study was selected. This case study was analysed in an asymmetric configuration, considering both fire wall positions and equipped with two of the six details conceived. Due to the large number of parametric analyses and their outcomes, it was decided to develop 3 models, and a conditional mean spectrum was defined for each of them. Next, a set of 20 ground motions was selected. Spectral acceleration at the structure's first period was selected as intensity measure (IM), while the capacity of the fusible links and the peak interstorey drift were chosen as local and global engineering demand parameters (EDP), respectively. The analyses performed to define the fragility functions were the Multiple Stripe Analyses (MSAs).

2 PARAMETRIC NUMERICAL STUDY OF THE RESISTANCE OF FUSIBLE LINKS

As part of the project, one of the fusible links consists of a steel profile assembled with aluminium bolts to a steel channel spanning horizontally between the steel structure columns. The profile is fixed to the wall column using four rods that pass through the firewall on one side and four bolts on the other. The profile can be either L-shaped or T-shaped. However, during the seismic testing, only the T-profile configuration was assessed. A parametric study was therefore conducted to compare the resistance of the fusible links in the two configurations. The aim was to confirm that both configurations could withstand a design force of either 40 kN or 90 kN with comparable dimensions, as specified in the project.

2.1 Investigated parameters

A parametric study has been carried out on the fusible link solution shown in Figure 2.1 by varying the parameters affecting its resistance. These parameters include the shape of the steel profile bolted to the channel (L or T), the number and diameter of the aluminium bolts, and the diameter of the steel rods. The chosen parameters are indicated in Table 1. In addition, Figure 2.2 illustrates the position of the steel rods considered. To reduce the number of calculations, only one dimension was considered for each type of steel profile (L and T profiles, as well as the steel channel). This is because the seismic test results indicated that the resistance of the studied fusible link solution primarily depends on the shear resistance of the aluminium bolts and the bending resistance of the steel rods. Excessive flexural deformation of the steel rods can result in additional moments being exerted on the aluminium bolt group, resulting in additional horizontal shear forces. All analyses in this parametric study considered a nominal yield strength of 275 MPa for the steel profiles (the most commonly used value nowadays) and an 8.8 steel grade for the rods and bolts.

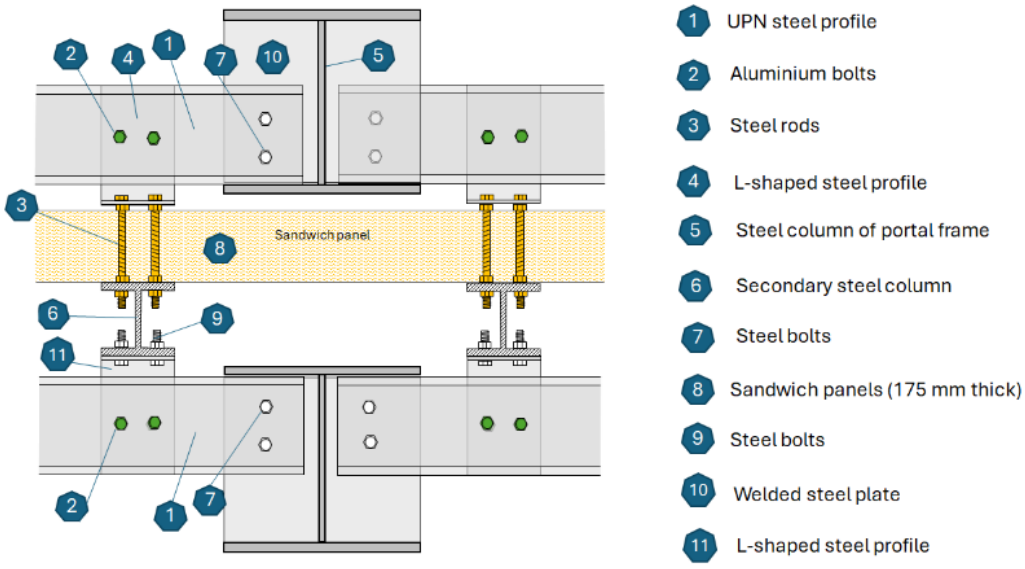

Figure 2.1: Schematic of the studied fusible link

Table 1 : Summary of the studied cases

Parameters		Specified value
UPN profile	Size	UPN 240
L shaped profile	Thickness	15 mm
	Size	250×250×180
L shaped profile	Thickness	15 mm
	Size	300×250×180
Steel rods	Diameter	M16 to M27
	number	2 rows of 2 bolts
	length	175mm
Steel bolts	Diameter	M20
	number	2 rows of 2 bolts
Aluminum bolts	diameter	M12 or 16
	number	1 row of four bolts, 2 rows of 2 bolts and 3 rows of 2 bolts

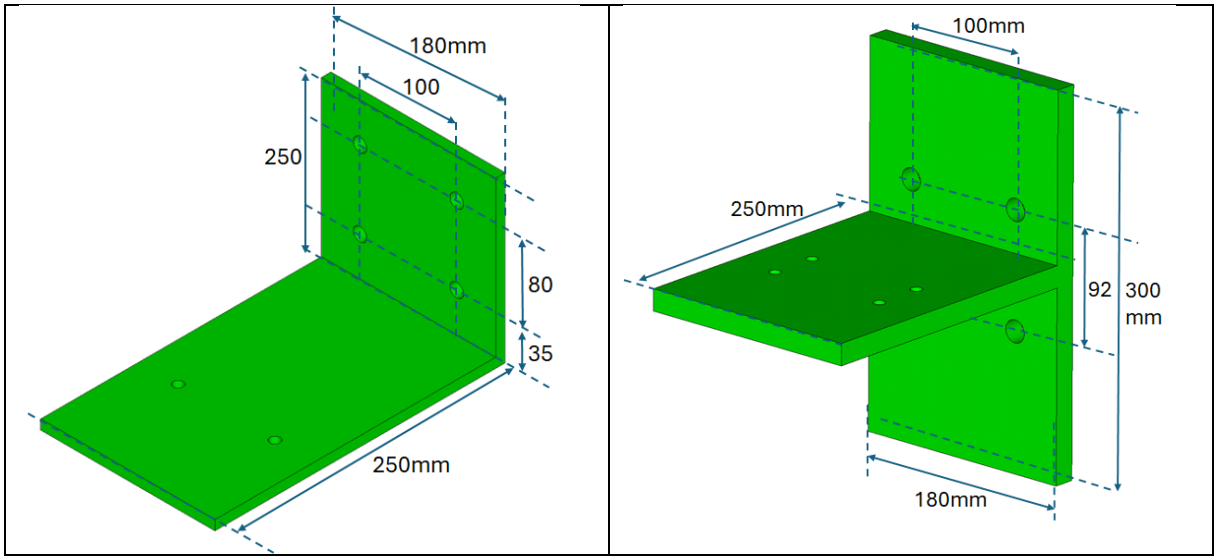

Figure 2.2: Geometrical dimensions of the considered L and T-shaped profile

2.2 Modelling considerations

The analyses were carried out using ANSYS with the same procedure and most of the modelling assumptions as those used in the numerical analysis of the seismic tests reported in deliverable D4.2 [2] . The main assumptions are outlined here:

- The studied cases are meshed with 20-nodes brick finite elements.
- Different loading cases were considered as illustrated in Figure 2.4, depending on the investigated link resistance: These were resistance to traction or compression in the plane of the steel portal frames and shear resistance in the perpendicular direction. Consequently, only part of the considered link is modelled, depending on the needs of the analysis. Supporting conditions from the parts of the study case that are not modelled are considered by introducing appropriate boundary conditions into the models to restrain the relevant degrees of freedom (displacements and rotations). These conditions are assumed to remain unchanged during loading.

- Bolts and steel rods are modelled in as much detail as possible. However, some geometric features that are assumed to have a negligible effect on the response of the fusible links are ignored. Firstly, since stripping of the nut threads was not observed in the tests, the threaded parts of the bolts, rods and nuts are omitted, and the bolt–nut assembly is modelled as a single component. This assumes that relative motion between the bolts and nuts, or loosening, does not occur during loading. Secondly, no washers are modelled. Bolts and rods were modelled using their effective diameter rather than the nominal diameter.
- Surface-to-surface contact with finite sliding was assumed for all contact surfaces. This includes contact between steel profiles and between bolts (heads and shanks) and steel profiles (upper surfaces and holes). A friction coefficient of $\mu = 0.25$ was adopted for all contact surfaces interacting with the bolts, as well as for surface contact between the steel profiles. The steel bolt shank, steel bolt head and steel bolt nut contact surfaces were always chosen to be master surfaces, as they are made of a stronger material. The same applies to steel rods. Additionally, the surface of the L- or T-shaped steel profile in contact with the channel web was also considered a master surface. All the other aforementioned contact surfaces were considered slave surfaces. Aluminium bolts are less resistant and rigid than steel members. Therefore, they are denoted as master surfaces in contact parts and are meshed more coarsely than slave surfaces.
- Pre-tension was not applied to the bolts during the analysis.
- The behaviour of structural steel is represented by a linear hardening plastic material model, defined by the means of a quadri-linear relationship as illustrated in Figure 2.3(a). Based on test results given in the project, a trilinear stress-strain relationship is assigned to aluminium bolts (see Figure 2.3(b)). A tri-linear model is also used for the steel of all bolts and rods. The material characteristics (Young's modulus, yield strength, and ultimate strength) considered at ambient temperature are reported in Table 2.
- The use of plasticity material models with isotropic type hardening is generally not recommended to investigate the mechanical behaviour of steel members under cyclic loading conditions. So, all components are modelled using a kinematic hardening constitutive model, considering the Von Mises yield criterion and related flow rules.
- The fracture of the aluminium bolts was not explicitly simulated in the analyses. Instead, a simplified approach was adopted, whereby bolt fracture is indirectly defined by a failure strain criterion that must not be exceeded. Therefore, the aluminium bolts are considered to have fractured in the analyses when the total mechanical strain obtained from the Von Mises analysis exceeds 5%.
- Each fusible link is subjected to monotonic or cyclic loading until failure, with each direction considered separately. For cyclic loading, the loading sequence follows the ECCS procedure, using parameters derived from the analyses of monotonic loading.

Table 2: Materials properties of steel components and aluminium bolts

Properties	Steel profile	Steel bolts and rods	Aluminium bolts
Young's modulus E (N/mm^2)	210000	210000	70000
Yield strength f_y (N/mm^2)	275	640	400
ultimate strength f_u (N/mm^2)	430	800	505
* According to the steel profile sizes			

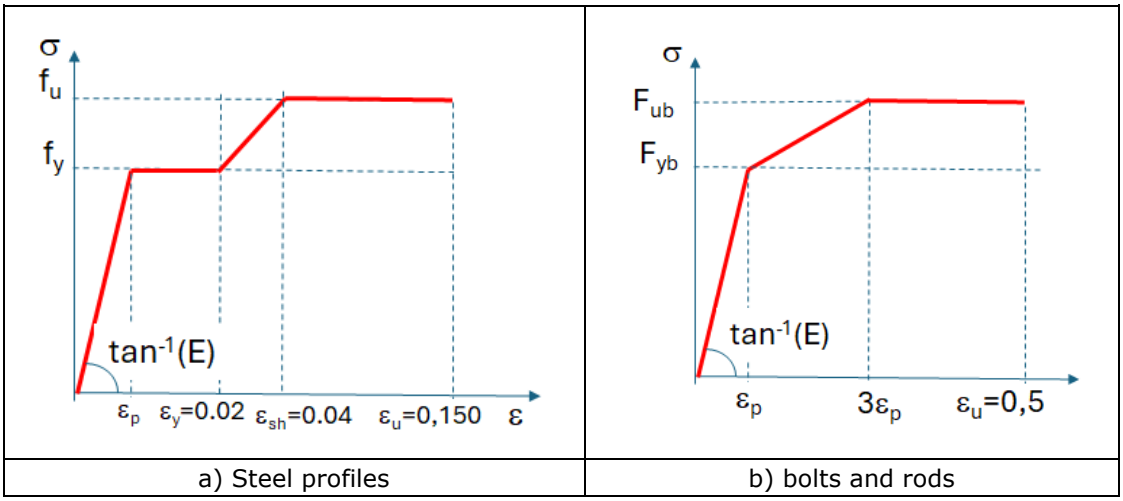

a) Steel profiles | b) bolts and rods

Figure 2.3: Idealised stress-strain models for materials adopted in modelling

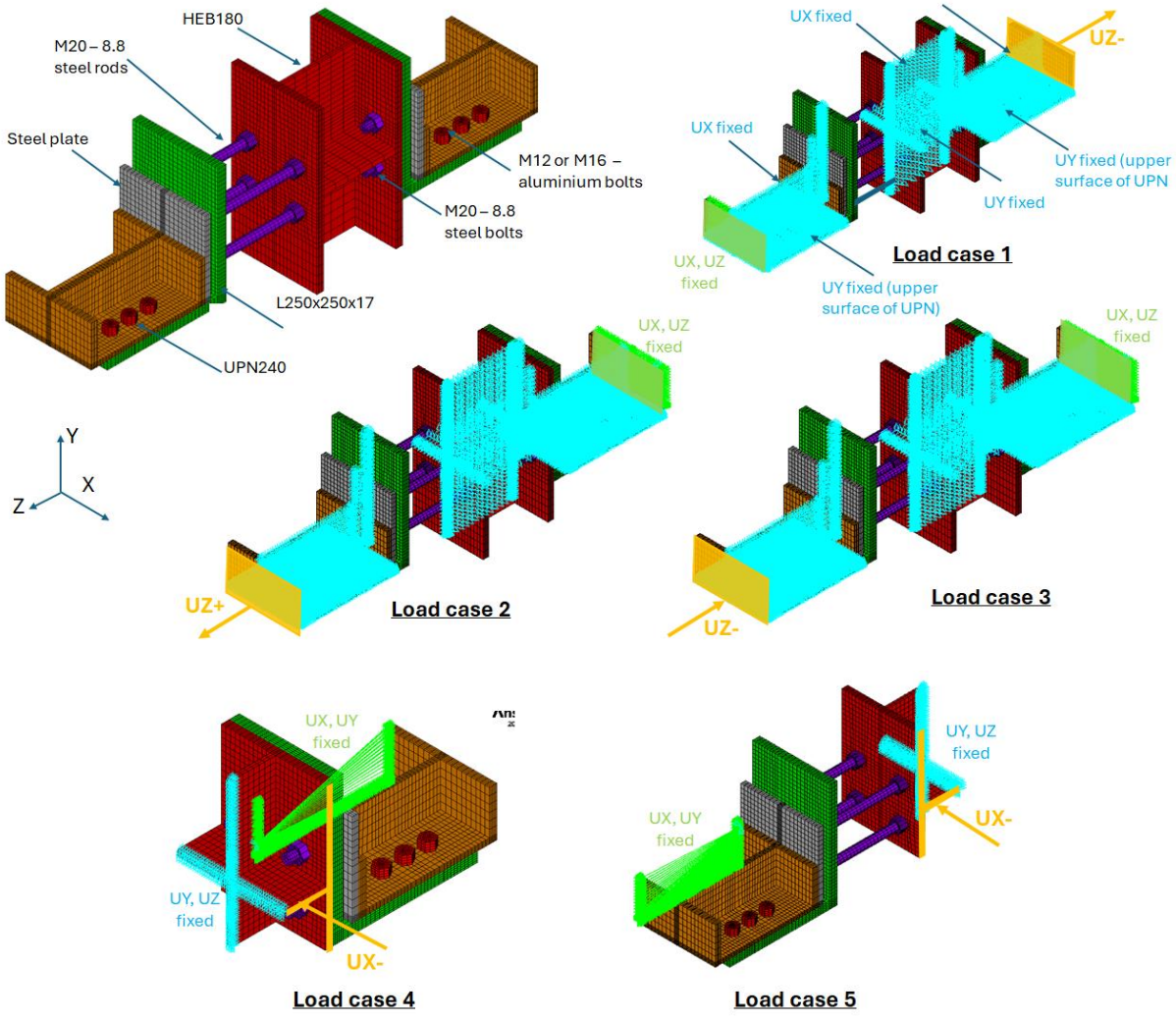

Figure 2.4: Modelling (boundary conditions and loading) of the study cases according to the investigated link resistance

For information purposes, following figure shows the models developed for the investigated link cases.

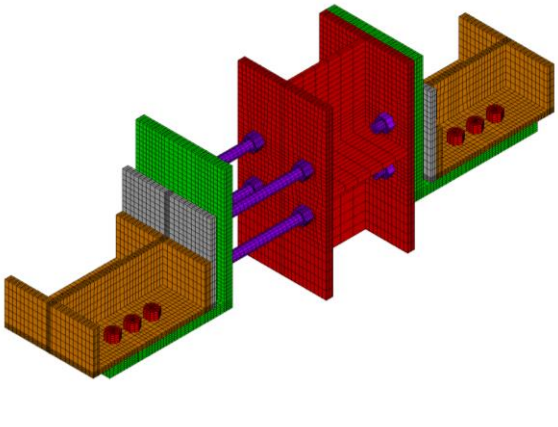

a) L-shape profile with 2x3 aluminium bolts

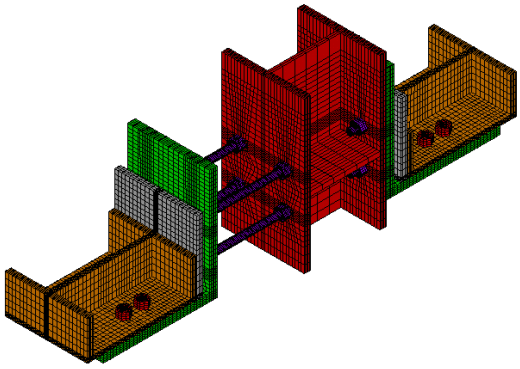

b) L-shape profile with 2x2 aluminium bolts

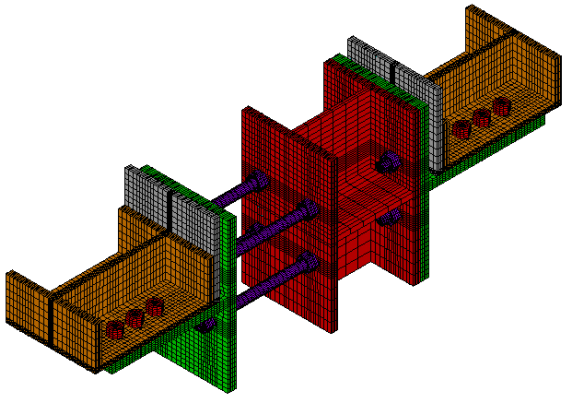

c) T-shape profile with 2x3 aluminium bolts

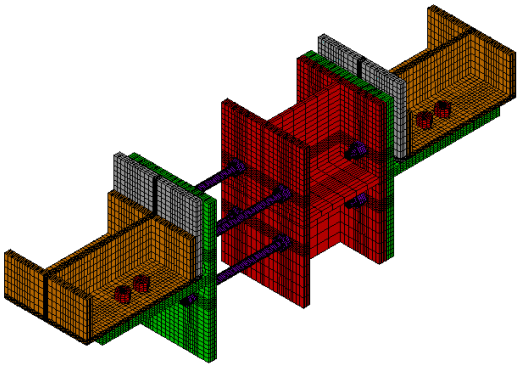

d) T-shape profile with 2x2 aluminium bolts

Figure 2.5: FE models developed using ANSYS for the study cases

2.3 Analysis results

The main results of the numerical finite element (FE) analyses are presented below. These results are presented as force-displacement curves.

2.3.1 Monotonic loading

Figure 2.6 to Figure 2.13 how the response in terms of force-displacement curve predicted for some of the studied link cases according to the considered loading conditions. Each predicted curve is a resulting plot of the total vertical force calculated by summing the reaction forces of all nodes at the fixed end of models against the prescribed vertical displacement.
It is worth noting that, in some cases, the final part of the predicted curves should be ignored since the link ductility can be over-estimated when the failure of the aluminium bolts occurs (which is not explicitly considered). In such cases, the figures indicate the moment at which the aluminium bolt group fractures.

Through these figures, it can be noted that:

- When links are subjected to shear loading in the plane of portal frames (.i.e. loading case n°2), the force–displacement curves initially appear linear (or slightly nonlinear), followed by a plateau stage corresponding to shear yielding in the cross-sectional area of all aluminium bolts (see Figure 2.7 and Figure 2.11). However, when approaching the link failure, the displacement-force curve obtained for the L-profile shows a slight stiffness degradation stage, which highlights the fusible link's nonlinear behaviour. This is believed to be due to the transverse bending deformation of the L-profile flanges, which are greater than those of the T-profile due to the profile shape. The links have the same resistance to traction in both configurations.
- When subjected to compression loading in the plane of portal frames (i.e. loading case n°1), links initially exhibit ductile behaviour rather than brittle behaviour by undergoing large plastic deformations (see Figure 2.7, Figure 2.6 and Figure 2.10). As the imposed displacement increases, the curves consist mainly of four stages: (i) an initial linear stage

corresponding to an elastic stiffness; (ii) a stage of stiffness degradation highlighting the nonlinear behaviour of the fusible link, where the load-bearing capacity reaches a peak value; and (iii) a failure stage characterised by a yield plateau or descending stage. The failure mode of the link is determined by the buckling of the steel rods. It is important to note that the resistance of the fusible links with a L-profile is higher than that of the link configuration with a T-profile. In the first link configuration, the four rods are in a state of compression. Conversely, in the other configuration, the loading eccentricity resulting from the positioning of the rods, in conjunction with the concomitant bending effect, leads to the upper rods being compressed and the second rod being under tension. This results in increased compression in the upper row, which decreases the load-bearing capacity. It is evident that an augmentation in rod diameter invariably results in an increase in link resistance.

- Regarding the loading cases applied perpendicular to portal frames, the predicted force-displacement curves differ between the two link configurations when loading is applied to the side of the steel bolts (loading case n°5). Firstly, there are differences in initial stiffness. Secondly, the resistance of the link is lower for the L-shaped steel profile than for the T-profile, and it decreases as the diameter of the aluminium bolts increases. In this case, the failure mode of the links is governed by the shear resistance of the aluminium bolts. As shown in Figure 2.8 and Figure 2.12, the fusible link with the L-shaped profile exhibits more pronounced non-linear behaviour as bolt failure approaches. As with loading case n°2, this is attributed to the transverse bending deformation of the L-profile flanges. Conversely, the same behaviour is observed between the two link configurations when loading is applied to the rods (loading case n°4). In this case, the failure mode of the links is also governed by the shear resistance of the aluminium bolts. However, the resistance achieved is lower than in the previous loading case due to the flexibility of the steel rods. This results in additional moments being exerted on the aluminium bolt group. The larger the rod diameter, the lower the additional bending moment and the higher the link resistance.
- With regard to the load-bearing capacity of the studied link, the most penalising load case is loading case n°4, due to the flexibility of the steel rods. This can drastically reduce the link's resistance, which is mainly provided by the shear resistance of the aluminium bolts, as previously mentioned.
- Despite differences in initial stiffness, the two studied link configurations with comparable dimensions demonstrate very similar load-bearing capacities when these resistances are provided by the shear resistance of aluminium bolts.

Summing up the results, Table 3 gives the predicted load-bearing capacity for some of the studies, highlighting the cases that can withstand a design force of either 40 kN or 90 kN, as specified in the project. The given resistance values are those obtained for the loading case n°5.

Table 3: Load-bearing capacity predicted for some of the studied lfusible ink cases

Case	Aluminium bolts		Steel rods	Load-bearing capacity (KN)	
	Bolt rows	diameter		T-profile	L-profile
1	2x2	M12	M20	35	x
2	2x2	M12	M24	38	x
3	2x2	M12	M27	41	x
4	2x2	M16	M16	35	x
5	2x2	M16	M20	44	43
6	2x2	M16	M24	69	68
7	2x2	M16	M27	77	79
8	3x2	M12	M20	36	x
9	3x2	M12	M20	38	x
10	3x2	M12	M24	46	44
11	3x2	M16	M20	56	54
12	3x2	M16	M24	73	70
13	3x2	M16	M27	91.2	94

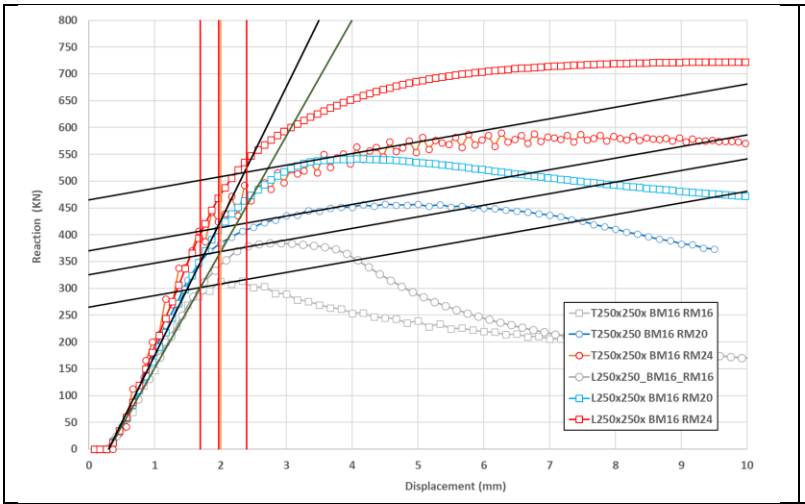

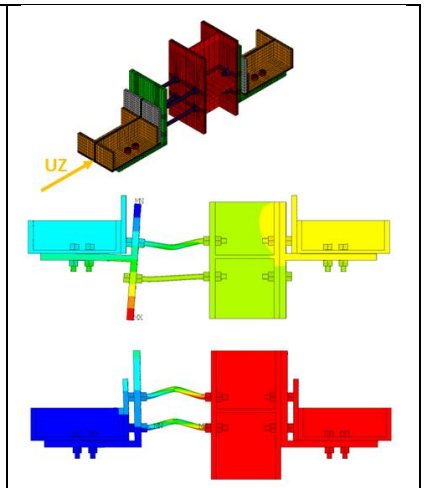

a) Force-displacement curves | b) deformed state at failure

Figure 2.6: Results of monotonic analyses for Links with 2x2 rows of aluminium bolts in compression (load case n°3)

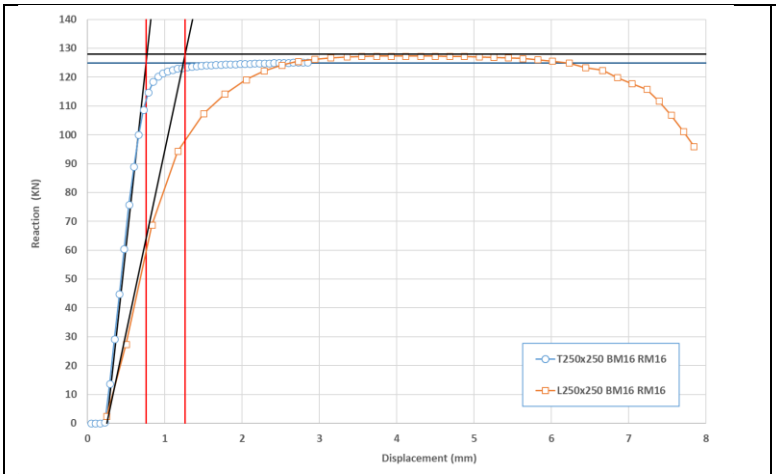

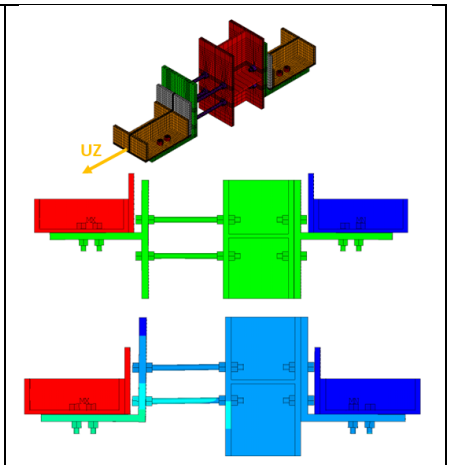

a) Force-displacement curves | b) deformed state at failure

Figure 2.7: Results of monotonic analyses for Links with 2x2 rows of aluminium bolts under in traction (load case n°2)

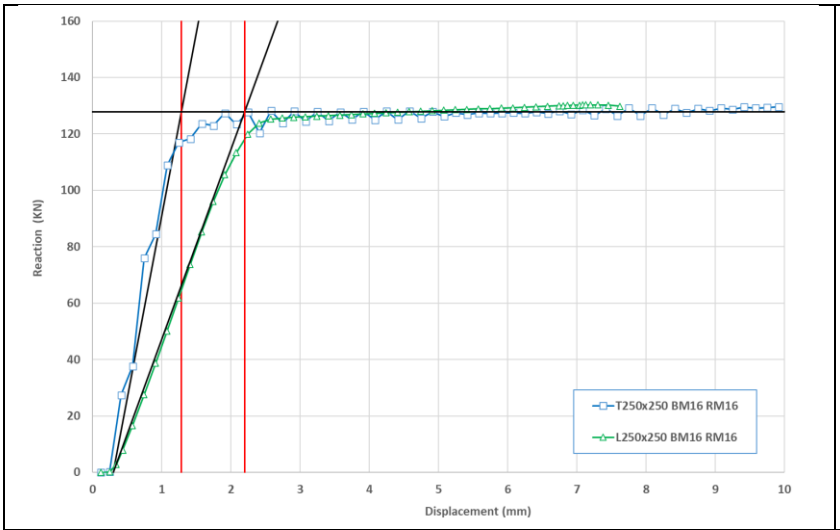

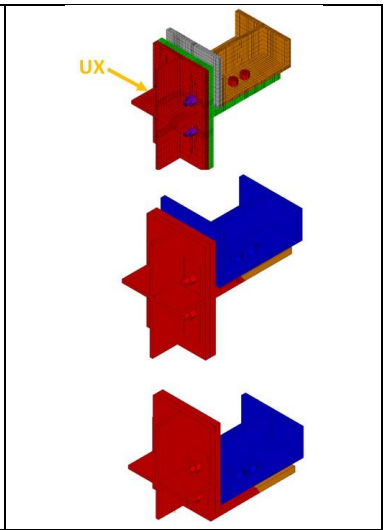

a) Force-displacement curves | b) deformed state at failure

Figure 2.8: Results of monotonic analyses for Links with 2x2 rows of aluminium bolts in shear (load case n°4)

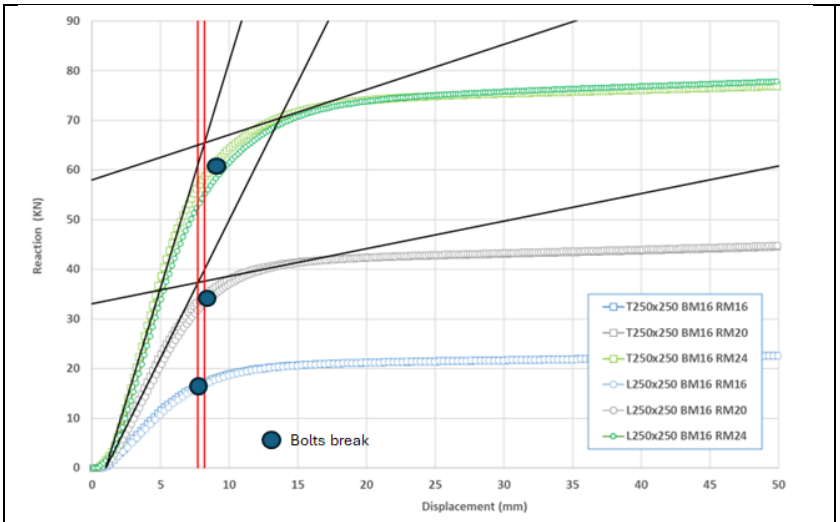

a) Force-displacement curves | b) deformed state at failure

Figure 2.9: Results of monotonic analyses for Links with 2x2 rows of aluminium bolts under in shear (load case n°5)

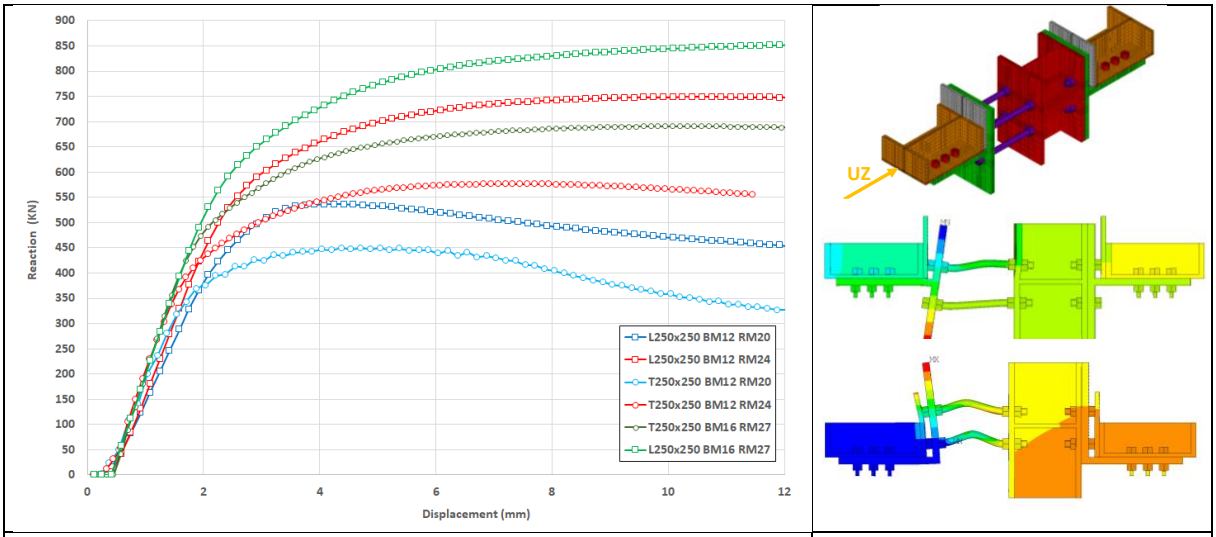

a) Force-displacement curves | b) deformed state at failure

Figure 2.10: Results of monotonic analyses for Links with 3x2 rows of aluminium bolts in compression (load case n°3

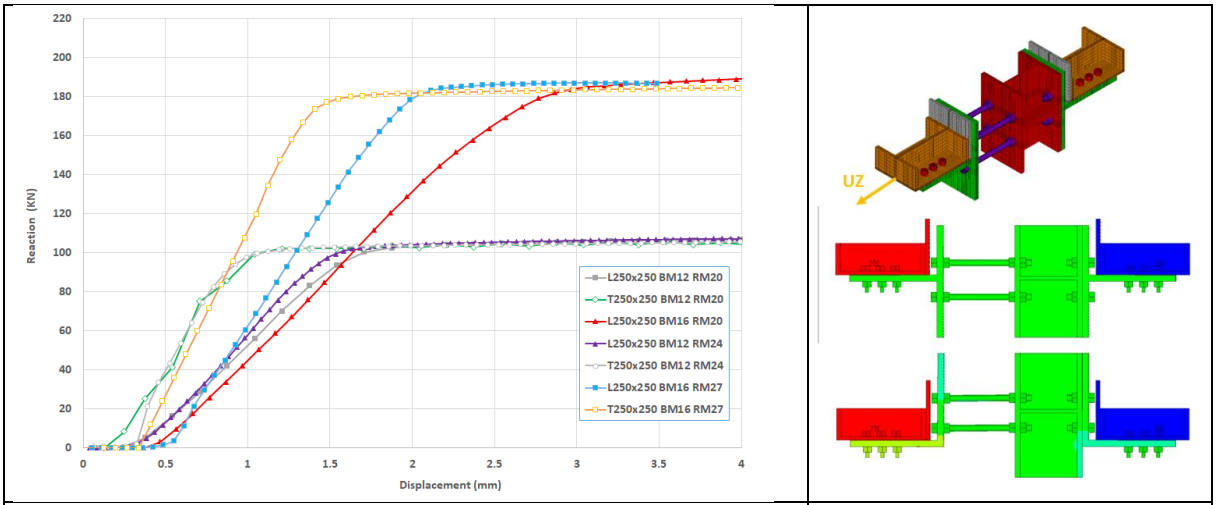

a) Force-displacement curves | b) deformed state at failure

Figure 2.11: Results of monotonic analyses for Links with 3x2 rows of aluminium bolts under in traction load case n°2)

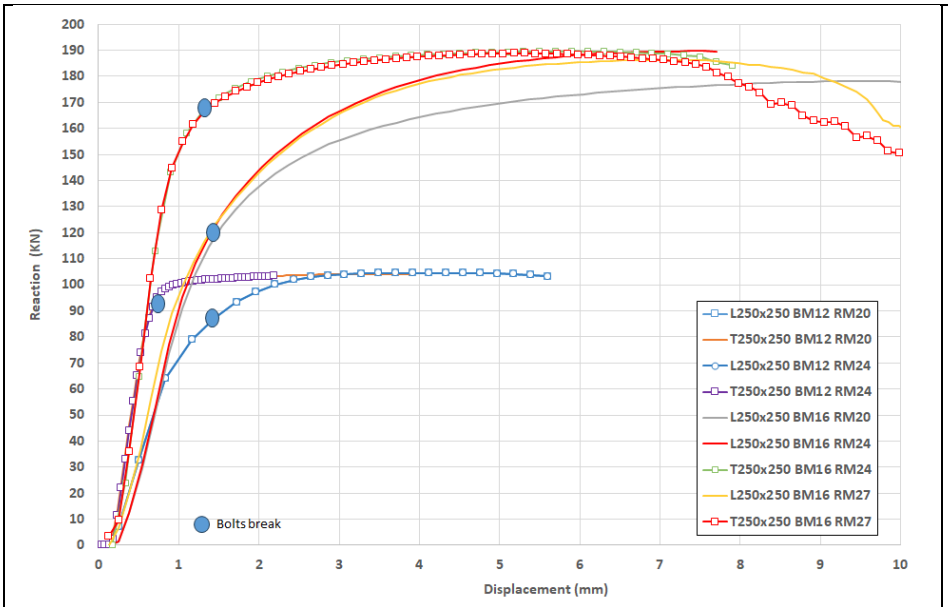

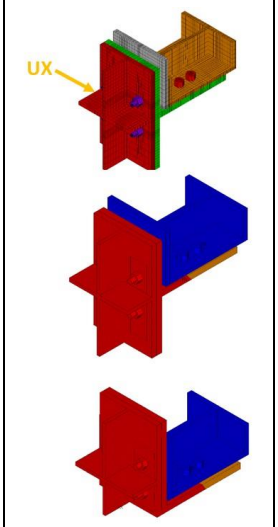

a) Force-displacement curves

b) deformed state at failure

Figure 2.12: Results of monotonic analyses for Links with 3x2 rows of aluminium bolts under in traction load case n°2)

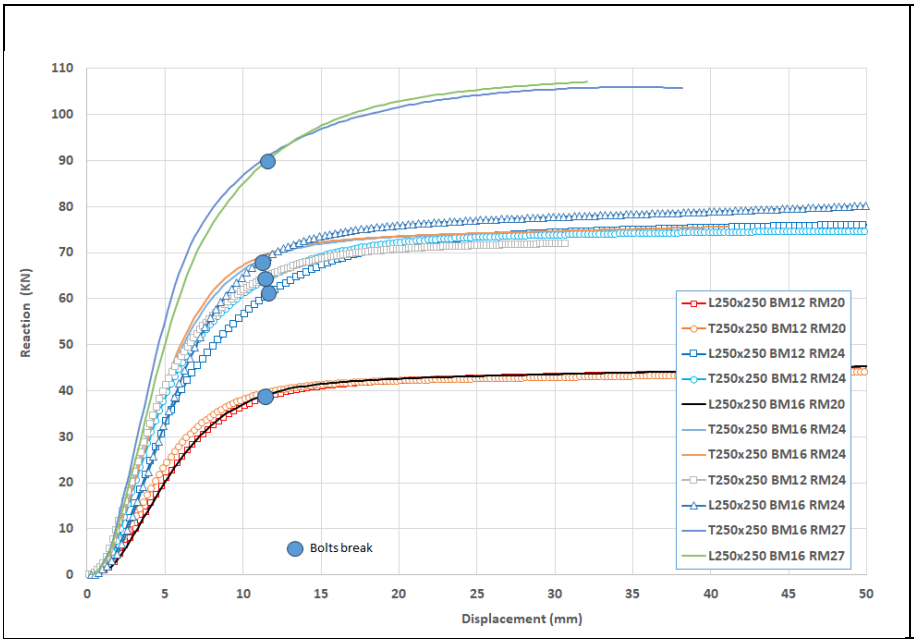

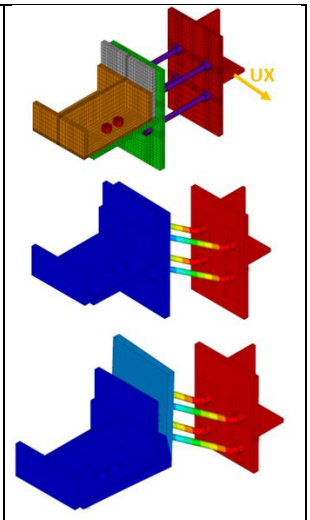

a) Force-displacement curves

b) deformed state at failure

Figure 2.13: Results of monotonic analyses for Links with 2x2 rows of aluminium bolts under in shear (load case n°5)

2.3.2 Cyclic loading

This section summarises the results of the analyses performed under cyclic loading for the three studied cases indicated in Table 3 that can withstand a design force of either 40 kN or 90 kN.

Numerical analyses based on cyclic loadings were performed, as recommended by the ECCS. For each studied fusible link, three loading cases were considered: loading applied in the plane of the steel portal frames, and loading applied perpendicular to this plane (distinguishing cases where the loading is applied to either the rod or the steel bolt side). Thus, the prescribed cycle-displacement curve was defined using yield displacements derived from the force-displacement curves predicted for loading cases 2 and 3 when applied in the plane of the portal frames, or for loading cases 4 and 5 when applied perpendicular to this plane. It should be noted that the negative and positive yield

displacements differ for the first cyclic loading case, whereas they are identical for the subsequent two.

Figure 2.14 and Figure 2.15 depict the predicted hysteresis curves for the selected fusible link cases. cases. The figures distinguish between cases with 2x2 or 3x2 rows of aluminium bolts.

It can be noted that in most cases, the loading-unloading loops predicted by the models overlap quite well during the prescribed cycling loading because the studied link remains in the elastic stage. The area of the hysteresis loops is very small and there is no residual deformation. Then, as loading displacement increases, the hysteresis loops become slightly bow-shaped as failure approaches, indicating that the studied cases enter the yielding stage. However, due to the lower resistance of aluminium bolts compared to other link components, and their brittle nature, the bow-shaped hysteresis loops remain limited.

It should be also underlined that the cyclic loading does not affect greatly the load-bearing capacity predicted for the studied fusible link. Indeed, they are in line with the resistance predicted from analyses carried out unde monotonic loading.

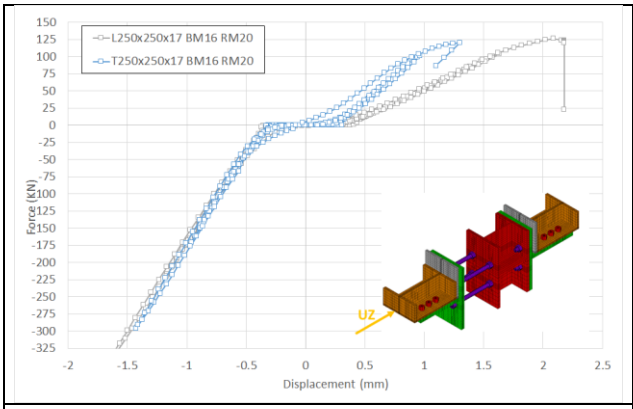

a) Cylcing loading n°1

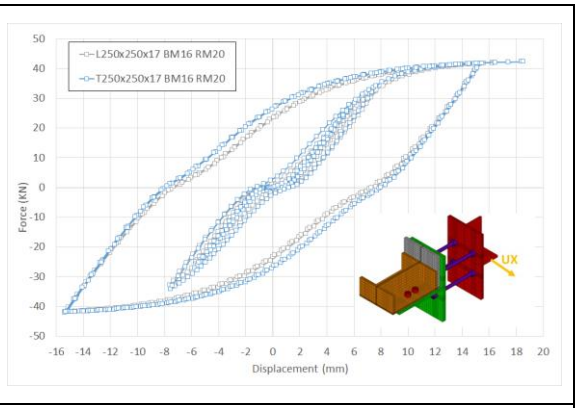

b) Cylcing loading n°1

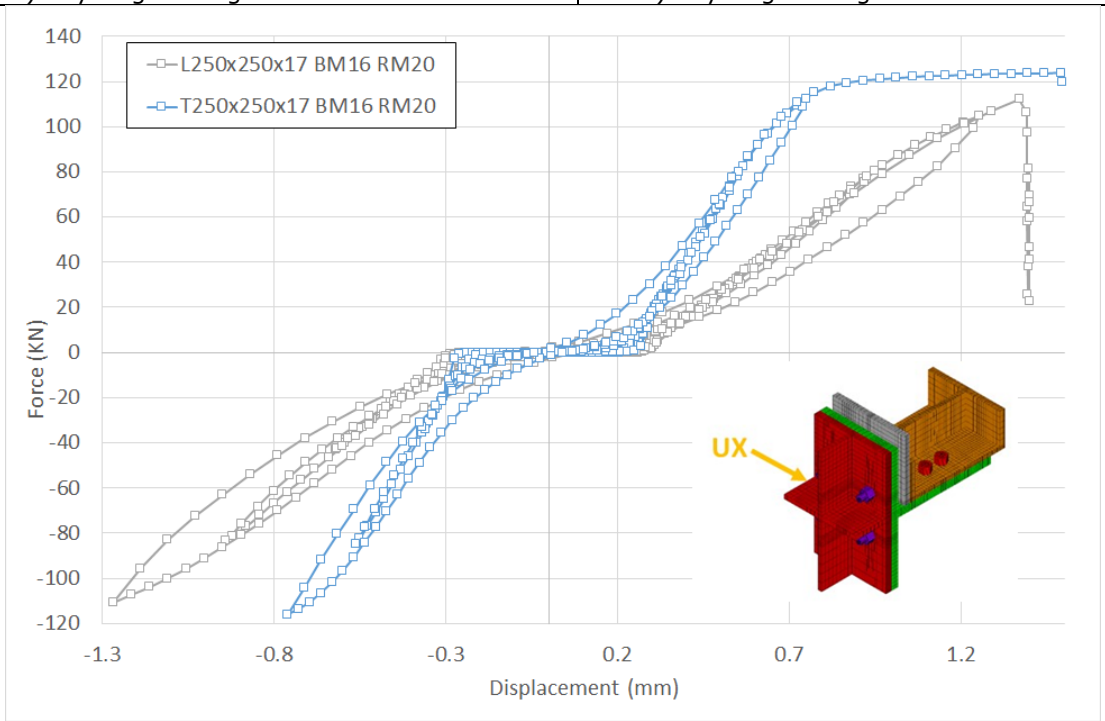

c) Cyclic loading n°3

Figure 2.14: Results of cyclic analyses for links with 2x2 rows of aluminium bolts

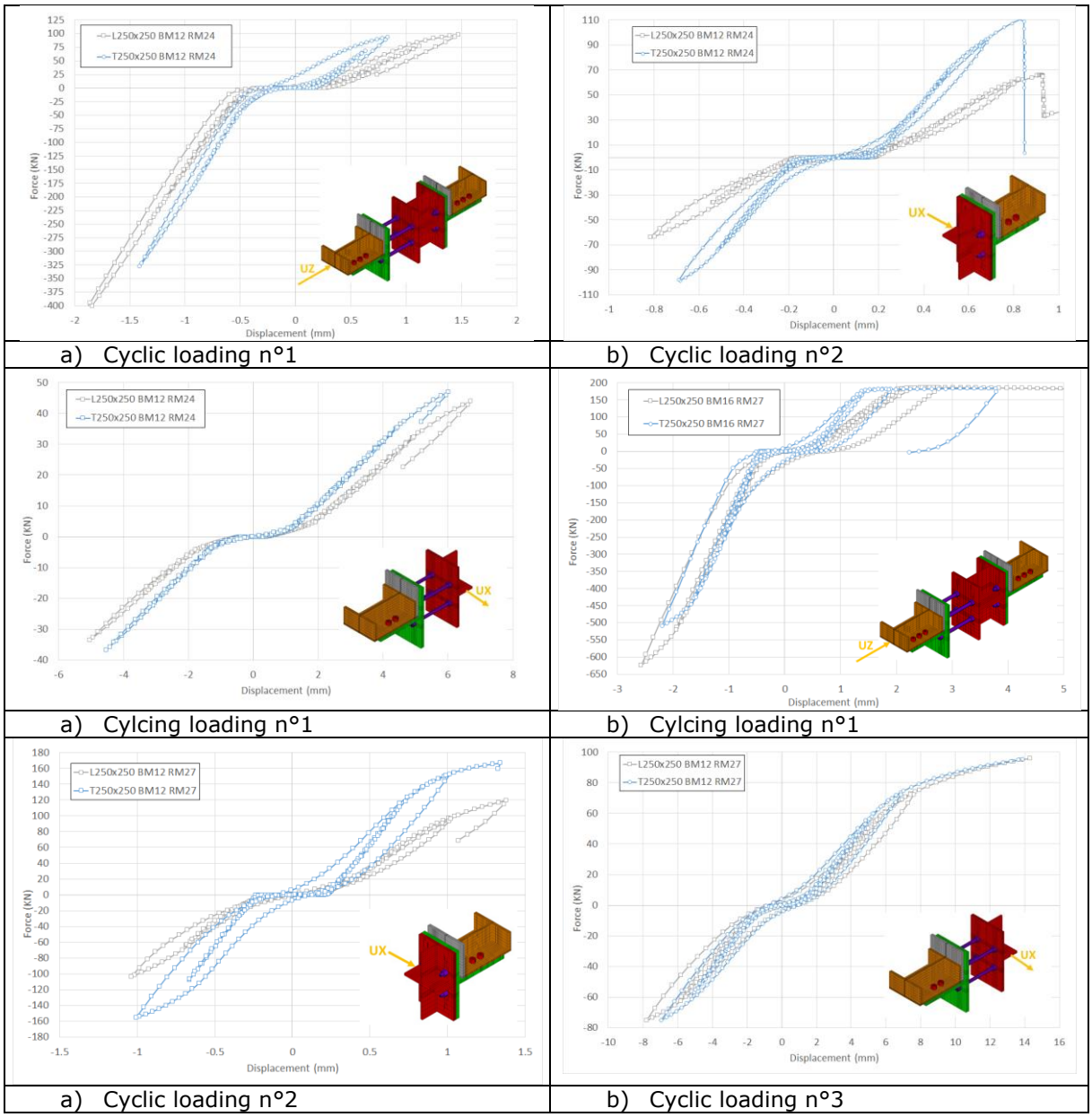

Figure 2.15: Results of cyclic analyses for links with 3x2 rows of aluminium bolts

2.4 Conclusions

The results of the numerical analyses showed that the resistance of the studied fusible link configurations with comparable dimensions could differ, with either the L-shaped or the T-shaped Link having lower resistance depending on the loading direction. However, for the most unfavourable loading case, the predicted resistances were very similar. The results also confirmed that both link configurations, which were designed to have comparable dimensions, could withstand a design force of either 40 kN or 90 kN.

3 GLOBAL NUMERICAL ANALYSES

3.1 Development of global numerical models

As reported in the Introduction, the case studies numerically modelled in this phase, were the same presented in the Deliverable D1.3 [1]. In detail, in this task three relevant case studies were considered from those initially selected: Case study 1, located in Carcassone, Case study 3, located in Pibrac, and Case study 4, located in Bressuire. Table 4 reports the characteristics of the three buildings. Greater details can be found in Deliverable D1.3 [1].

Table 4. Case studies main features.

	Case study 1	**Case study 3**	**Case study 4**
Floor area [m^2]	1400 m^2	6000 m^2	12000 m^2
Steel grade	S275	S355 and S275	S355 and S275
Column section	HEA600	Welded section	Welded section
Rafters section	IPE600	Welded section	Welded section
Facades	IPE200 and cold-formed sections	From IPE 200 to IPE360 and cold-formed section	IPE300 and cold-formed sections
Purlins section	C cold-formed section	C cold-formed section	C cold-formed section
Bracing system section	L70x7	L60x6	L70x7
Design PGARegion seismicity level	Low0.04g	0.04gLow	Moderate0.12g

3.1.1 Modelling assumptions

The numerical models of the case studies were developed in the OpenSees software [3].

Below the modelling assumptions that were used developing the models:

- The nonlinear steel material constitutive law was defined according to the uniaxial *Steel02* material [4], which is characterized by isotropic strain hardening;
- Columns, beams and bracing system were modelled as nonlinear beam finite elements with distributed plasticity;
- Geometric imperfections were introduced on the bracing system to allow for buckling phenomena;
- Facades, purlins and support elements were modelled as elastic beam finite elements;
- Columns were pinned at the base;
- Gravity loads were applied to the purlins by considering the seismic load combination as provided by the Eurocode 8 [5] and the masses were applied to the nodes at the intersections between the purlins and the beams;
- The fusible links details were inserted through the calibrated models presented in Deliverable D4.2 [2];
- Damping sources are modelled through the Rayleigh damping matrix where the values of the mass-related and stiffness-related damping coefficients are considered for a damping factor of 4% for the first two vibration modes.

In addition to the aforementioned assumptions, for each case study, specific choices were made to achieve high quality models. In fact, for Case study 3 all the elements were modelled at their precise location, including the offset of purlins with respect to the rafters. This was done because of the reasonable small size of model. Conversely, for Case study 4, given its significant plan dimensions and the number of elements, some simplifications were applied without hindering the accuracy in the global response. For instance, no offset was introduced between purlins and rafters and the effect of the horizontal bracing system perpendicular to the portal frames was introduced through an equivalent *equaldof* constraint.

3.1.2 Analysed configurations

In order to study the behaviour of the fusible links details, several configurations were considered. As shown in Deliverable D1.3 [1], the case studies are composed of two identical buildings divided by the firewall located orthogonally or parallelly to the portal frames. As expected, taking into account that the fusible links are not deemed to withstand horizontal forces and the perfect symmetry between the structures and the fusible links, limited forces in the fusible links were observed, because of very small differential displacements between the fusible link system and the structures. Therefore, an asymmetric configuration of the models was developed to obtain two structures characterized by different dynamic properties and consequently expecting different responses. In Figure 3.1 a schematic representation of the two main analysed configurations symmetric and asymmetric, is reported.

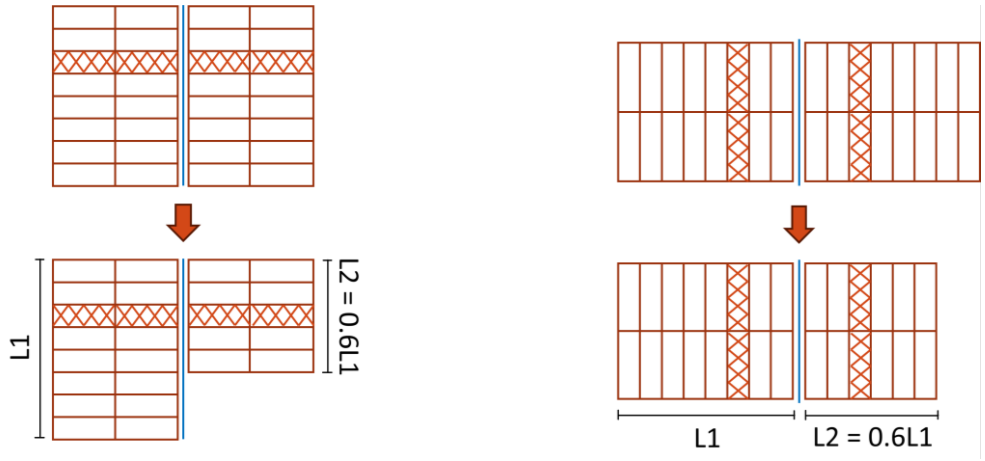

Figure 3.1. Symmetrical and asymmetrical configuration of the analysed building: a) firewall orthogonal to the portal frames and b) firewall parallel to the portal frames.

3.1.3 Configuration of the fusible link system

As already mentioned, the six fusible links details investigated in the previous tasks were inserted in the global numerical models by means of the calibrations performed against their experimental behaviour. In order to properly develop the global models, some adaptations were introduced. The fusible links details were applied to the portal frames columns, when the firewall is located orthogonal to the portal frames, and to the facades columns, when the firewall is positioned parallel to the portal frames. The fusible links details were applied at the roof level. In addition, in accordance with the sandwich panels producer indications, when the distance between these abovementioned columns was over 5 m, an additional column, equipped with the fusible link, was added. The additional columns were linked to main structure by means of horizontal elastic elements at the fusible links level. Figure 3.2 reports a schematic representation of this concept.

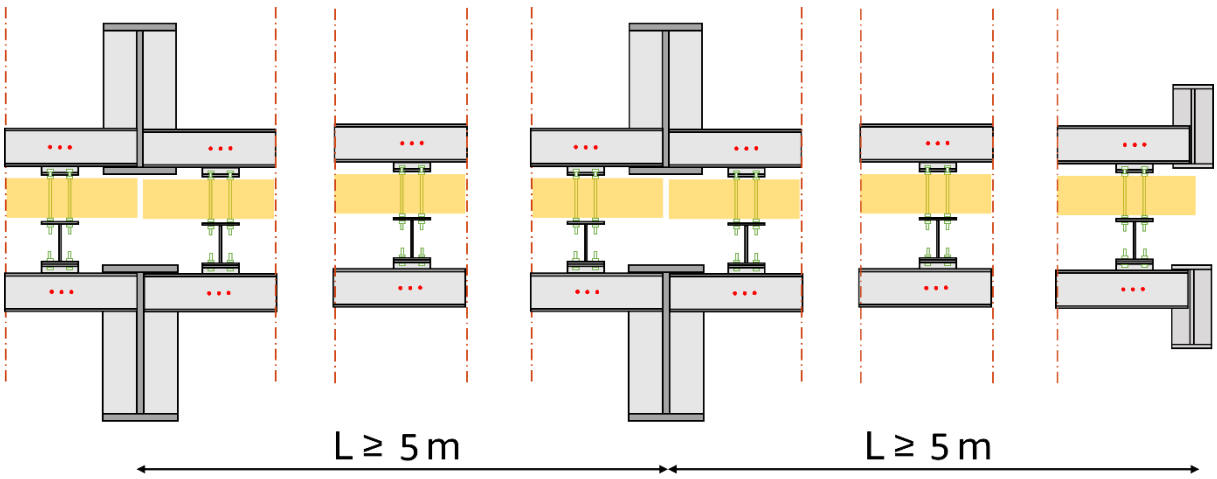

Figure 3.2. Building configuration.

Regarding the tested fusible link details, also in this case it was necessary to evaluate some adaptations. As presented in Deliverable D4.1 [11], the details were conceived from two different reference details, and they were tested in one direction. Therefore, it was possible to combine the experimental results to obtain the global behaviour of the details to be used into the numerical models of the investigated structures. Figure 3.3a and Figure 3.3b recall the two reference details that inspired the development of the six tested in the laboratory, while Figure 3.3c shows a schematic view of the details, where each group of aluminium bolts is represented by a couple of nonlinear springs, with different colours for different directions.

In order to characterize the behaviour of the nonlinear springs in each direction, some evaluations were conducted on the details. It is worth noting that, in the configurations described in the following, the interaction between two directions is not directly captured into the model. Thus, the resultant shear force was also checked a posteriori.

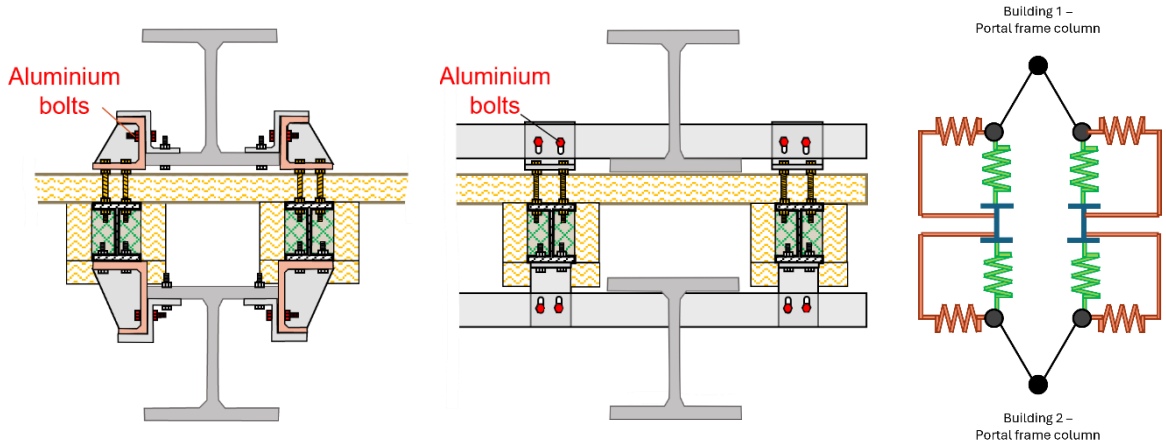

a) b) c)

Figure 3.3. a) and b) reference details and c) numerical model of the fusible links details.

3.1.3.1 Detail 3145

The first detail conceived for the numerical analyses is a combination of Detail 3.1, Detail 4 and Detail 5, depicted in Figure 3.4.

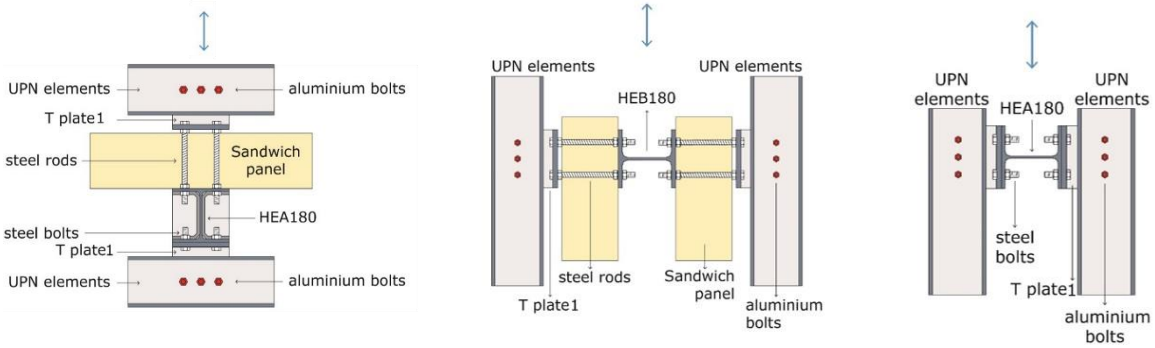

a) b) c)

Figure 3.4. Images of a) Detail 3.1, b) Detail 4 and c) Detail 5.

Firstly, Detail 4 and Detail 5, as widely explained in Deliverable D4.1 [11] were conceived to better characterize the influence of the sandwich panel on the fusible links. Figure 3.5 reports the geometric combination of the abovementioned details. Considering that the two were originally symmetric, under a numerical point of view, for each detail was taken half of the corresponding detail response and it was applied to the proper nonlinear spring.

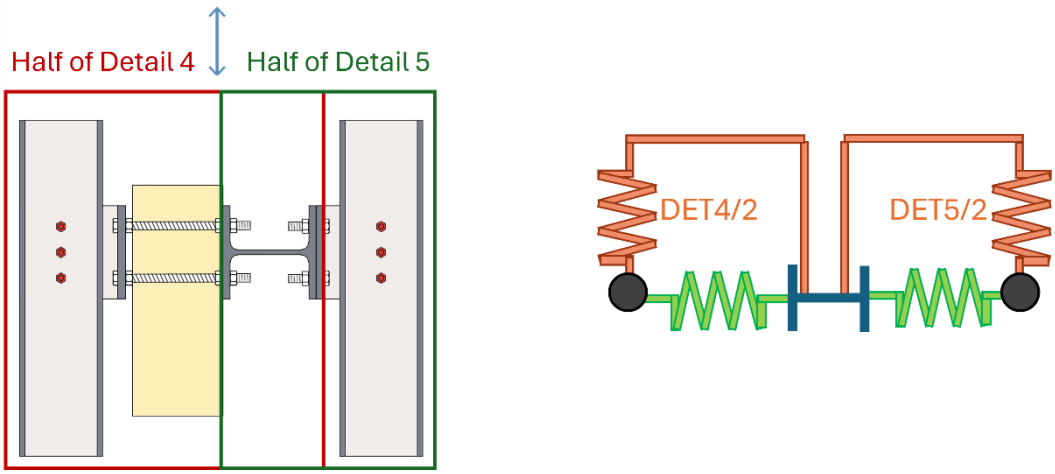

a) b)

Figure 3.5. a) geometrical combination of Detail 4+5 and b) numerical application to the appropriate nonlinear springs

Comparing Detail 3.1 and Detail 4+5, it can be highlighted that the latter represents the first one rotated of 90 degrees, therefore their combination can describe the behaviour of the detail in two directions. Figure 3.6 reports the application of the details to the springs composing the numerical detail.

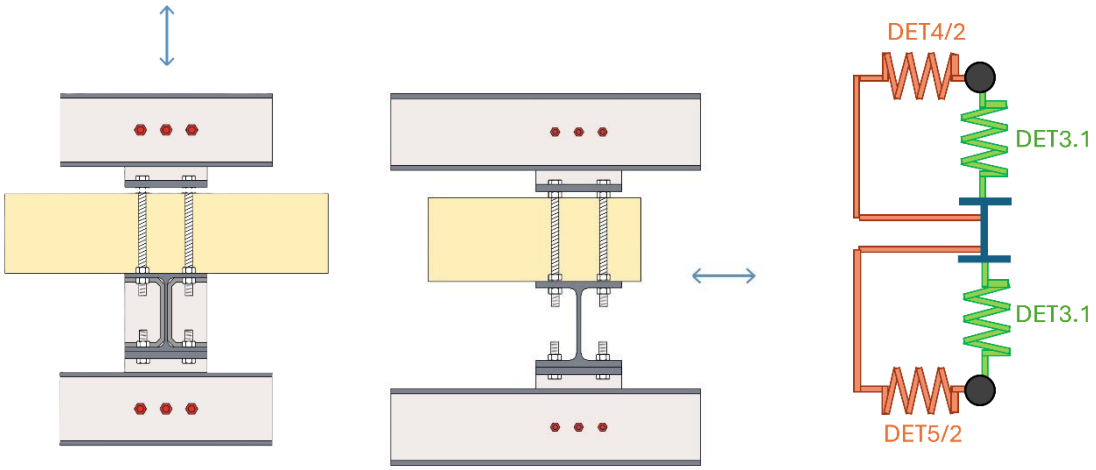

a) b) c)

Figure 3.6. a) Detail 3.1, b) Detail 4+5 c) numerical combination of Detail 3145.

In addition, it was considered that the two details combined were conceived and tested with different size of aluminium bolts, Detail 3.1 with M16 aluminium bolts and both Detail 4 and Detail 5 with M12 aluminium bolts. Consequently, in order to make the two details effectively comparable, a scale factor (SF) in terms of resistance area on the bolts area was calculated and applied to the calibrated curves of Detail 4 and Detail 5. The two new numerical curves applied can be observed in Figure 3.7b and Figure 3.7c.

$$SF = \frac{A_{resM16}}{A_{resM12}}$$

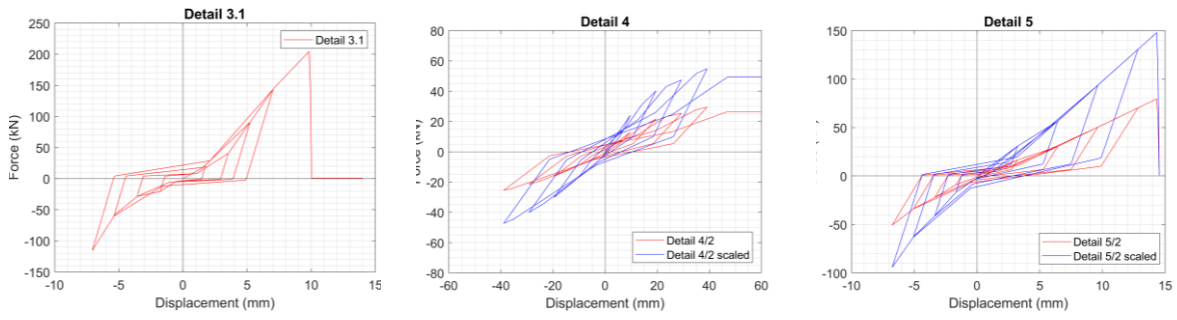

a) b) c)

Figure 3.7. Numerical models applied to detail 3145 a) Detail 3.1, b) Detail 4 scaled and c) Detail 5 scaled.

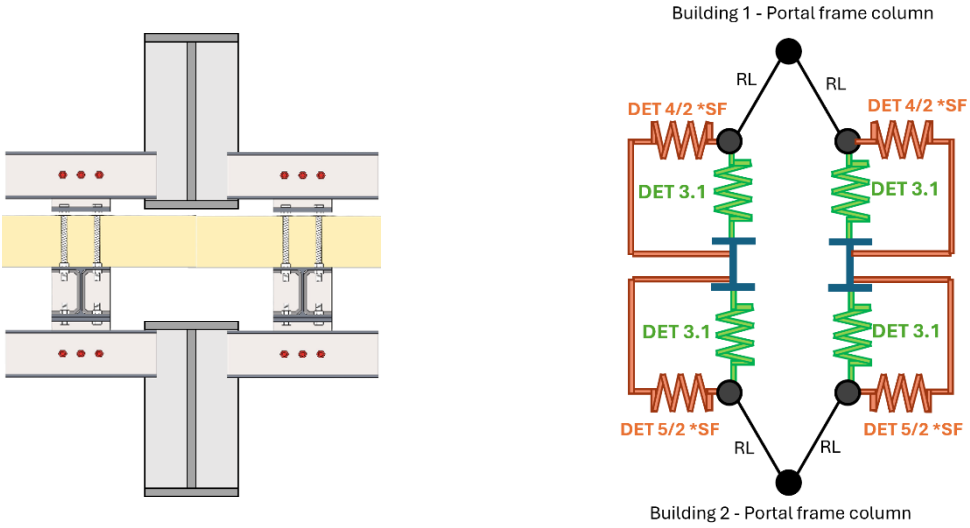

a) b)

Figure 3.8. a) geometrical and b) numerical model of Detail 3145.

The combination of the details presented is suitable for representing the fusible link joint in both directions, as shown in Figure 3.8. Considering the necessity of adding supporting columns between the portal frames equipped with fusible links, Detail 3145 configuration resulted suitable also for that location.

3.1.3.2 Detail 3245

Based on the assumptions made on Detail 3.1, the same concept was applied to Detail 3.2, considering that they were designed for seismicity levels characterised with a PGA = 0.12g. Indeed, the two details differ only for the size of aluminium bolts (M16 Detail 3.1 and M12 Detail 3.2); therefore, with respect to the relationship with Detail 4 and Detail 5, the same conclusions were drawn. On these premises, it was possible to combine Detail 3.2 with Detail 4 and Detail 5 as performed for Detail 3.1. Figure 3.9 reports the combination of details and the final numerical model of Detail 3245.

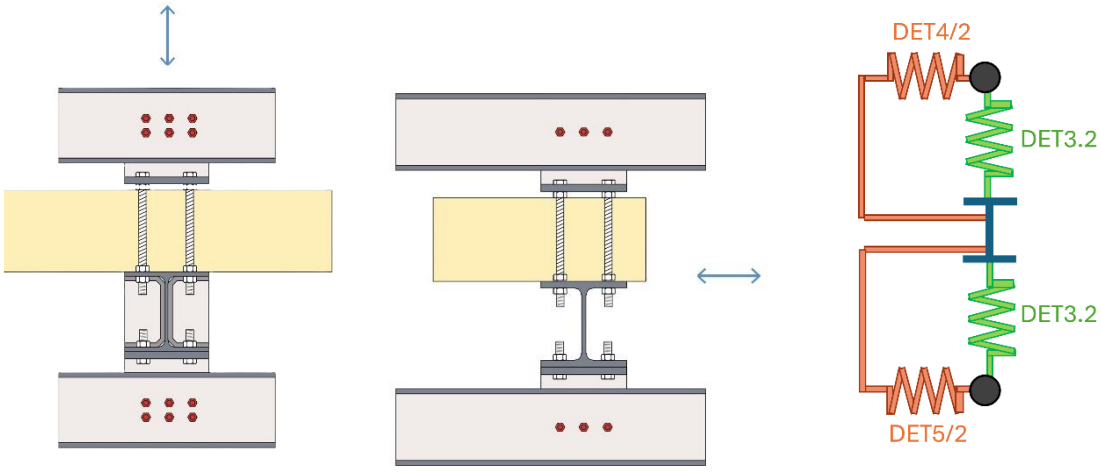

a) b) c)

Figure 3.9. a) Detail 3.2, b) Detail 4+5 c) numerical combination of Detail 3245.

Additionally, as occurred for Detail 3145, a scale factor (SF) was necessary to compare the three details. In this case, the difference between the details was not the diameter of the bolts, but the different resistance of the details in the two directions due to the different number of the aluminium bolts. Therefore, a scale factor equal to 2 was applied to Detail 4 and Detail 5, as hereafter shown

$$SF = \frac{6 * A_{resM12}}{3 * A_{resM12}}$$

The numerical curves applied to the nonlinear springs are reported in Figure 3.10.

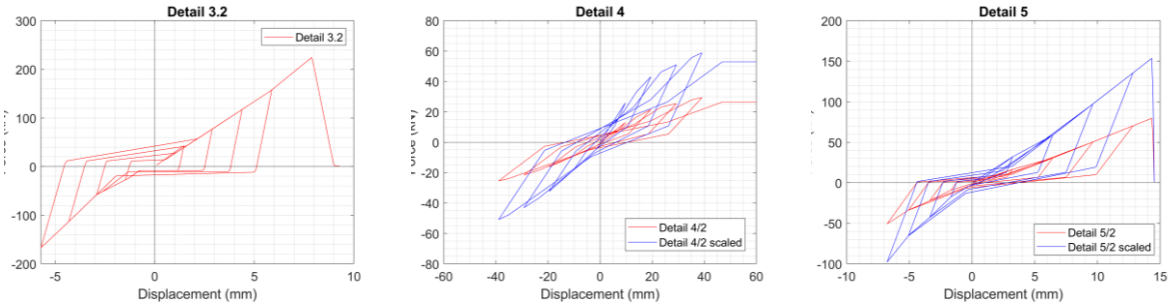

a) b) c)

Figure 3.10. Numerical models applied to detail 3245 a) Detail 3.2, b) scaled Detail 4 and c) scaled Detail 5

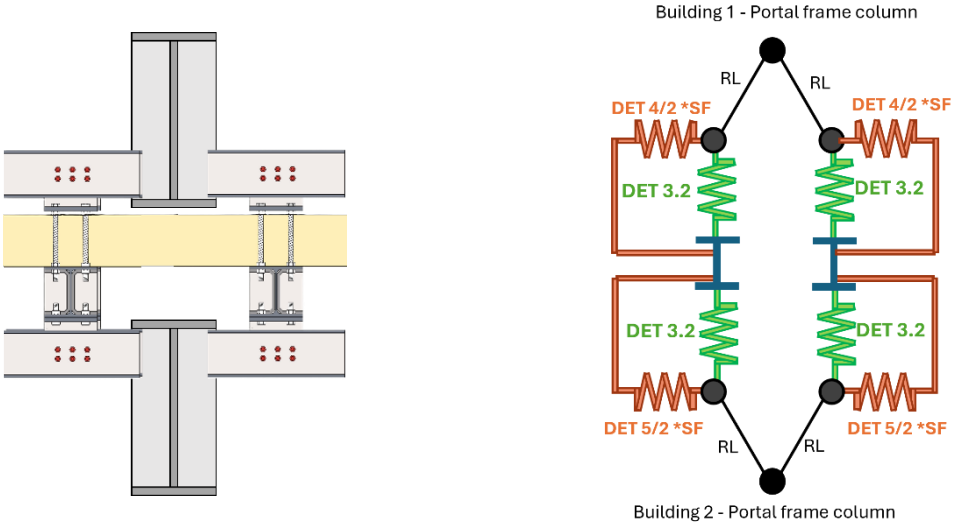

a) b)

Figure 3.11. a) geometrical and b) numerical model of Detail 3245.

This combination of the details is suitable for representing the fusible link joint in both directions, see Figure 3.11. Considering the necessity of adding supporting columns between the portal frames equipped with fusible links, Detail 3245 configuration resulted suitable also for that location.

3.1.3.3 Detail 1

Figure 3.12a depicts the geometric configuration of Detail 1. The geometric representation highlights the presence of the building portal frame column in the configuration of the details, making it primarily appropriate for a wall configuration perpendicular to the portal frames. Therefore, the detail was tested in the direction perpendicular to the sandwich panels while the behaviour of the fusible links in the other horizontal direction was neglected, because of the presence of the vertical bracing system in that direction that would withstand the lateral forces. Considering the numerical model of Detail 1, the behaviour observed during the experimental campaign and successively calibrated, was split between the two green springs, see Figure 3.12b, while the behaviour on the other direction, as abovementioned, was defined through a stiff material.

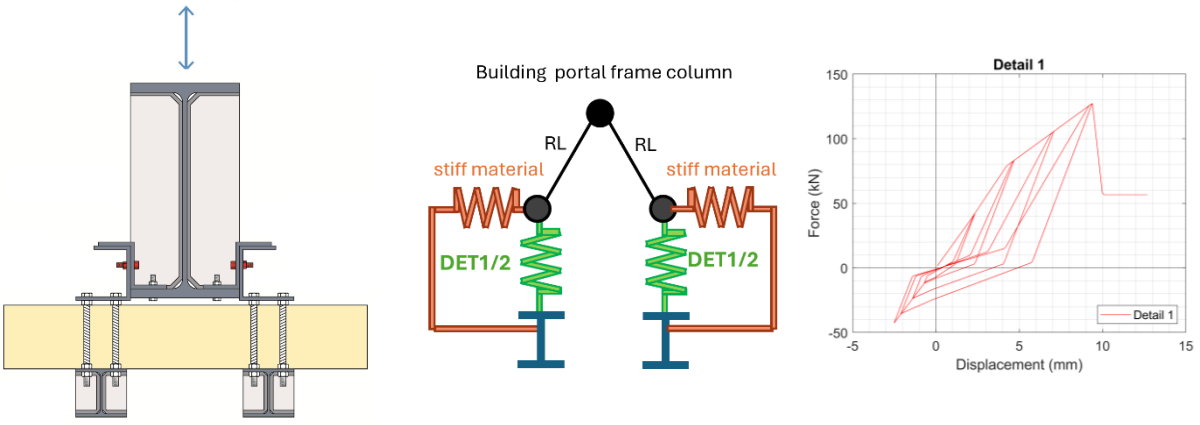

a) b) c)

Figure 3.12. a) Detail 1; b) numerical model of Detail 1 and c) calibration of Detail 1 experimental behaviour.

Figure 3.13 shows the building configuration of Detail 1 in its geometry configuration and numerical configuration. As highlighted in the previous section, this detail set-up was related to the connection with the building portal frame perpendicular to the fire wall. Therefore, in the building configuration where it was necessary to add supporting columns between the portal frames that spanned more than 5 m, as presented in Section 3.1.2, was not possible to apply this kind of detail.

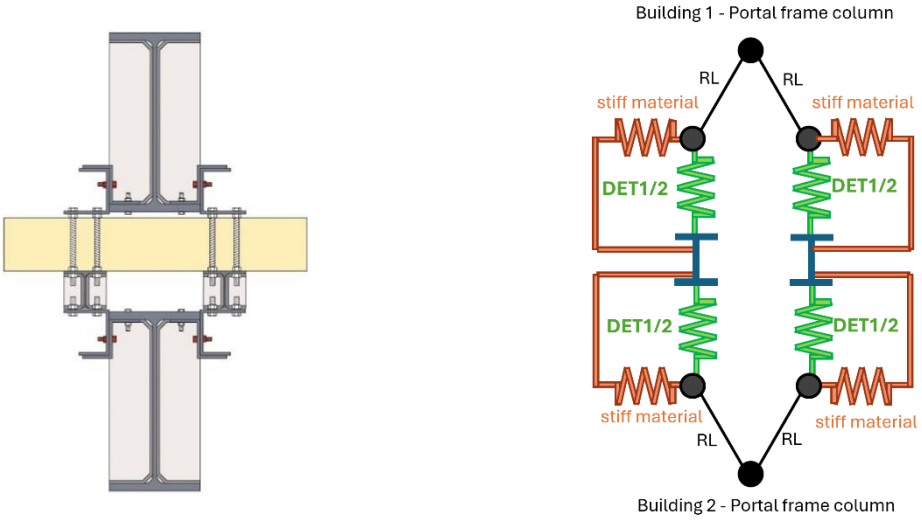

a) b)

Figure 3.13. a) Detail 1 building configuration and b) corresponding numerical model

To overcome this issue, it was decided to apply to the additional supporting columns, one of the details presented that was readily applicable. Thus, it was decided to apply the numerical model built for Detail 3245, considering that the details, Detail 1 and Detail 3245, were tested with the same size of aluminium bolts. However, the two were designed for different levels of seismicity; therefore, to simplify, the resistance of Detail 3245 was halved to make it comparable to a low seismicity level. The final conceived building configuration can be observed in Figure 3.14.

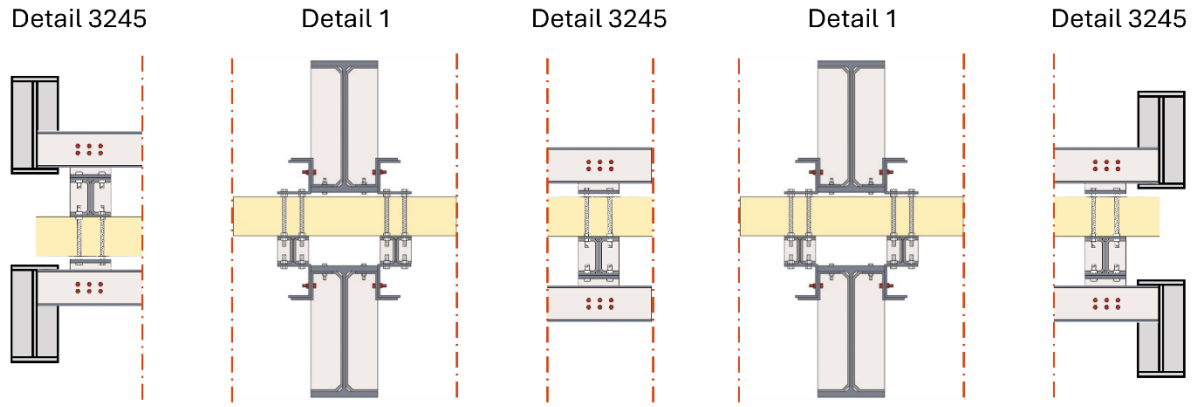

Figure 3.14. Building configuration with firewall orthogonal to the portal frames equipped with Detail 1 + Detail 3245.

3.1.3.4 Detail 2

Considering the configuration similarities, the same assumptions made on Detail 1, were applied to Detail 2. The detail was tested orthogonally to the sandwich panels while the behaviour of the fusible links in the other horizontal direction was neglected, because of the presence of the vertical bracing system in that direction that would withstand the lateral forces. The numerical model of Detail 2 was split between the two green springs, see Figure 3.12b, while the behaviour on the other direction, as abovementioned, was defined through a stiff material.

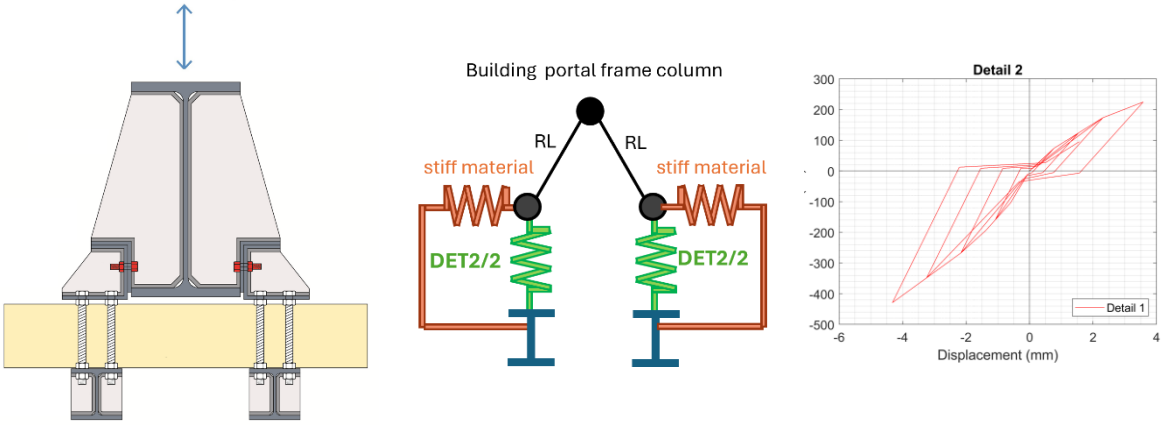

a) b) c)

Figure 3.15. a) Detail 2 and b) numerical model of Detail 2 and c) calibration of Detail 2 experimental behaviour.

Figure 3.16 shows the building configuration of Detail 2 in its geometry configuration and numerical configuration. The fusible link system is directly connected to the buildings columns. Therefore, it is not suitable for the additional columns between the portal frames. Thus, it was decided to apply the numerical model built for Detail 3145, considering that the details, Detail 2 and Detail 3145, were tested with the same size of aluminium bolts and designed for the same level of seismicity. The final conceived building configuration can be observed in Figure 3.17.

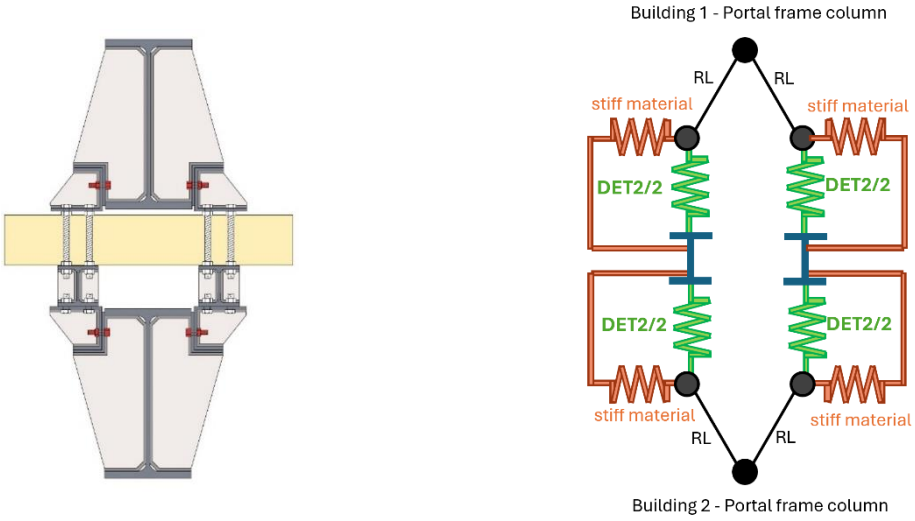

a) b)

Figure 3.16. a) Detail 2 building configuration and b) corresponding numerical model

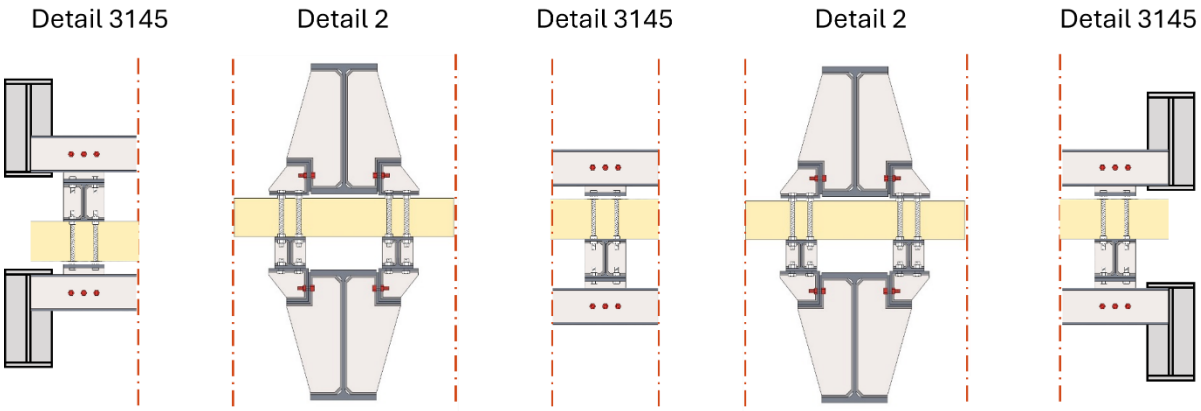

Figure 3.17. Building configuration Detail 2 + Detail 3145.

3.2 Spectrum - compatible accelerograms selection

In order to perform the nonlinear dynamic analyses, a series of spectrum compatible accelerograms were selected for the two level of seismicity considered, design PGA = 0.04g and design PGA = 0.12g (see Deliverable D1.3. Therefore, the ground motions selection was made from both the European database, the Engineering Strong Motion Database [12], and the Italian one, ITalian Accelerometric Archive 4.0 [13], part of the National Institute of Geophysics and Vulcanology. The selection followed some criteria hereafter reported:

- For each case study, a spectrum target was defined considered the two levels of seismicity;
- A range of periods, in which spectral compatibility is satisfied, was defined in accordance with both the Eurocode 8 [14] and the Italian national code [15];
- A range of magnitude and distances for the events was selected in order to find a satisfactory numbers of ground motions;
- The compatible directions of the events were the horizontal ones;
- Events characterized by different soil classification were selected to investigate the effect.

Figure 3.1 reports the requirements of the two codes in relation to a target spectrum, considered as the elastic spectrum defined by EN-1998-1, and a first period T_1 taken as an example. Figure 3.1a depicts the spectrum-compatibility range of periods between $0.2T_1$ and $1.5T_1$ and the range of spectral accelerations between 75% and 130% of the corresponding target response spectrum, as specified in Annex C of Eurocode 8 [14]. In addition, a minimum limitation of 50% is defined. Alongside, Figure 3.1b shows the spectrum-compatibility range of periods between 0.15 T_1 and $2T_1$ and the range of spectral accelerations between 90% and 130% of the corresponding target response spectrum, as specified in the Italian national code. The selected accelerograms were recorded in Italy, Greece, Turkey and Armenia, and, given the ground motion variability, the seismicity levels varied from low to moderate, with PGA values as low as 0.02g up to 0.28g.

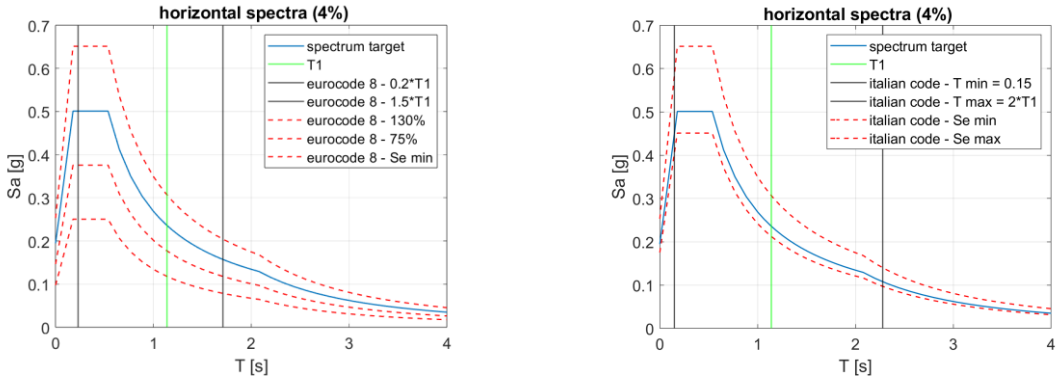

a) b)

Figure 3.1. Range of periods and spectral acceleration according to a) EC8 and b) Italian code.

In agreement with the two codes abovementioned, 3 ground motions were selected for each level of seismicity and the maximum value on the fusible links, out of the three nonlinear dynamic analyses carried out with them, was in the end compared with the relative capacity obtained through the experimental tests.

Considering that from the databases was possible to select a minimum of 7 accelerograms and the mean in the range of spectral accelerations was obtained from all of them, the three used for the analyses were the ones closer to the target spectrum at the first period of the structure T_1. For each case study, this selection is hereafter presented.

3.2.1 Case study 1

In this section, the spectrum compatible accelerograms selected for Case study 1 are reported. A modal analysis was performed to evaluate the first period of the structures that will serve to determine the spectrum compatible accelerograms, for each analysed configuration. The main difference in the periods was detected between the symmetric and asymmetric models, rather than the orthogonal and parallel modes. Table 5 and Table 6 report the periods and the modal masses found for the analysed structures.

Table 5. Case study 1 - wall orthogonal configuration - dynamic properties.

Symmetric configuration					Asymmetric configuration				
Mode	T [s]	Ux [%]	Uy [%]	Rz [%]	Mode	T [s]	Ux [%]	Uy [%]	Rz [%]
1°	0.63	50.6	0.0	4.1	1°	0.56	13.8	0.00	8.39
7°	0.58	0.0	77.0	10.8	3°	0.54	0.04	71.1	10.8
8°	0.55	0.0	16.5	38.6	10°	0.42	0.00	19.7	41.7

Table 6. Case study 2 - wall parallel configuration - dynamic properties.

Symmetric configuration					Asymmetric configuration				
Mode	T [s]	Ux [%]	Uy [%]	Rz [%]	Mode	T [s]	Ux [%]	Uy [%]	Rz [%]
1°	0.63	27.8	0.0	29.5	1°	0.63	23.6	0.0	27.2
4°	0.62	24.2	0.0	27.8	4°	0.61	25.2	0.0	35.2
13°	0.58	0.0	92.3	0.2	11°	0.53	0.0	90.3	0.2

Based on the dynamic properties of the symmetric configurations, parallel and orthogonal, it was decided to select the same set of accelerograms. The same principle was applied to the asymmetric ones.

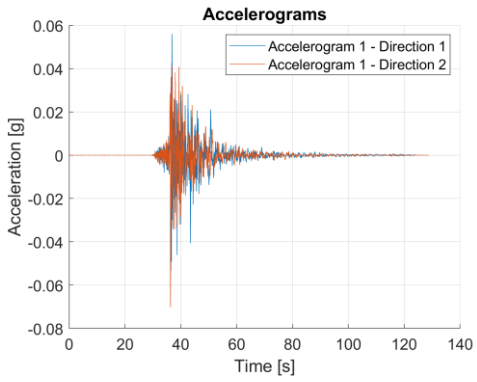

a)

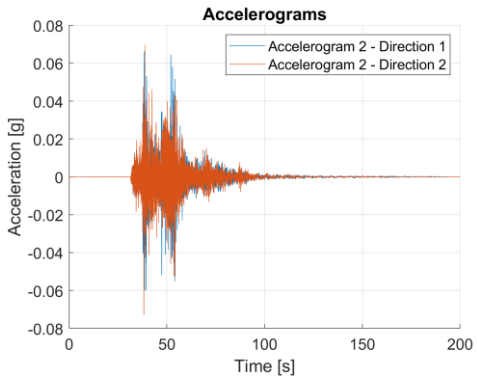

b)

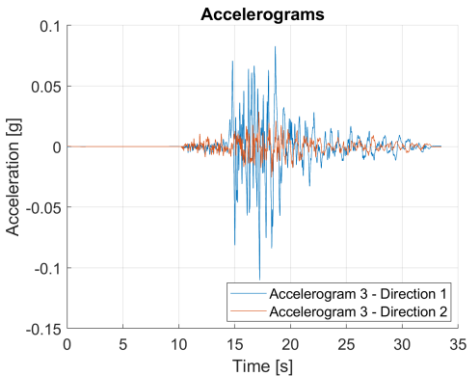

c)

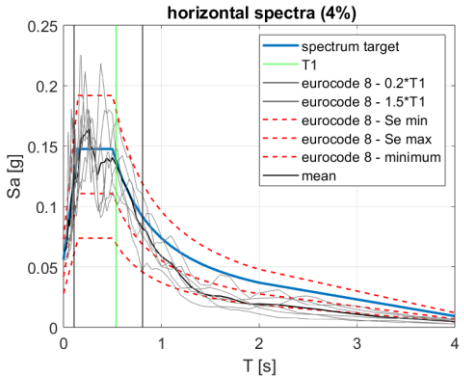

d)

Figure 3.2. Case study 1, symmetric configuration a) – c) low seismicity accelerograms selected, d) spectrum-compatibility.

Table 3.1. Case study 1 – low seismicity ground motions–symmetric configuration (orthogonal and parallel).

Number	Event ID/Station code	Event	PGA [g]	Mw	R [km]	Soil classification
1	EMSC-20161026_0000095/ 3A.MZ27	Italy	0.05	5.9	35.5	B
2	EMSC-20140524_0000026/ HL.LIA	Greece	0.07	6.9	45.1	B
3	IS-2000-0053/ SM.104	Greece	0.10	6.5	30.5	B

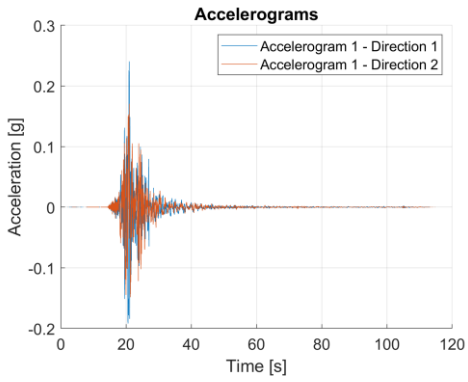

a)

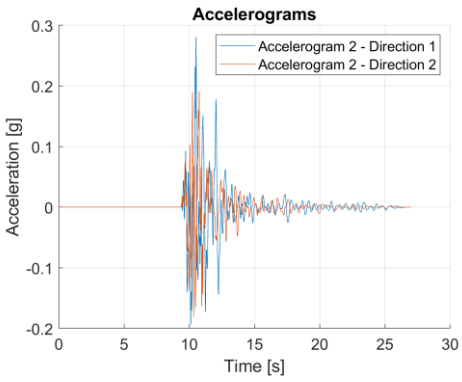

b)

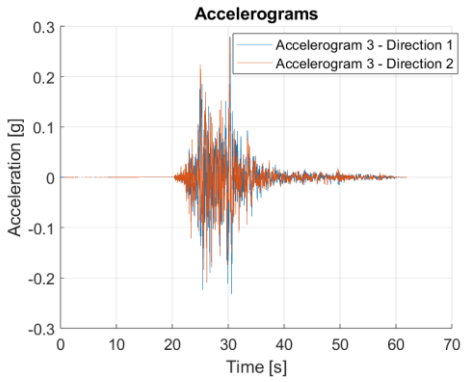

c)

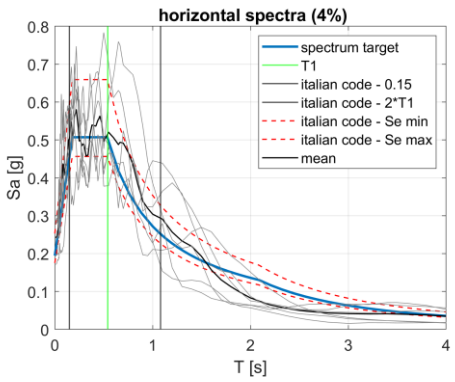

d)

Figure 3.3. Case study 1, symmetric configuration a) – c) moderate seismicity accelerograms selected, d) spectrum-compatibility.

Figure 3.2 and Figure 3.3 report the three accelerograms and the relative response spectra selected for both seismicity intensities in the symmetric configuration.

As reported in the criteria followed for selecting the accelerograms, only the two horizontal directions were spectrum-compatible with the spectrum target, and only them are illustrated in the figures. Nevertheless, the analyses were performed considering the vertical component. In addition, the Arias Intensity function was applied to the ground motions to reduce the computational burden and the energy content below 0.1% and over 99.5% was disregarded in accordance with the following equations:

$$I_A = \frac{\pi}{2g} \cdot \int_0^t a^2(t)dt \qquad H(\%) = \frac{\int_0^t a^2(t)dt}{\int_0^\infty a^2(t)dt}$$

Table 3.2. Case study 1 – moderate seismicity ground motions–asymmetric configuration (orthogonal and parallel).

Number	Event ID/Station code	Event	PGA [g]	Mw	R [km]	Soil classification
1	IT-2012-0011/ IT.MOG0	Italy	0.23	6.0	15.8	C
2	EMSC-20170821_0000072/ IV.IOCA	Italy	0.27	3.9	1.0	C
3	EMSC-20161030_0000029/ IV.T1212	Italy	0.26	6.6	11.6	A

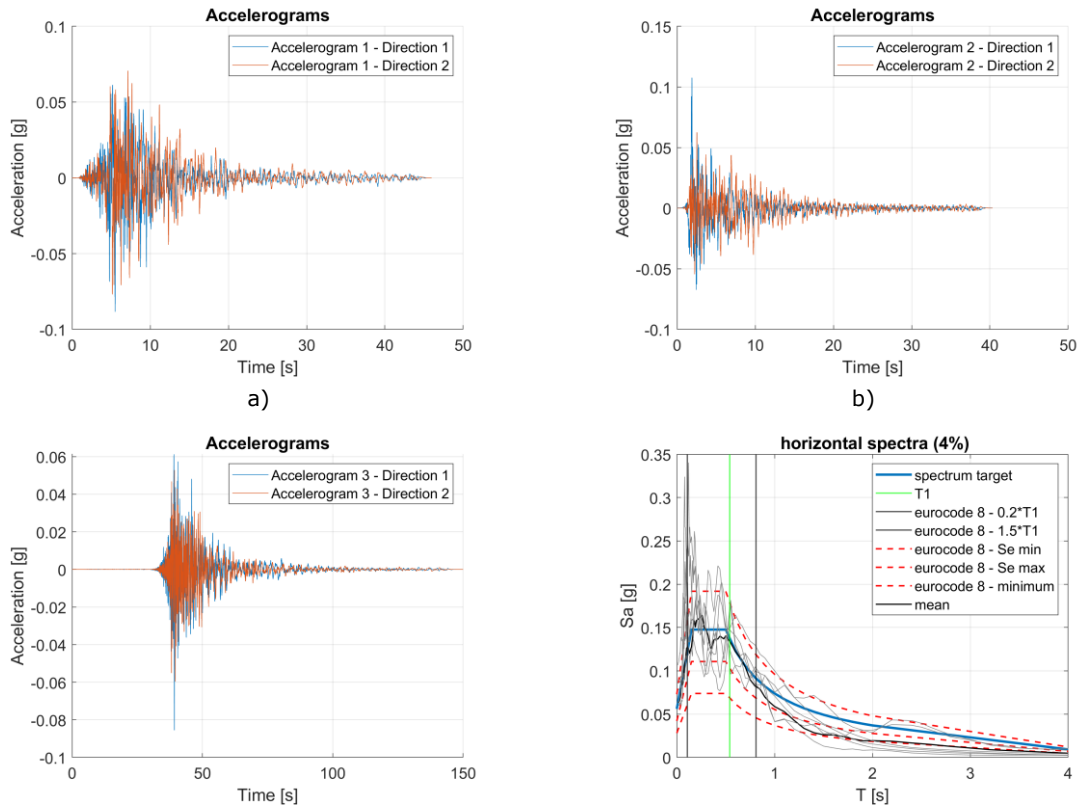

Figure 3.4. Case study 1, asymmetric configuration a) – c) low seismicity accelerograms selected, d) spectrum-compatibility.

Table 3.3. Case study 1 – low seismicity ground motions–asymmetric configuration (orthogonal and parallel).

Number	Event ID/Station code	Event	PGA [g]	Mw	R [km]	Soil classification
1	IT-1990-0001/ IT. RNR	Italy	0.08	5.8	31.1	B

2	IT-1990-0003/ IT. SRT	Italy	0.10	5.6	36.9	A
3	IT-2012-0011/ TV. CAS05	Italy	0.08	6.0	27.6	C

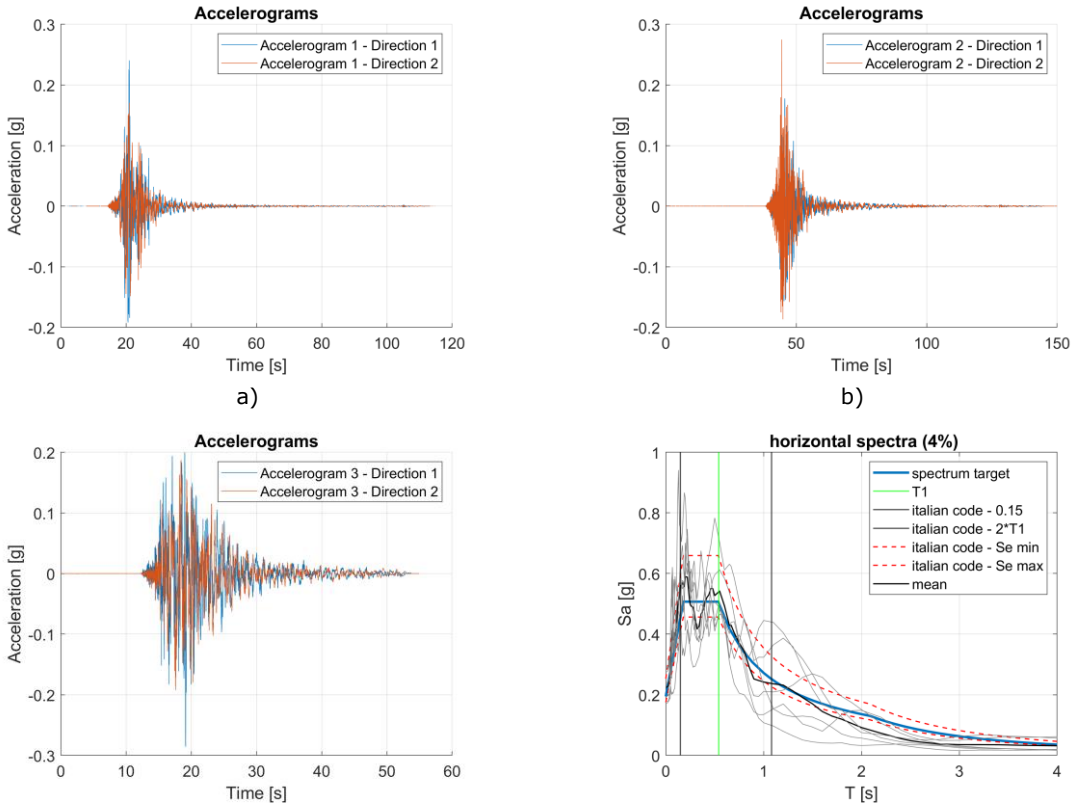

Figure 3.5. Case study 1, asymmetric configuration a) – c) moderate seismicity accelerograms selected, d) spectrum-compatibility.

Figure 3.4 and Figure 3.5 report the accelerograms and relative response spectra calculated for Case study 1 at the two levels of seismicity considered for the symmetric model.
As reported in the criteria followed for selecting the accelerograms, only the two horizontal directions were spectrum-compatible with the spectrum target, and only them are illustrated in the figures. Nevertheless, the analyses were performed considering the vertical component. Also in this case, the Arias Intensity function was applied to the ground motions.

Table 3.4. Case study 1 – moderate seismicity ground motions– asymmetric configuration (orthogonal and parallel).

Number	Event ID/Station code	Event	PGA [g]	Mw	R [km]	Soil classification
1	IT-2012-0011/ IT. MOG0	Italy	0.23	6.0	15.8	C
2	IT-2012-0011/ IT. MIR05	Italy	0.26	6.0	15.8	C
3	EMSC-20161030_0000029 / IV. T1244	Italy	0.28	6.6	16.9	B

3.2.2 Case study 3

In this section, the spectrum compatible accelerograms selected for Case study 3 are reported. Firstly, a modal analysis was performed to evaluate the first period of the structures that will serve to determine the spectrum compatible accelerograms for each configuration presented in Section

3.1.2. The main difference in the periods was expected between the symmetric and asymmetric models, however, as can be seen in Table 7 and in Table 8, the first periods had the same results in the two configurations, due to a proportional distribution of mass and stiffness between the symmetric and asymmetric configuration.

Table 7. Case study 3 - wall orthogonal configuration - dynamic properties.

Symmetric configuration					Asymmetric configuration				
Mode	T [s]	Ux [%]	Uy [%]	Rz [%]	Mode	T [s]	Ux [%]	Uy [%]	Rz [%]
1°	1.14	0.04	39.4	5.78	1°	1.14	0.02	45.5	3.18
2°	1.11	0.04	32.8	7.98	2°	1.11	0.06	29.5	13.2
3°	1.09	61.4	0.02	9.21	3°	1.09	21.9	0.44	4.35

Table 8. Case study 3 - wall parallel configurations - dynamic properties.

Symmetric configuration					Asymmetric configuration				
Mode	T [s]	Ux [%]	Uy [%]	Rz [%]	Mode	T [s]	Ux [%]	Uy [%]	Rz [%]
1°	1.13	0.05	19.1	24.1	1°	1.13	0.02	21.7	23.4
2°	1.11	0.25	19.3	23.7	2°	1.11	0.01	21.4	33.4
4°	1.09	81.3	0.08	0.41	6°	1.05	75.4	0.04	0.15

As a result, the same spectrum-compatible accelerograms were selected to perform the nonlinear dynamic analyses.

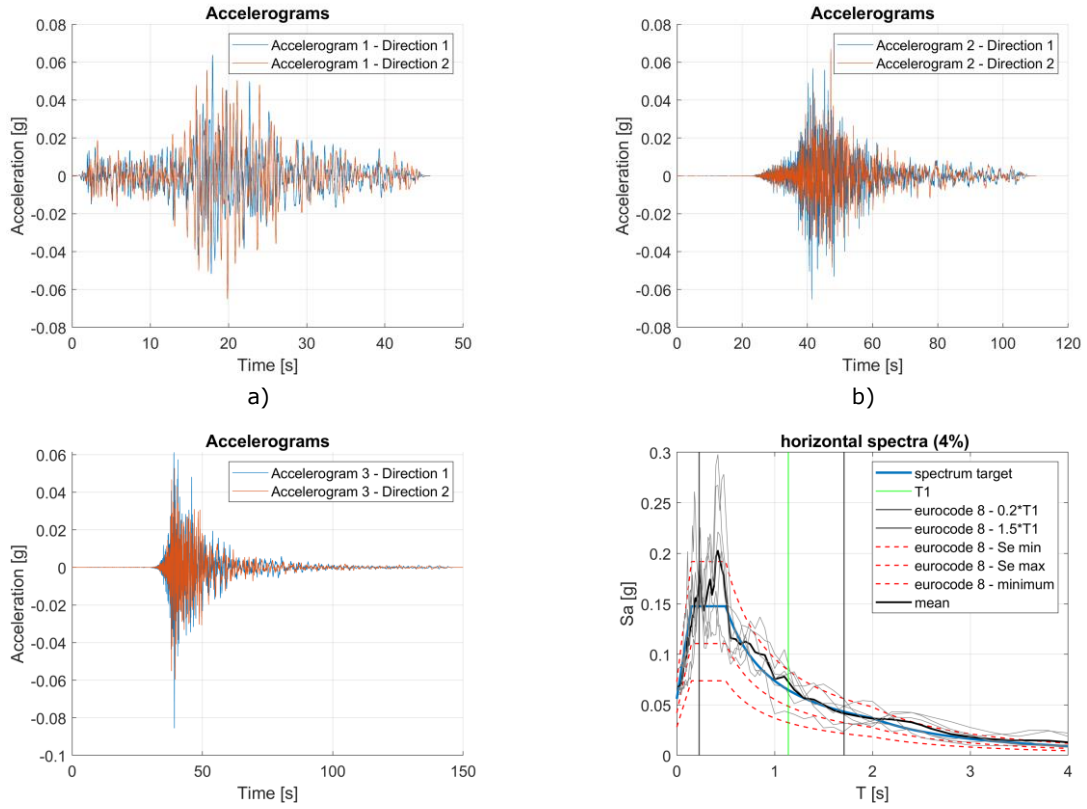

Figure 3.6. Case study 3 a) – c) low seismicity accelerograms selected, d) spectrum-compatibility.

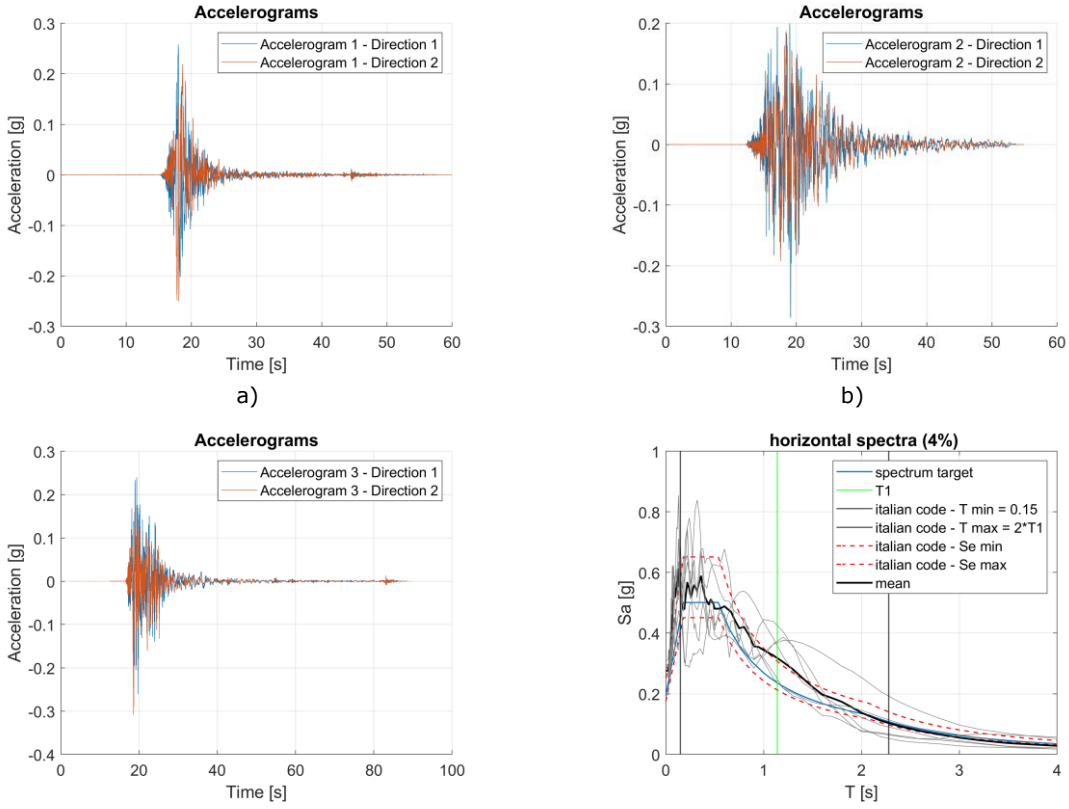

Figure 3.7. Case study 3 a) – c) moderate seismicity accelerograms selected, d) spectrum-compatibility.

Figure 3.6 and Figure 3.7 report the accelerograms and relative response spectra calculated for Case study 3 at the two levels of seismicity considered. As reported in the criteria followed for selecting the accelerograms, only the two horizontal directions were spectrum-compatible with the spectrum target, and only them are illustrated in the figures. Nevertheless, the analyses were performed considering the vertical component as well. In addition, the Arias Intensity function was also applied to the ground motions to reduce the computational cost

Table 9. Case study 3 – low seismicity ground motions.

Number	Event ID/Station code	Event	PGA [g]	Mw	R [km]	Soil classification
1	GR-1983-0001/ HI.LEF1	Greece	0.06	5.0	90.3	C
2	EMSC-20181025_0000087/ HL.LXRA	Greece	0.06	4.8	84.1	B
3	IT-2012-0011/ TV.CAS05	Italy	0.08	4.9	27.6	C

Table 10. Case study 3 – moderate seismicity ground motions.

Number	Event ID/Station code	Event	PGA [g]	Mw	R [km]	Soil classification
1	IT-2012-0010/ IV.T0819	Italy	0.25	5.5	6.8	C
2	EMSC-20161030_0000029/ IV.T1244	Italy	0.28	6.2	16.9	B
3	IT-2009-0009/ MN.AQU	Italy	0.25	6.1	2.5	B

3.2.3 Case study 4

In this section, the spectrum-compatible accelerograms selected for Case study 4 are reported. Firstly, a linear dynamic analysis was performed to evaluate the first period of the structures that will serve to determine the spectrum compatible accelerograms, for each configuration developed. The first periods are reported in Table 11 and Table 12 along with the modal masses.

Table 11. Case study 4 - wall orthogonal configurations – dynamic properties.

Symmetric configuration					Asymmetric configuration				
Mode	T[s]	Ux [%]	Uy [%]	Rz [%]	Mode	T[s]	Ux [%]	Uy [%]	Rz [%]
1°	2.38	67.1	0.00	0.11	1°	2.48	25.5	0.00	3.66
3°	2.27	0.00	98.5	0.00	2°	2.16	39.8	0.00	2.18
52°	0.66	0.00	0.00	61.5	4°	1.98	0.64	82.9	0.13

Table 12. Case study 4 - wall parallel configurations – dynamic properties.

Symmetric configuration					Asymmetric configuration				
Mode	T [s]	Ux [%]	Uy [%]	Rz [%]	Mode	T[s]	Ux [%]	Uy [%]	Rz [%]
1°	2.59	24.1	0.00	4.29	1°	2.59	29.8	0.00	0.47
2°	2.59	20.2	0.00	4.78	2°	2.39	18.7	0.00	2.14
5°	2.24	0.00	98.5	0.00	8°	1.88	0.00	98.2	0.15

Based on the dynamic properties of the symmetric configurations, parallel and orthogonal, it was decided to select the same set of accelerograms. The same principle was applied to the asymmetric ones. It has to be noted that for the low seismicity level, the same set of accelerograms were used for the symmetric and asymmetric configuration.

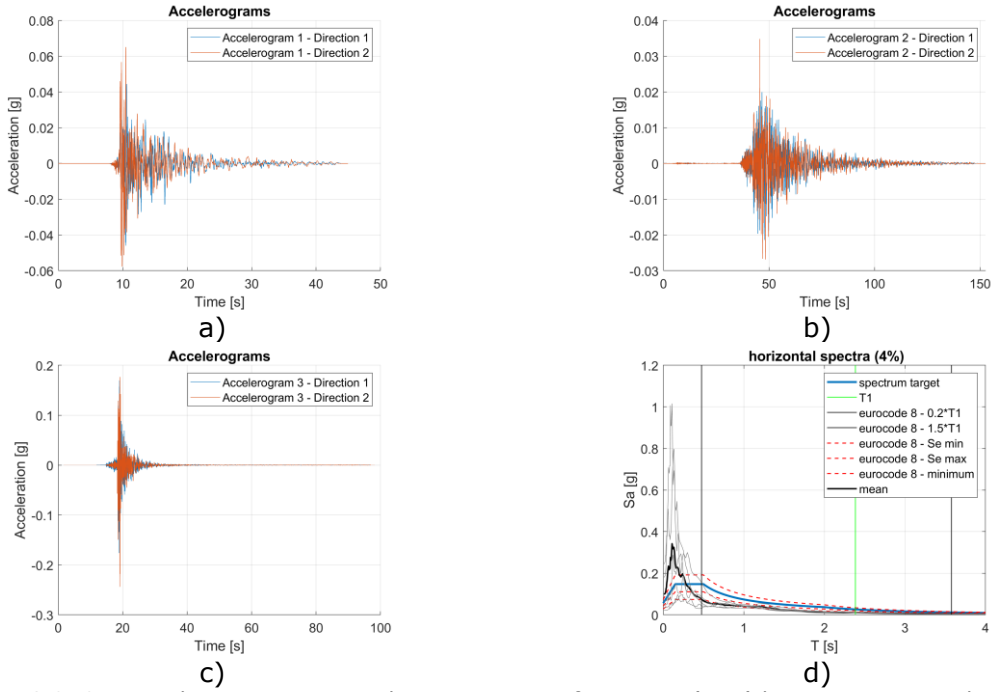

Figure 3.8. Case study 4, symmetric and asymmetric configuration a) – c) low seismicity accelerograms selected, d) spectrum-compatibility.

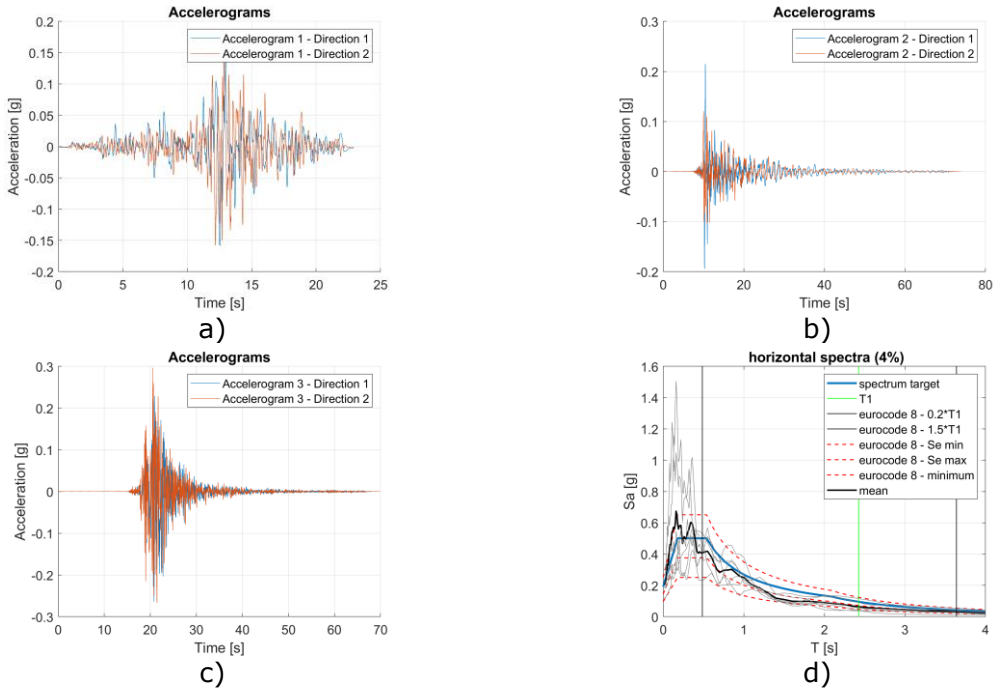

Figure 3.9. Case study 4, symmetric configuration a) – c) moderate seismicity accelerograms selected, d) spectrum-compatibility.

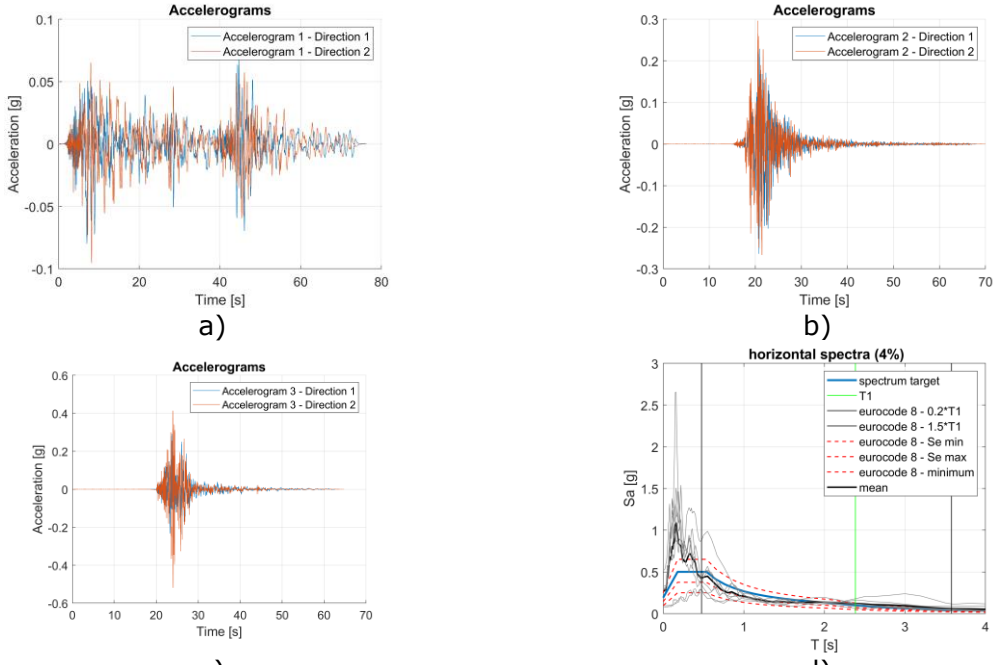

Figure 3.10. Case study 4, asymmetric configuration a) – c) moderate seismicity accelerograms selected, d) spectrum-compatibility.

Figure 3.8 and Figure 3.9 report the accelerograms and relative response spectra calculated for Case study 4 at the two levels of seismicity considered for the symmetric model. Figure 3.10 reports the accelerograms and relative response spectra at the moderate seismicity level for the asymmetric model. As reported in the criteria followed for selecting the accelerograms, only the two horizontal directions were spectrum-compatible with the spectrum target, and only them are illustrated in the figures. Nevertheless, the analyses were performed considering the vertical component. In addition, the Arias Intensity function was applied to the ground motions to reduce the computational burden.

Table 3.5, Table 3.6 and Table 3.7 report the ground motions selected for both levels of seismicity.

Table 3.5. Case study 4 – low seismicity ground motions

Number	Event ID/Station code	Event	PGA [g]	Mw	R [km]	Soil classification
1	EMSC-20140921_0000002/ HL.ARIA	Greece	0.04	5.0	6.5	C
2	IT-2012-0012/ IV.T0826	Italy	0.17	4.9	12.1	C
3	EMSC-20151029_0000038/ KO.ERCV	Turkey	0.02	4.8	33.7	B

Table 3.6. Case study 4 - moderate seismicity ground motions - symmetric configuration (orthogonal and parallel)

Number	Event ID/Station code	Event	PGA [g]	Mw	R [km]	Soil classification
1	AM-1988-0001/ A.GUK	Armenia	0.18	6.7	35.4	C
2	EMSC-20161026_0000095/ IT.NOR	Italy	0.21	5.9	13.7	B
3	IT-2012-0011/ IV.T0802	Italy	0.25	6	9.9	C

Table 3.7. Case study 4 – moderate seismicity ground motions– asymmetric configuration (orthogonal and parallel)

Number	Event ID/Station code	Event	PGA [g]	Mw	R [km]	Soil classification
1	IT-1980-0012/ IT.BSC	Italy	0.08	6.9	28.3	A
2	IT-2012-0011/ IV.T0802	Italy	0.25	6	9.9	C
3	TK-2003-0038/ IV.T0802	Italy	0.28	6.4	11.6	B

3.3 Results of the time-history analyses

3.3.1 Case study 1: Carcassone

In this section, the results of the time-history analyses carried out on Case study 1 are presented.

Considering the configurations presented in section 3.1.2, Table 13 depicts all the numerical analyses that were performed on Case study 1, while Figure 3.18 illustrates the different building configurations.

Table 13. Case study 1 analyses

Wall position / building configuration	Low seismicity (Design PGA=0.04g)	Moderate seismicity (Design PGA=0.12g)		
Orthogonal / Symmetric	Detail 1	Detail 2	Detail 3145	Detail 3245
Orthogonal / Asymmetric	Detail 1	Detail 2	Detail 3145	Detail 3245
Parallel / Symmetric	-	-	Detail 3145	Detail 3245
Parallel / Asymmetric	-	-	Detail 3145	Detail 3245

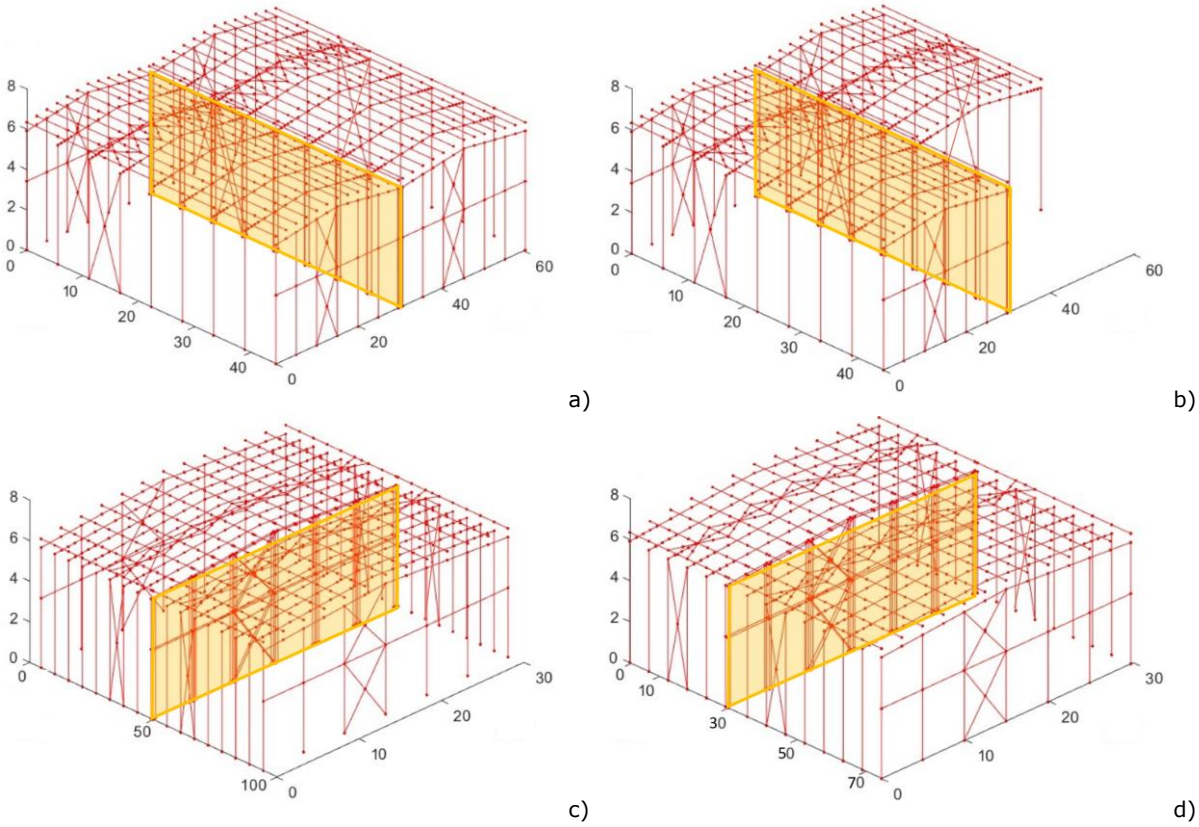

Figure 3.18. Case study 1 structure configuration: a) Orthogonal – Symmetric; b) Orthogonal – Asymmetric; c) Parallel – Symmetric; d) Parallel – Asymmetric.

3.3.1.1 Low seismicity

For each building configuration, some main relevant global results are reported, while the results on the fusible links are presented in detail.

In this section, the outcomes of the time-history analyses performed on Case study 1 subjected to low seismicity ground motions, modified by means of Arias Intensity function, are presented. In addition to the results on the fusible links details, some global outcomes are reported as well. As reported in Table 13, Detail 1 was included only when the fire wall is orthogonal to the portal frames, in both symmetric and asymmetric configuration. The results, both global and local are presented as a comparison between the two configurations.

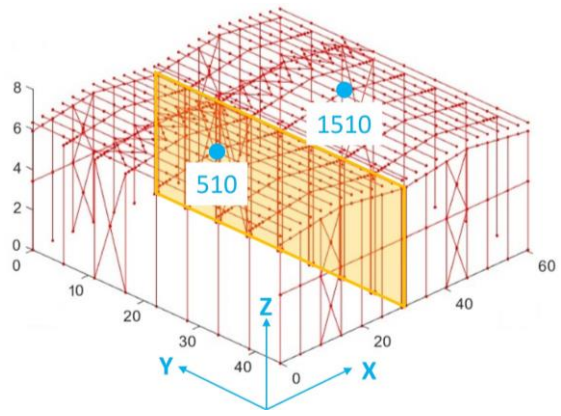

(a1)

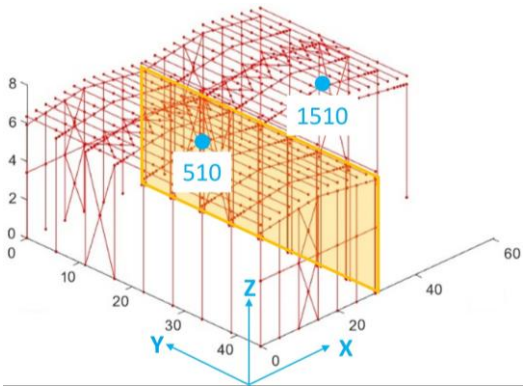

(b1)

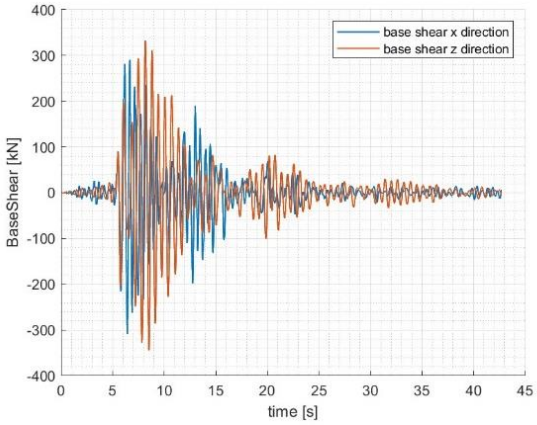

(a2)

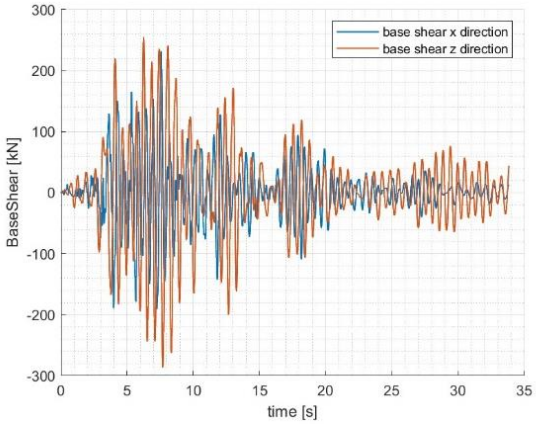

(b2)

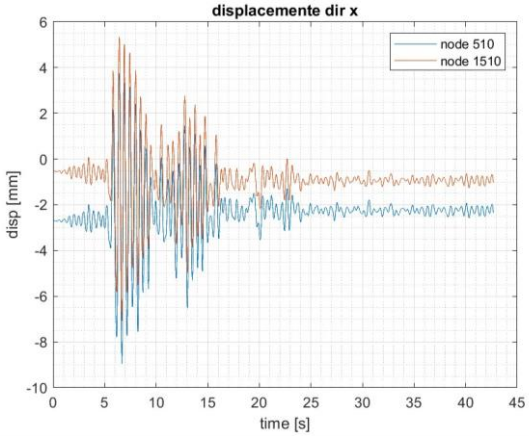

(a3)

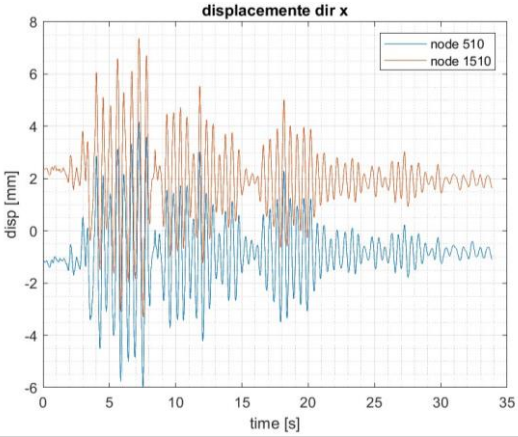

(b3)

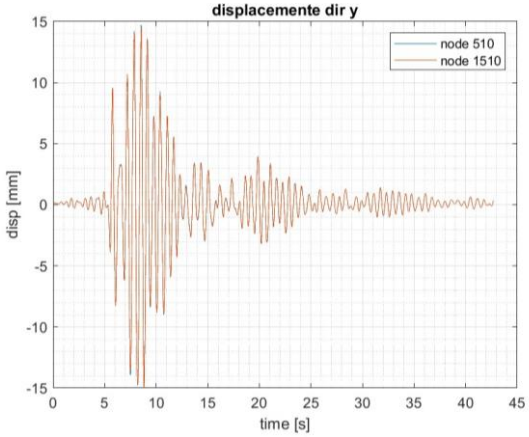

(a4)

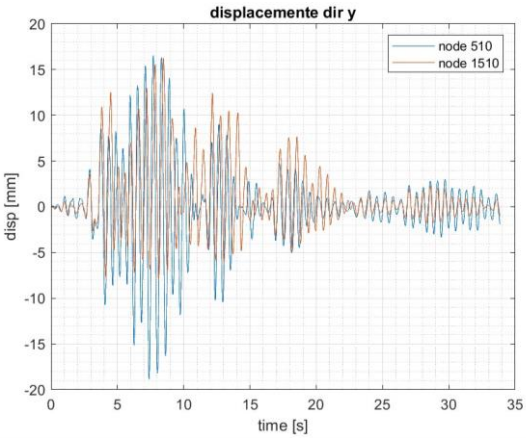

(b4)

Figure 3.19. Case study 1 global outputs (a) symmetric model with firewall orthogonal to the portal frames and (b) asymmetric model with firewall orthogonal to the portal frames.

Figure 3.19 reports the global outputs of one of the time-history analyses performed on Case study 1 equipped with Detail 1. Considering the base shear, a slight decrease of values can be observed on the asymmetric configuration with respect to the symmetric one, which is in line with the asymmetry introduced. Moreover, in terms of global displacement, the effect of the asymmetry is well denoted in the direction orthogonal to the portal frames, see Figure 3.19b4. On the contrary, on the direction parallel to the portal frames, the global displacement is symmetric despite the asymmetry between the structures.

In terms of local outputs on the fusible links, hereafter the results obtained on Detail 1 from the three accelerograms are reported.

Figure 3.20 and Figure 3.21 depict the outputs on the fusible links for each of the accelerograms run in the symmetric (SYM) and the asymmetric (ASYM) configurations, respectively. As can been noticed, the magnitude of the results is very similar both in terms of forces and displacements. The magnitude of the latter is rather small. Moreover, observing the maximum values reached during the analyses in comparison with the capacity of Detail 1, reported in Table 14, the detail is stressed only for half of its maximum resistance and no damage occurred.

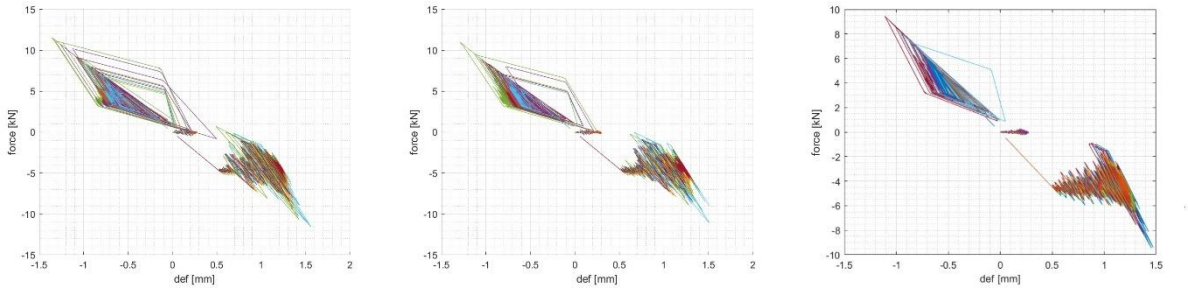

a) b) c)

Figure 3.20Results on fusible links of the symmetric configuration equipped with Detail 1 from analyses performed with a) Accelerogram 1, b) Accelerogram 2 and c) Accelerogram 3.

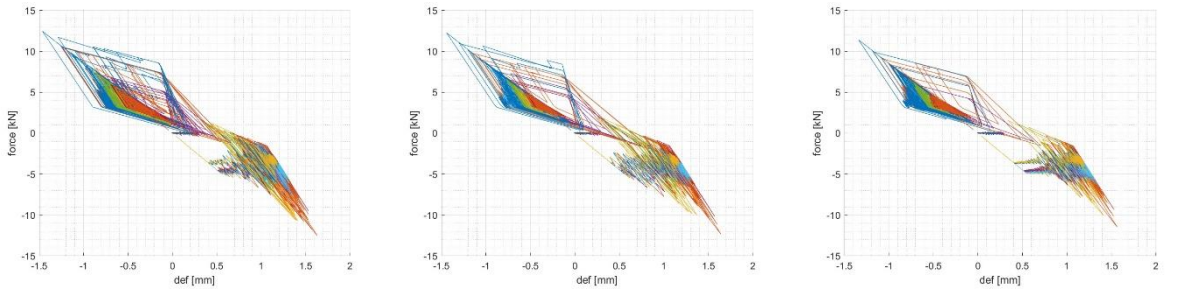

a) b) c)

Figure 3.21. Results on fusible links of the asymmetric configuration equipped with Detail 1 obtained from analyses performed with a) Accelerogram 1, b) Accelerogram 2 and c) Accelerogram 3.

Table 14. Forces obtained on fusible links in comparison with the detail capacity.

Accelerogram	Accelerogram 1	Accelerogram 2	Accelerogram 3	Capacity
Maximum force SYM configuration	11.5 kN	11.0 kN	9.5 kN	22.0 kN
Maximum force ASYM configuration	12.5 kN	12.5 kN	11.5 kN	22.0 kN

3.3.1.2 Moderate seismicity

Detail 2, Detail 3145 and Detail 3245 were designed and tested for a seismicity level characterised by PGA = 0.12g. The moderate seismicity accelerograms presented in Section 3.2.1 and modified by means of the Arias Intensity function, were used in the time-history analyses. For the sake of completeness, in addition to the results on the fusible links details, some global outcomes are reported as well. As reported in Table 13, Detail 2 was tested only in orthogonal models, in both symmetric and asymmetric configuration, while Detail 3145 and Detail 3245 were tested with the firewall in both positions, orthogonal and parallel to the portal frames. The results, both global and local are presented as a comparison between the symmetric and asymmetric configurations.

3.3.1.2.1 Configuration with the firewall orthogonal to the portal frames

Figure 3.22 reports the global results in the orthogonal symmetric and asymmetric configurations equipped with one of three details covered in this section.

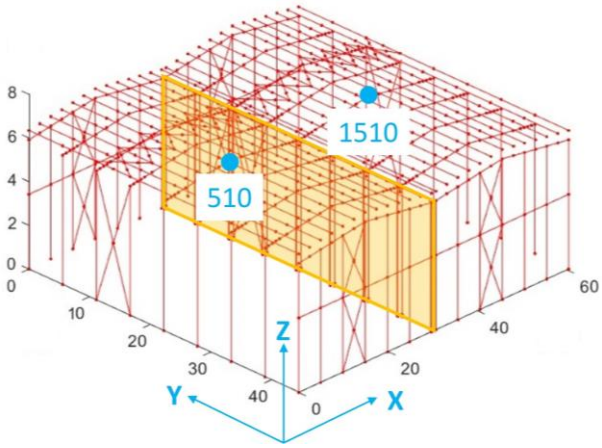

(a1)

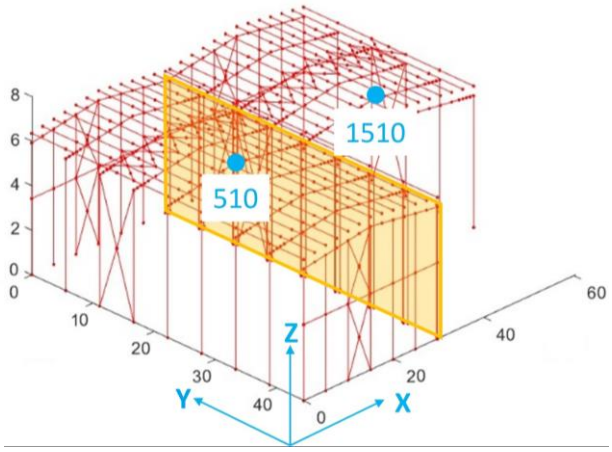

(b1)

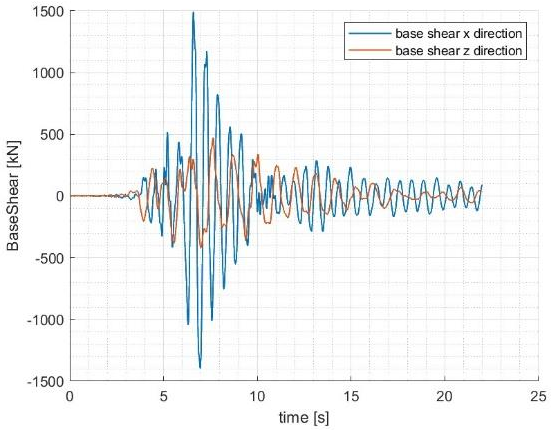

(a2)

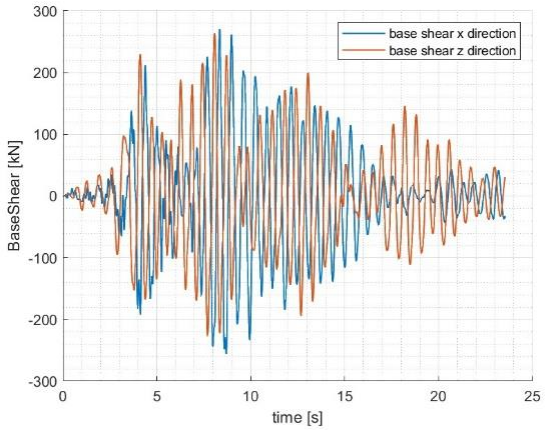

(b2)

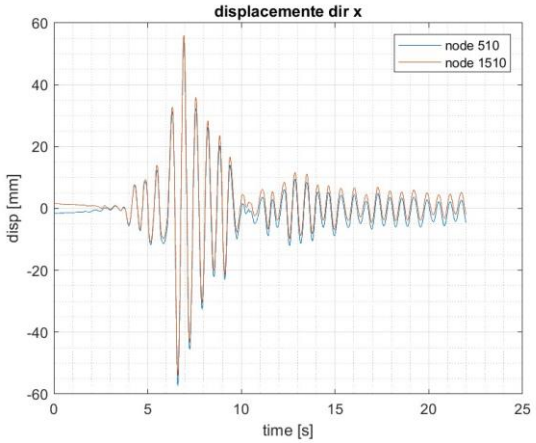

(a3)

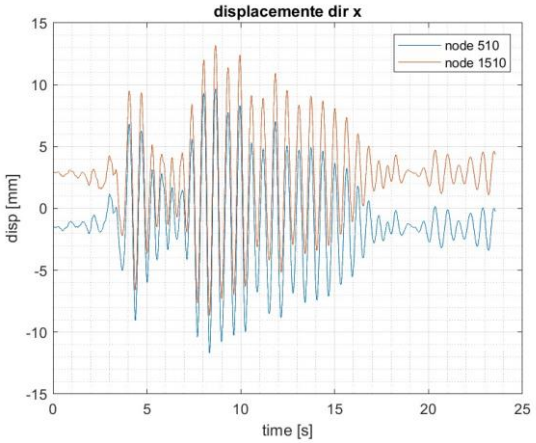

(b3)

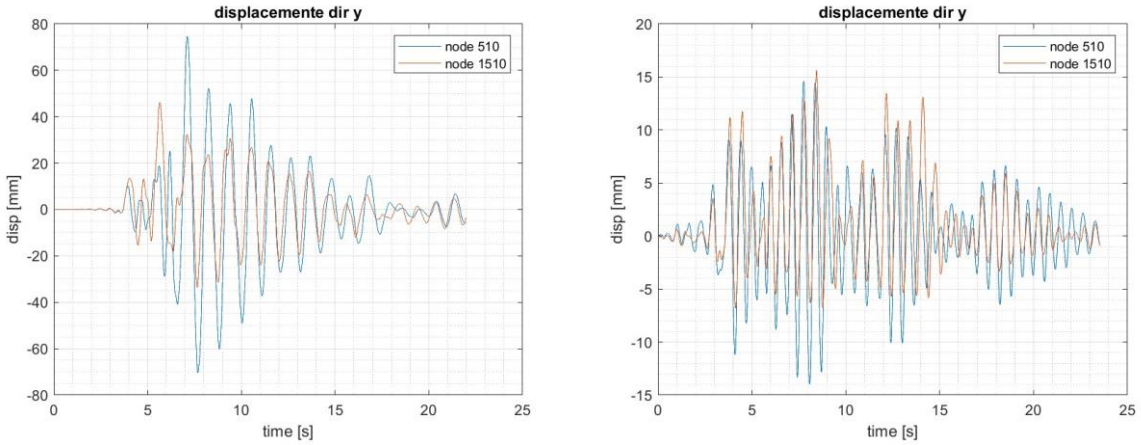

(a4) (b4)

Figure 3.22. Case study 1 global outputs (a) symmetric model with firewall orthogonal to the portal frames and (b) asymmetric model with firewall orthogonal to the portal frames.

In line with the results observed on the global models subjected to low seismicity accelerograms, despite the different accelerograms used to run the analyses, the asymmetry determined a significant decrease of forces in terms of base shear, in particular in the direction parallel to the portal frames. In terms of global displacements, the same trend recorded on the previous case was noticed. In fact, the asymmetry is more emphasized in the direction orthogonal to the portal frames, while in the direction parallel to the portal frames, despite a different initial displacement due to the gravity analyses, the symmetry between the structures is kept. A decrease of displacement reached was observed in both directions in the asymmetric configuration.

Figure 3.23 depicts the outputs on the fusible links on the symmetric (SYM) configuration for each of the accelerograms run. As can be noticed the results are very similar. The same consideration could be point out for the asymmetric (ASYM) results reported in Figure 3.24. Moreover, observing the maximum values reached during the analyses, in comparison with the capacity of Detail 2, reported in Table 15 and obtained from the experimental test extensively presented in Deliverable D4.1 [11], the detail stress in both cases are below the capacities.

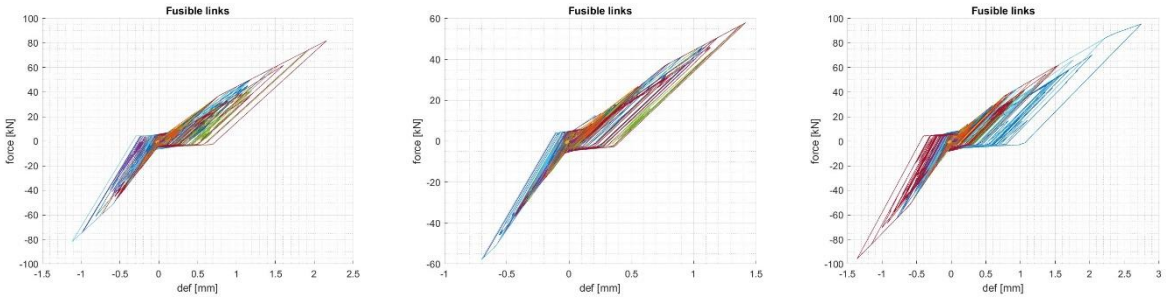

a) b) c)

Figure 3.23. Results on fusible links of the symmetric configuration equipped with Detail 2 from analyses performed with a) Accelerogram 1, b) Accelerogram 2 and c) Accelerogram 3.

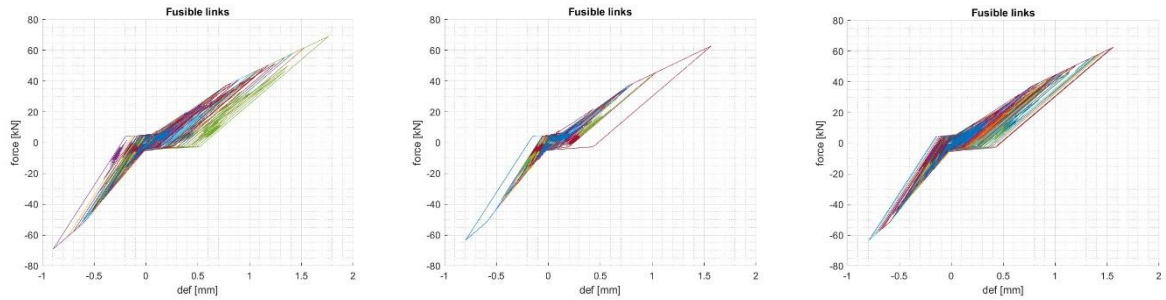

a) b) c)

Figure 3.24. Results on fusible links of the asymmetric configuration equipped with Detail 2 from analyses performed with a) Accelerogram 1, b) Accelerogram 2 and c) Accelerogram 3.

Table 15. Forces obtained on Detail 2 fusible links in comparison with the detail capacity.

Accelerogram	Accelerogram 1	Accelerogram 2	Accelerogram 3	Capacity
Maximum force SYM configuration	80.0 kN	58.0 kN	95.0 kN	110.0 kN
Maximum force ASYM configuration	70.0 kN	65.0 kN	65.0 kN	110.0 kN

Concerning the results obtained in this case study configuration, equipped with Detail 3145, they are hereafter reported.

Figure 3.25 depicts the outputs on the fusible links on the symmetric configuration for each accelerogram. As can be noticed, the result shape is very similar, while the values increase and decrease with the accelerograms intensities. Figure 3.26 depicts the outputs on the fusible links in the asymmetric configuration. As can be noticed, the magnitude of forces is lower, owing to the smaller differential displacement recorded on the fusible links. Table 16 reports the maximum values reached in comparison with the capacities calculated for each detail configuration. Indeed, while on one direction the fusible link is characterized only by Detail 3.1, on the other direction, the behaviour could be represented by Detail 4 or Detail 5. However, the results obtained were under the maximum capacities.

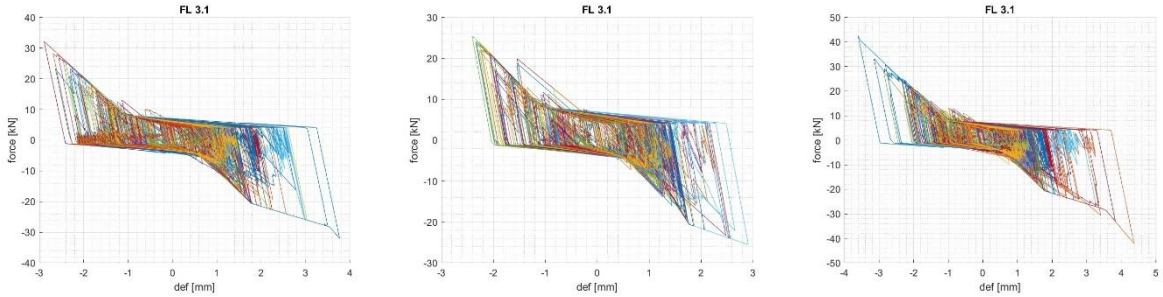

a) b) c)

Figure 3.25. Results on fusible links of CS1_SO equipped with Detail 3145 from analyses performed with a) Accelerogram 1, b) Accelerogram 2 and c) Accelerogram 3.

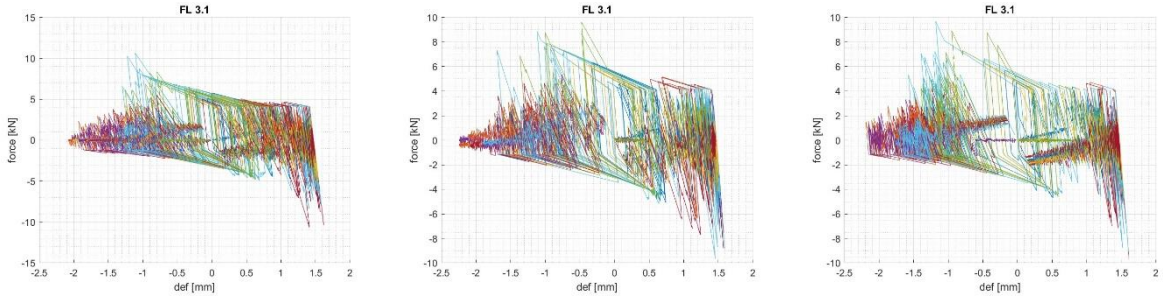

a) b) c)

Figure 3.26. Results on fusible links of CS1_AO equipped with Detail 3145 from analyses performed with a) Accelerogram 1, b) Accelerogram 2 and c) Accelerogram 3.

Table 16. Forces obtained on Detail 3145 fusible links in comparison with the detail capacity.

Symmetric configuration				
Component	Accelerogram 1	Accelerogram 2	Accelerogram 3	Capacity
Detail 3.1	32.00 kN	26.00 kN	42.00 kN	115.00 kN
Detail 4	25.14 kN	18.62 kN	20.49 kN	26.30 kN
Detail 5	26.07 kN	20.49 kN	21.42 kN	50.50 kN
Asymmetric configuration				
Component	Accelerogram 1	Accelerogram 2	Accelerogram 3	Capacity
Detail 3.1	11.00 kN	9.50 kN	9.50 kN	115.00 kN
Detail 4	11.17 kN	10.24 kN	11.17 kN	26.30 kN
Detail 5	12.11 kN	11.17 kN	11.17 kN	50.50 kN

With regard to the configurations equipped with Detail 3245, in terms of local outputs on the fusible links, the results obtained on Detail 3.2 in Figure 3.27 are reported.

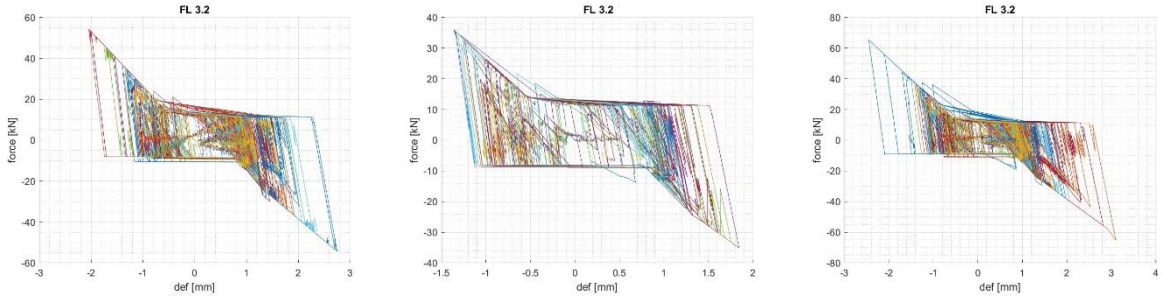

a) b) c)

Figure 3.27. Results on fusible links of the symmetric configuration equipped with Detail 3245 from analyses performed with a) Accelerogram 1, b) Accelerogram 2 and c) Accelerogram 3.

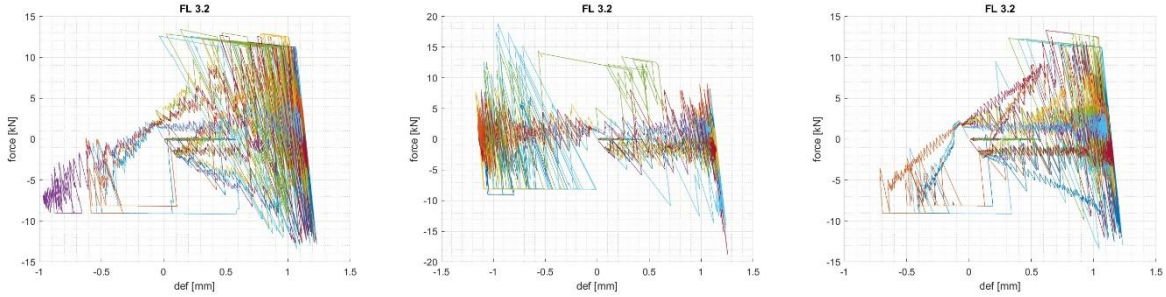

a) b) c)

Figure 3.28. Results on fusible links of the asymmetric configuration equipped with Detail 3245 from analyses performed with a) Accelerogram 1, b) Accelerogram 2 and c) Accelerogram 3.

Figure 3.27 depicts the outputs on the fusible links for each of the accelerograms run. As can been noticed the shape and the magnitude of the results are similar. Figure 3.28 depicts the outputs on the fusible links for each accelerogram. As can be noticed the displacements are very small that affect force-displacement diagram. In fact, in comparison with the symmetric configuration results, the differential displacement reached in this case is smaller and therefore less defined shape of the results can be observed. Table 17 reports the maximum values reached in comparison with the capacities calculated for each detail configuration. For each configuration the maximum forces were lower than the maximum capacities. It is worth to recall that the symmetric and asymmetric models were analysed with different set of spectrum-compatible accelerograms, as reported in Section 3.2.1. This is the reason of the different forces in the fusible links between the symmetric and asymmetric cases.

Table 17. Forces obtained on Detail 3245 fusible links in comparison with the detail capacity.

Symmetric configuration				
Component	Accelerogram 1	Accelerogram 2	Accelerogram 3	Capacity
Detail 3.2	55.00 kN	35.00 kN	65.00 kN	115.00 kN
Detail 4	26.00 kN	22.00 kN	22.00 kN	26.30 kN
Detail 5	28.00 kN	22.00 kN	23.00 kN	50.50 kN
Asymmetric configuration				
Component	Accelerogram 1	Accelerogram 2	Accelerogram 3	Capacity
Detail 3.2	13.00 kN	19.00 kN	13.00 kN	115.00 kN
Detail 4	13.00 kN	12.00 kN	12.40 kN	26.30 kN
Detail 5	13.40 kN	12.00 kN	13.00 kN	50.50 kN

3.3.1.2.2 Configuration with the firewall parallel to the portal frames

As reported in Table 13, the last two details presented were involved also in the models with the wall parallel to the portal frames. Figure 3.29 reports the global output obtained in both configurations, symmetric and asymmetric in comparison.

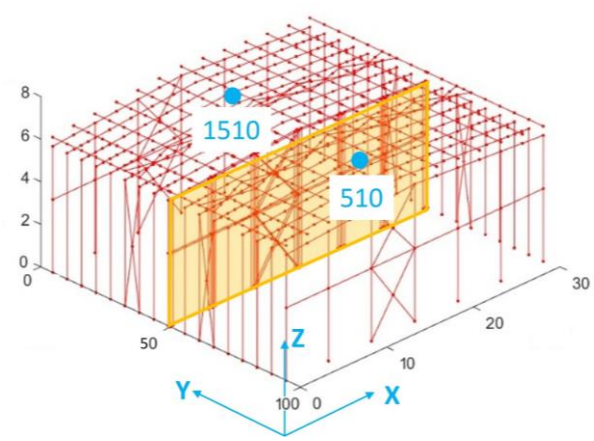

(a1)

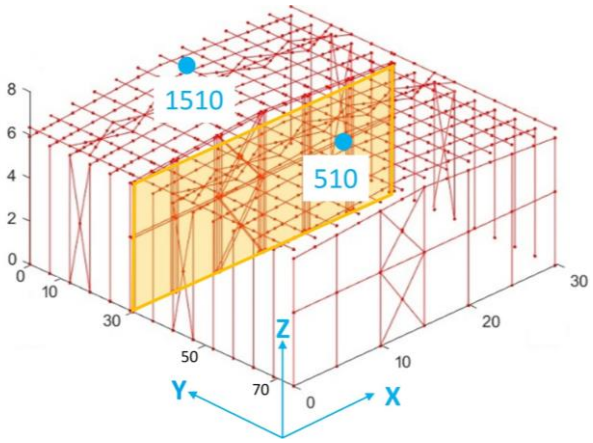

(b1)

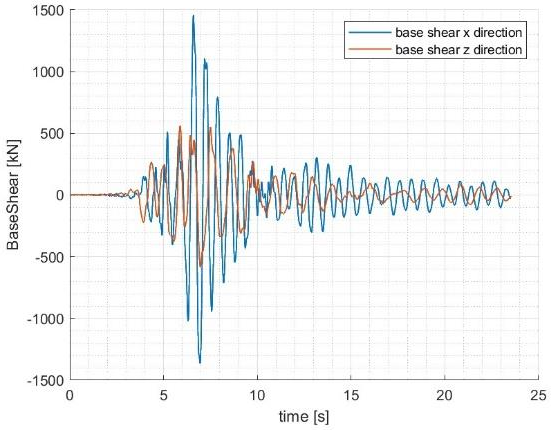

(a2)

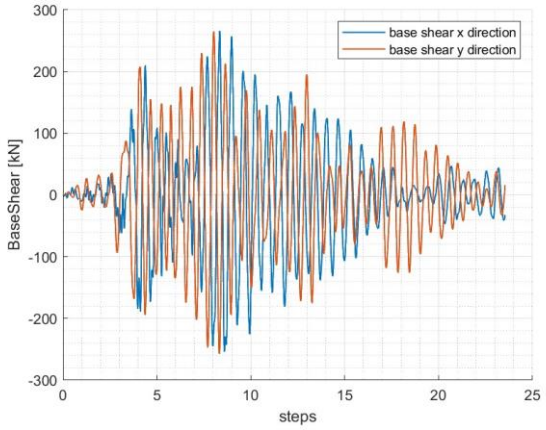

(b2)

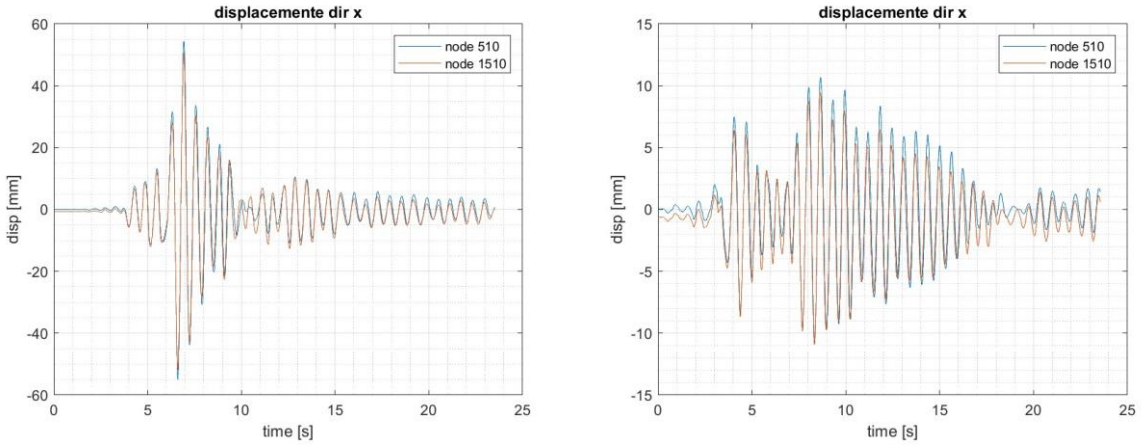

((a3))

(b3)

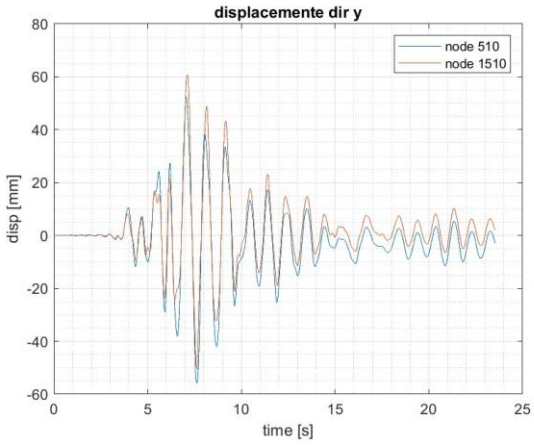

((a4))

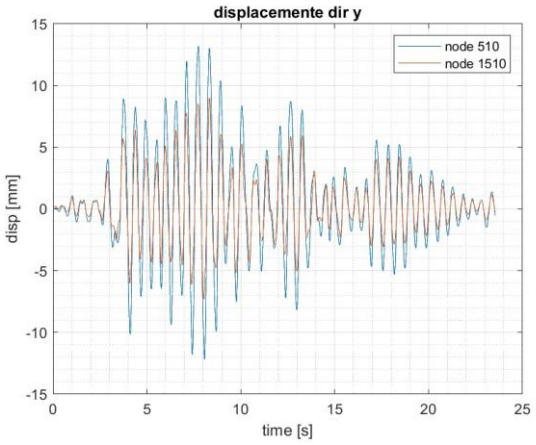

(b4)

Figure 3.29. Case study 1 global outputs (a) symmetric model with firewall parallel to the portal frames and (b) asymmetric model with firewall parallel to the portal frames.

In line with the results observed on the global models of the orthogonal configuration, despite the different accelerograms used to run the analyses, Figure 3.29 shows that the asymmetry introduced determined a significant decrease of forces in terms of base shear, in particular in the direction parallel to the portal frames. In terms of global displacements, the asymmetry is evident in the direction orthogonal to the portal frames, while in the direction parallel to the portal frames the symmetry between the structures is such that the global displacements between the two buildings are very similar. A decrease of displacement was observed in both directions in the asymmetric configuration.

Concerning the results obtained in this configuration, when equipped with Detail 3145, they are hereafter reported.

Figure 3.30 depicts the outputs on the fusible links for the symmetric configuration, for each accelerogram. As can be noticed the shape of the results are very similar, while the maximum forces range between 45 and almost 60 kN. Figure 3.30 depicts the outputs on the fusible links for the asymmetric configuration. As can be seen the level of forces reached is lower with respect to the symmetric configuration. This result is in line with the smaller differential displacements reached in the second case. Table 18 reports the maximum values reached in comparison with the capacities calculated for each detail component and the results obtained were under the maximum capacities.

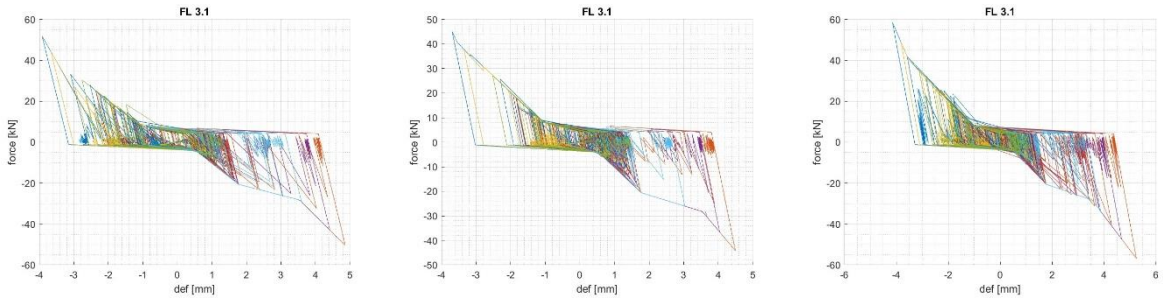

a) b) c)

Figure 3.30. Results on fusible links of the symmetric configuration equipped with Detail 3145 from analyses performed with a) Accelerogram 1, b) Accelerogram 2 and c) Accelerogram 3.

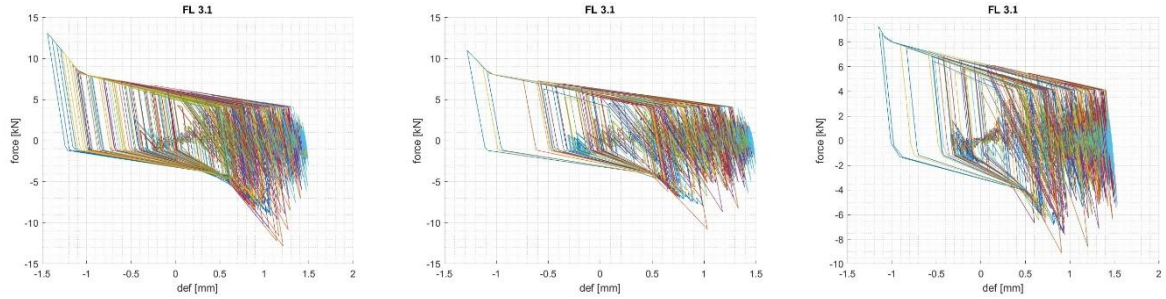

a) b) c)

Figure 3.31. Results on fusible links of the asymmetric configuration equipped with Detail 3145 from analyses performed with a) Accelerogram 1, b) Accelerogram 2 and c) Accelerogram 3.

Table 18. Forces obtained on fusible links in comparison with the detail capacity.

Symmetric configuration				
Component	Accelerogram 1	Accelerogram 2	Accelerogram 3	Capacity
Detail 3.1	50.00 kN	45.00 kN	58.00 kN	115.00 kN
Detail 4	2.50 kN	2.40 kN	3.00 kN	26.30 kN
Detail 5	3.00 kN	2.50 kN	3.50 kN	50.50 kN
Asymmetric configuration				
Component	Accelerogram 1	Accelerogram 2	Accelerogram 3	Capacity
Detail 3.1	13.00 kN	11.00 kN	8.00 kN	115.00 kN
Detail 4	1.00 kN	1.10 kN	1.20 kN	26.30 kN
Detail 5	1.50 kN	1.50 kN	1.60 kN	50.50 kN

With respect to Detail 3245, similar evaluations in terms of local outputs on the fusible links can be provided.

Figure 3.32 and Figure 3.33 depicts the outputs on the fusible links for each of the accelerograms run on the symmetric and asymmetric configurations. As can be noticed, the displacements reached in both cases are very small and so the magnitude of the forces in the fusible links. Table 19 reports the maximum force values in comparison with the capacities for each detail configuration. The capacities were not overcome that led to no failure of the fusible link.

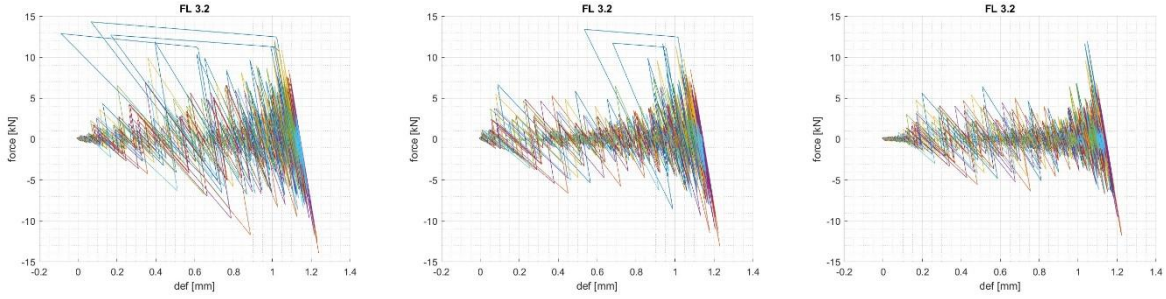

a) b) c)

Figure 3.32. Results on fusible links of the symmetric configuration with Detail 3145 from analyses performed with a) Accelerogram 1, b) Accelerogram 2 and c) Accelerogram 3.

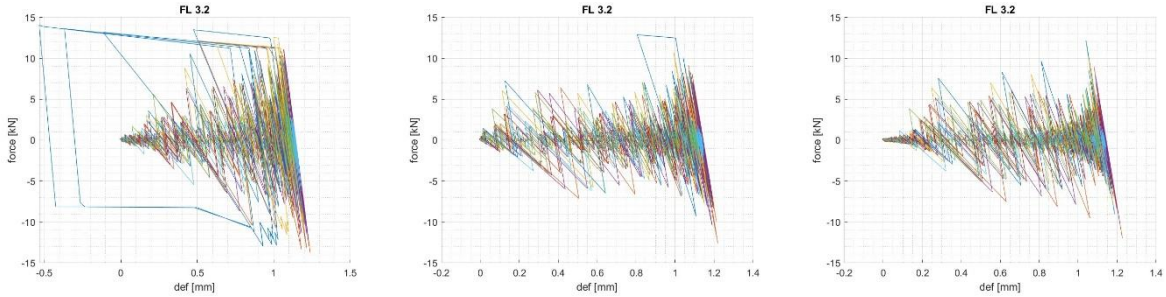

a) b) c)

Figure 3.33. Results on fusible links of the asymmetric configuration with Detail 3245 from analyses performed with a) Accelerogram 1, b) Accelerogram 2 and c) Accelerogram 3.

Table 19. Forces obtained on fusible links in comparison with the detail capacity.

Symmetric configuration				
Component	Accelerogram 1	Accelerogram 2	Accelerogram 3	Capacity
Detail 3.1	14.00 kN	13.50 kN	12.00 kN	115.00 kN
Detail 4	1.50 kN	1.60 kN	2.40 kN	26.30 kN
Detail 5	1.60 kN	1.80 kN	3.00 kN	50.50 kN
Asymmetric configuration				
Component	Accelerogram 1	Accelerogram 2	Accelerogram 3	Capacity
Detail 3.1	14.00 kN	13.50 kN	12.00 kN	115.00 kN
Detail 4	1.80 kN	1.60 kN	1.60 kN	26.30 kN
Detail 5	3.00 kN	1.80 kN	1.60 kN	50.50 kN

3.3.2 Case study 3: Pibrac

In this section, the results of the time-history analyses carried out on Case study 3 are presented.

In this section, the results of the time-history analyses on Case study 3 are presented. Considering the configurations presented in Section 3.1.2, Table 20 depicts all the numerical analyses that were performed on Case study 3, where are highlighted the details involved in the analyses, connected to the main columns of the steel structures. Figure 3.34 illustrates the different building configurations analysed.

Table 20. Case study 3 analyses

Wall position / building configuration	Low seismicity (Design PGA=0.04g)	Moderate seismicity (Design PGA=0.12g)		
Orthogonal/ Symmetric	Detail 1	Detail 2	Detail 3145	Detail 3245
Orthogonal /Asymmetric	Detail 1	Detail 2	Detail 3145	Detail 3245
Parallel /Symmetric	-	-	Detail 3145	Detail 3245
Parallel /Asymmetric	-	-	Detail 3145	Detail 3245

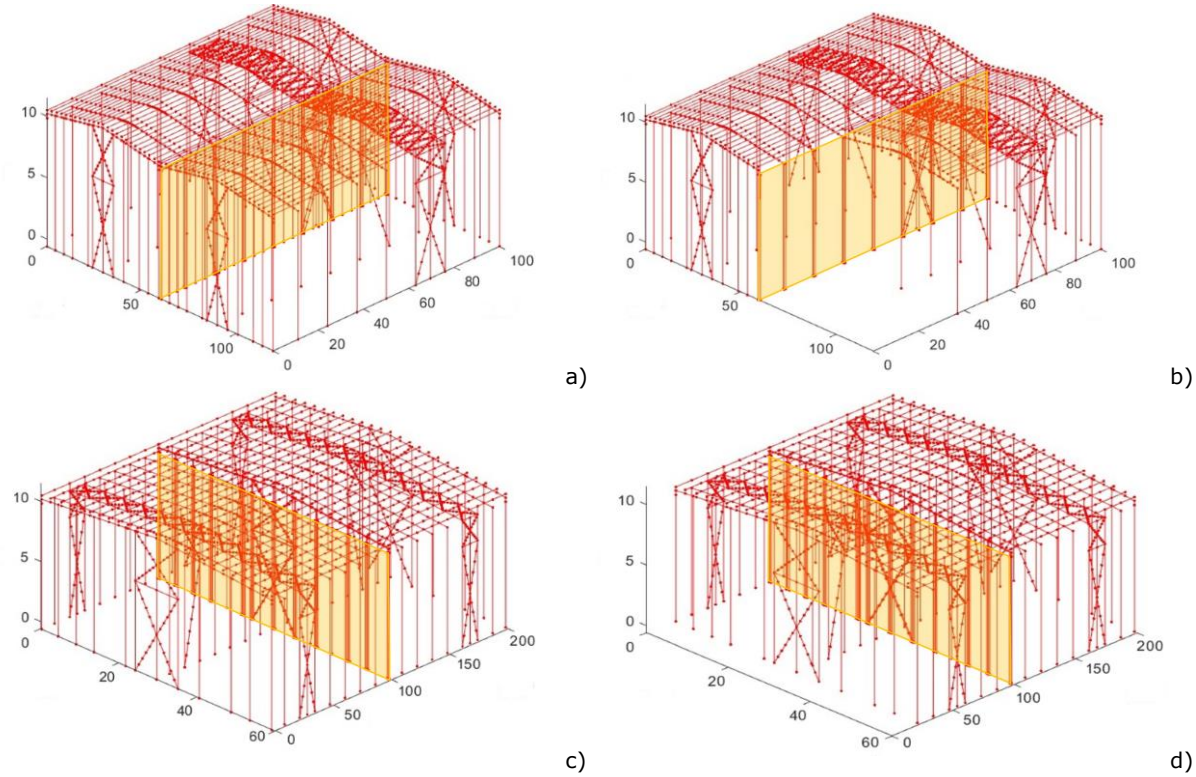

Figure 3.34. Case study n.3 structure configuration: a) Orthogonal – Symmetric; b) Orthogonal – Asymmetric; c) Parallel – Symmetric; d) Parallel – Asymmetric.

3.3.2.1 Low seismicity

In this section, the outcomes of the time-history analyses performed on Case study 3 subjected to low seismicity ground motions, modified by means of Arias Intensity function, are presented. In addition to the results on the fusible links details, some global outcomes are reported as well. As reported in Table 20, Detail 1 was tested only in orthogonal models, in both symmetric and asymmetric configuration. The results, both global and local are presented as a comparison between the two configurations.

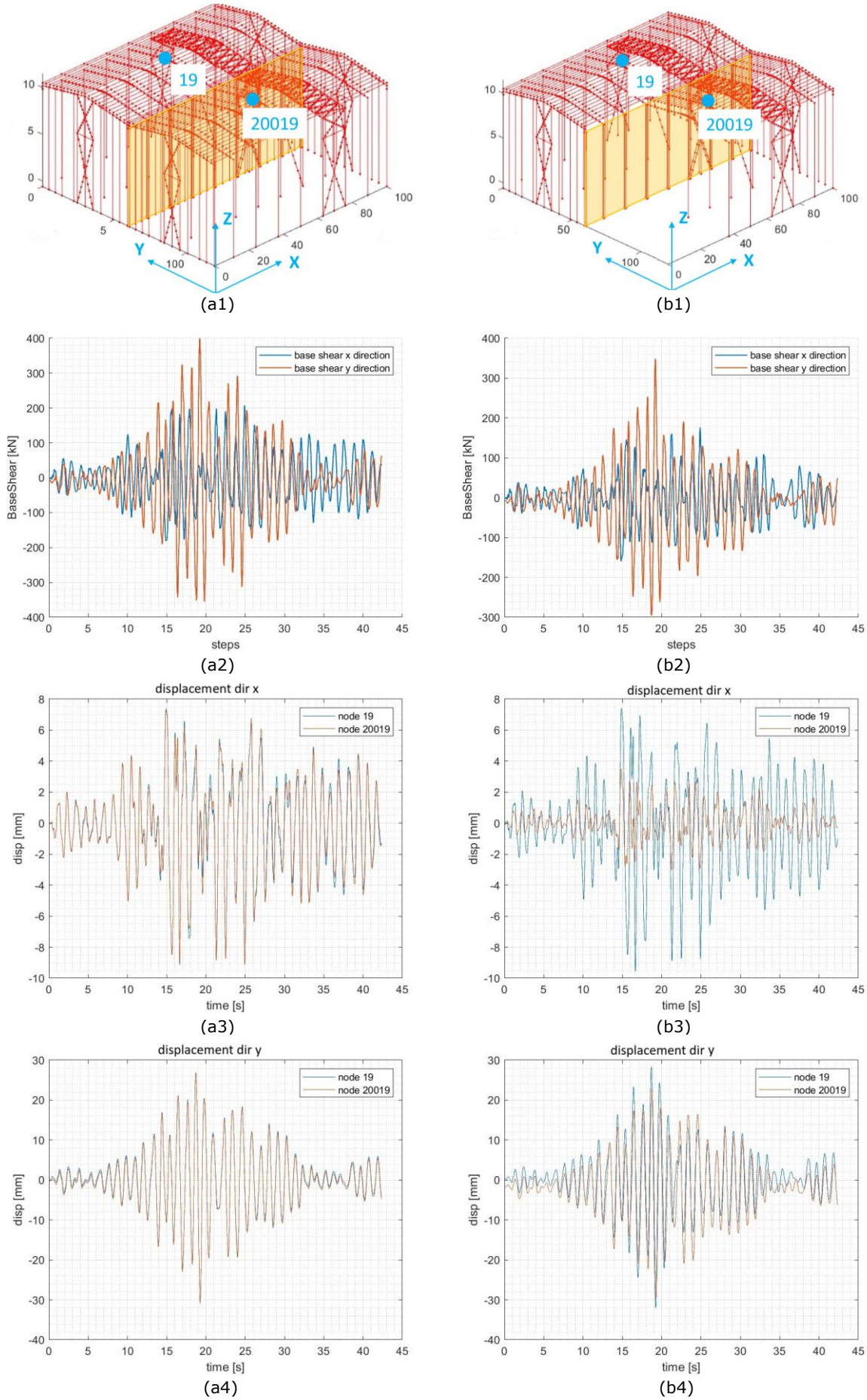

Figure 3.35. Case study 3 global outputs (a) symmetric model with firewall orthogonal to the portal frames and (b) asymmetric model with firewall orthogonal to the portal frames.

Figure 3.35 reports the global outputs of one of the time-history analyses performed on Case study 3 equipped with Detail 1. Considering the base shear, a slight decrease of values can be observed on the asymmetric configuration with respect to the symmetric one. Moreover, in terms of global displacement, the effect of the asymmetry is well denoted on global displacement in the direction orthogonal to the portal frames, see Figure 3.35b3. On the contrary, on the direction parallel to the portal frames, the global displacement symmetry between the structures is similar despite the asymmetry.

In terms of local outputs on the fusible links, hereafter the main results obtained on Detail 1 from the three accelerograms are reported. Figure 3.36 and Figure 3.37 illustrates the curves obtained for all the fusible links characterized by Detail 1 calibration. Additionally, as explained in Section 3.1.2, the columns added between the portal frames were equipped with Detail 3245, therefore, in Table 21, the results regarding all the components involved in the model can be read.

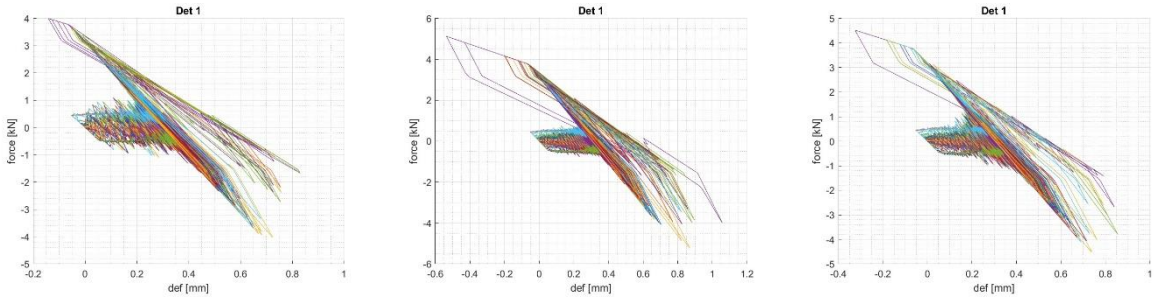

a) b) c)

Figure 3.36. Results on fusible links of the symmetric configuration equipped with Detail 1 from analyses performed with a) Accelerogram 1, b) Accelerogram 2 and c) Accelerogram 3.

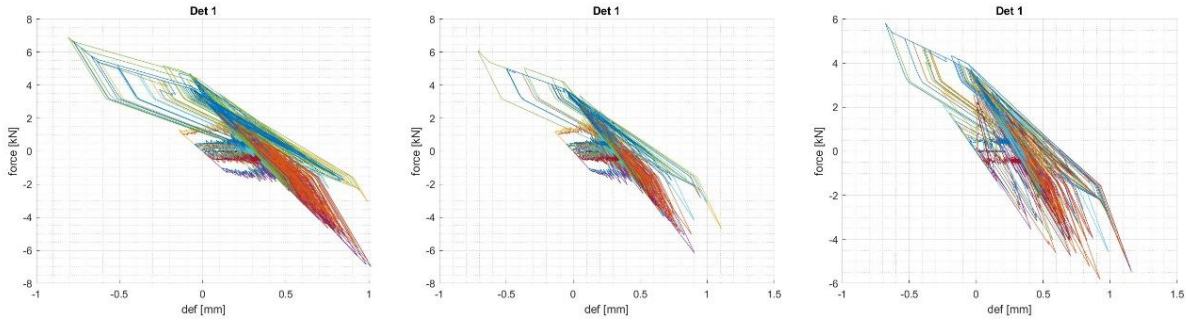

a) b) c)

Figure 3.37. Results on fusible links of the asymmetric configuration equipped with Detail 1 obtained from analyses performed with a) Accelerogram 1, b) Accelerogram 2 and c) Accelerogram 3.

Table 21. Forces obtained on fusible links in comparison with the detail capacity.

Symmetric configuration				
Component	Accelerogram 1	Accelerogram 2	Accelerogram 3	Capacity
Detail 1	4.00 kN	5.00 kN	4.50 kN	22.00 kN
Detail 3.2	9.00 kN	9.50 kN	10.00 kN	57.50 kN
Detail 4	0.70 kN	0.70 kN	0.50 kN	26.30 kN
Detail 5	0.80 kN	0.70 kN	0.60 kN	50.50 kN
Asymmetric configuration				
Component	Accelerogram 1	Accelerogram 2	Accelerogram 3	Capacity
Detail 1	7.00 kN	6.00 kN	6.00 kN	22.00 kN
Detail 3.2	9.25 kN	9.50 kN	10.50 kN	57.50 kN
Detail 4	0.65 kN	0.55 kN	0.50 kN	26.30 kN
Detail 5	0.75 kN	0.65 kN	0.50 kN	50.50 kN

From the results reported in the table above, a general low level of stress in the fusible links can be highlighted due to a little differential displacement. The comparison with the maximum capacity highlighted that no damage occurred in the details. The asymmetry determined an increase of forces in the fusible link represented by Detail 1, while the other details kept the same level of forces.

3.3.2.2 Moderate seismicity

Detail 2, Detail 3145 and Detail 3245 were designed and tested for seismicity level characterised by PGA = 0.12g. The moderate seismicity accelerograms presented in Section 3.2.2 and modified my means of the Arias Intensity function, were used in the time-history analyses. For the sake of completeness, in addition to the results on the fusible links details, some global outcomes are reported as well. As reported in Table 20, Detail 2 was tested only in orthogonal models, in both symmetric and asymmetric configuration, while Detail 3145 and Detail 3245 were tested with the firewall in both positions, orthogonal and parallel to the portal frames. The results, both global and local are presented as a comparison between the symmetric and asymmetric configurations.

3.3.2.2.1 Configuration with the firewall orthogonal to the portal frames

Figure 3.38 reports the global results in the orthogonal symmetric and asymmetric configurations equipped with one of three details covered in this section.

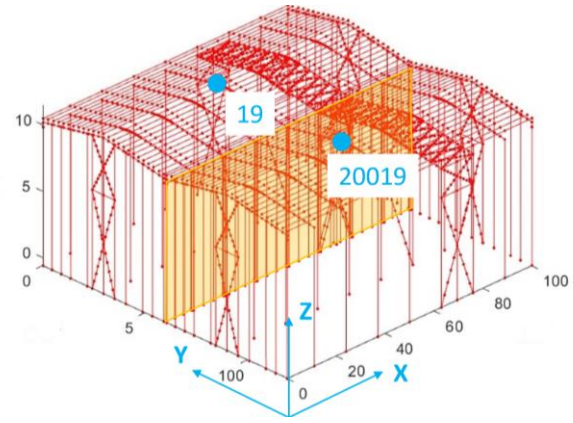

(a1)

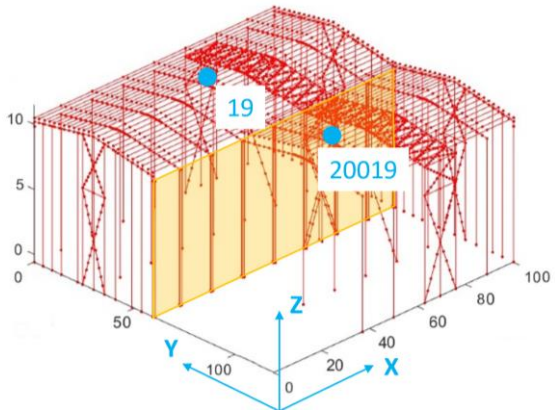

(b1)

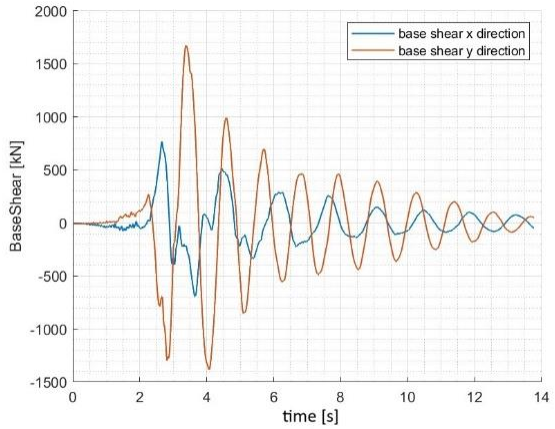

(a2)

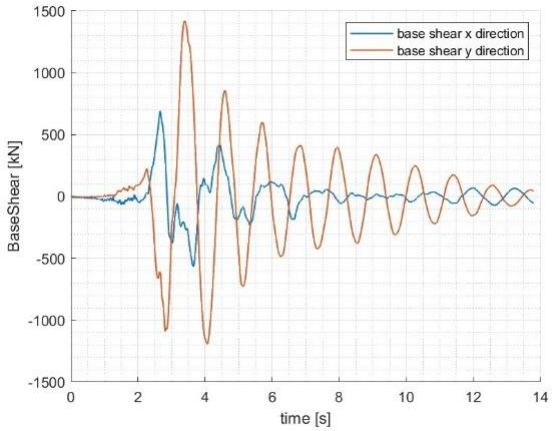

(b2)

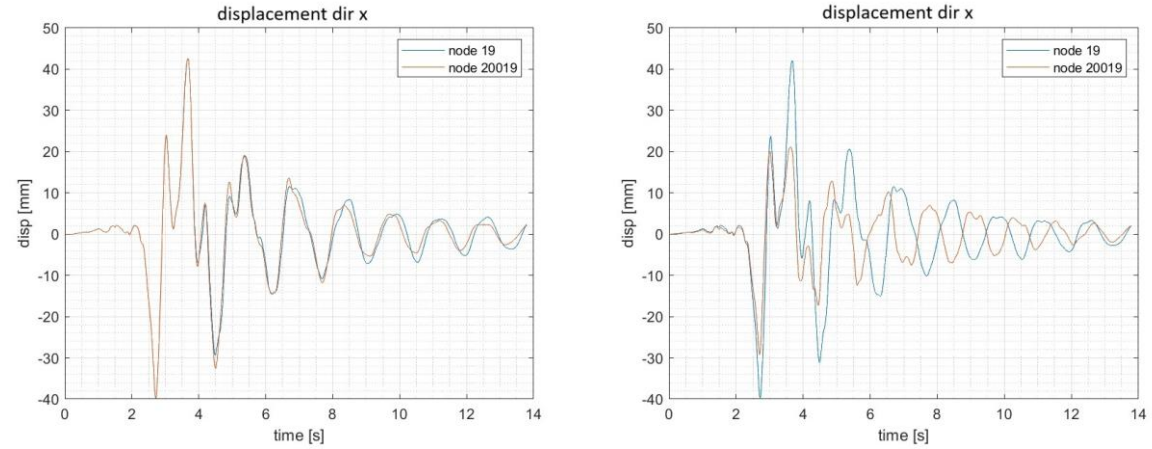

(a3)

(b3)

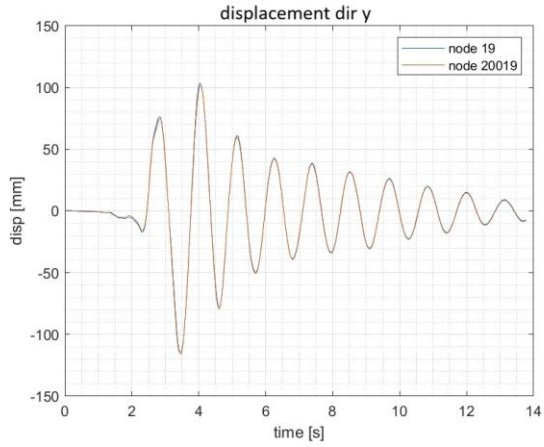

(a4)

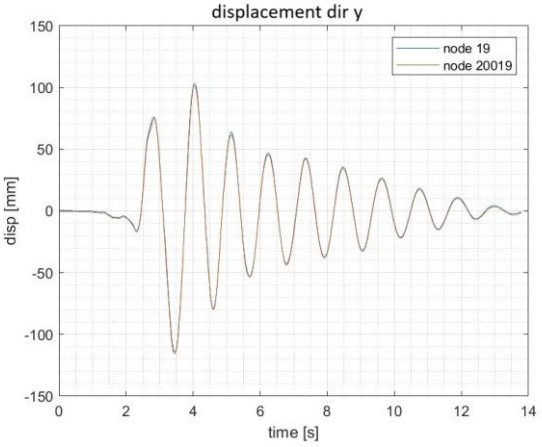

(b4)

Figure 3.38. Case study 3 global outputs (a) symmetric model with firewall orthogonal to the portal frames and (b) asymmetric model with firewall orthogonal to the portal frames.

In line with the results observed on the global models subjected to low seismicity accelerograms, despite the different levels of forces reached at the base shear, the comparison between the two configurations highlighted a slight decrease of forces in the second one. In terms of global displacements, the same trend recorded on the previous case was noticed: the asymmetry is evident on the direction orthogonal to the portal frames, while on the direction parallel to the portal frames the symmetry and the same level of displacement was observed for the two structures.

In terms of local outputs on the fusible links, hereafter the results obtained on Detail 2 from the three accelerograms are reported and in Table 22 the results regarding both Detail 2 and Detail 3145, that is located on the columns between the portal frames, can be read.

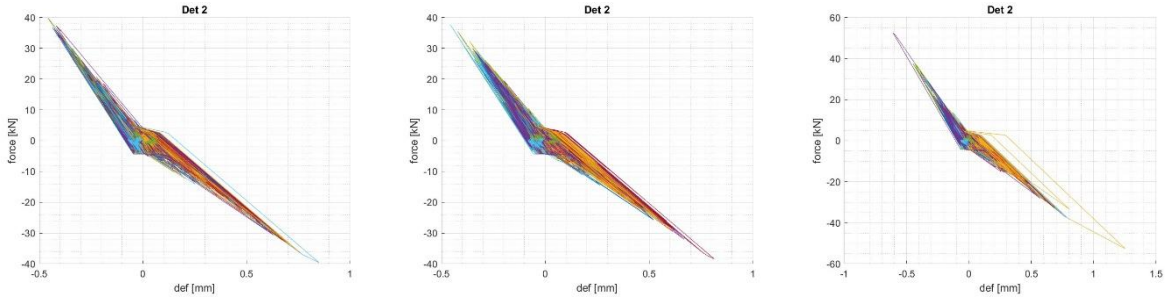

a) b) c)

Figure 3.39. Results on fusible links of the symmetric configuration equipped with Detail 2 from analyses performed with a) Accelerogram 1, b) Accelerogram 2 and c) Accelerogram 3.

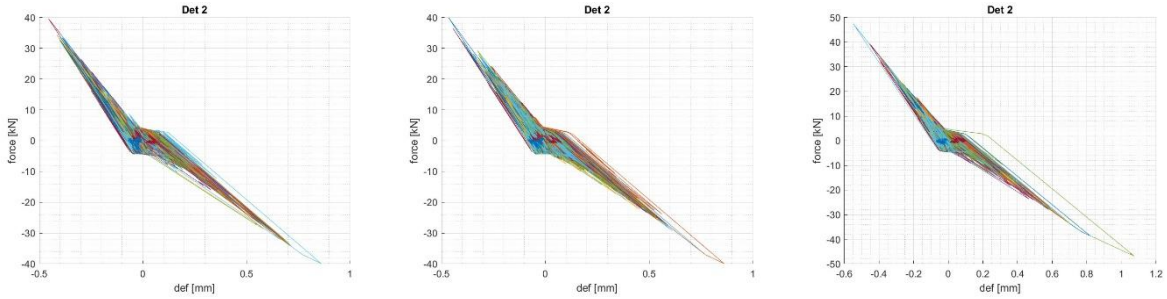

a) b) c)

Figure 3.40. Results on fusible links of the asymmetric configuration equipped with Detail 2 from analyses performed with a) Accelerogram 1, b) Accelerogram 2 and c) Accelerogram 3.

Table 22. Forces obtained on fusible links in comparison with the detail capacity.

Symmetric configuration				
Component	Accelerogram 1	Accelerogram 2	Accelerogram 3	Capacity
Detail 2	40.00 kN	38.00 kN	52.50 kN	110.00 kN
Detail 3.1	3.20 kN	4.20 kN	5.50 kN	115.00 kN
Detail 4	0.50 kN	1.40 kN	0.60 kN	26.30 kN
Detail 5	1.25 kN	1.80 kN	1.00 kN	50.50 kN
Asymmetric configuration				
Component	Accelerogram 1	Accelerogram 2	Accelerogram 3	Capacity
Detail 2	40.00 kN	40.00 kN	48.00 kN	110.00 kN
Detail 3.1	4.00 kN	5.25 kN	5.50 kN	115.00 kN
Detail 4	1.00 kN	1.40 kN	0.60 kN	26.30 kN
Detail 5	1.70 kN	1.80 kN	1.00 kN	50.50 kN

The maximum values obtained from the two series of analyses presented similar forces in the configurations studied, symmetric and asymmetric. This is due to similar dynamic properties of the two structural configurations. In fact, on the fusible links directly applied to the portal frame columns, Detail 2, a minimum difference was noted, while any difference was observed analysing the results on the additional columns equipped with Detail 3145.

Concerning the results obtained in this configuration, when equipped with Detail 3145, they are hereafter reported.

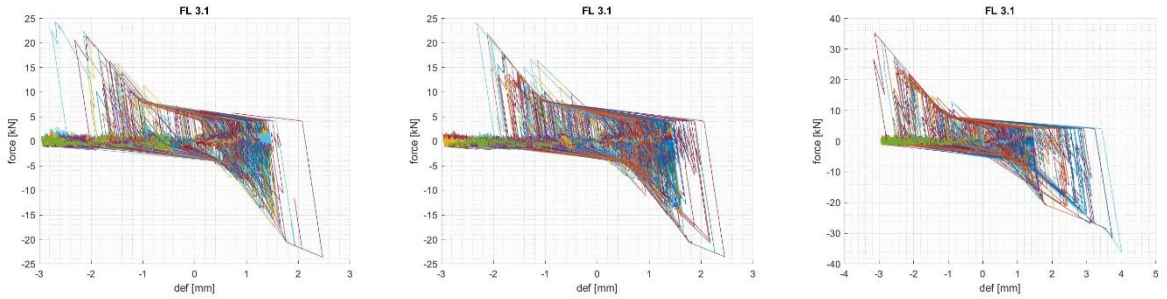

a) b) c)

Figure 3.41. Results on fusible links of the symmetric configuration equipped with Detail 3145 from analyses performed with a) Accelerogram 1, b) Accelerogram 2 and c) Accelerogram 3.

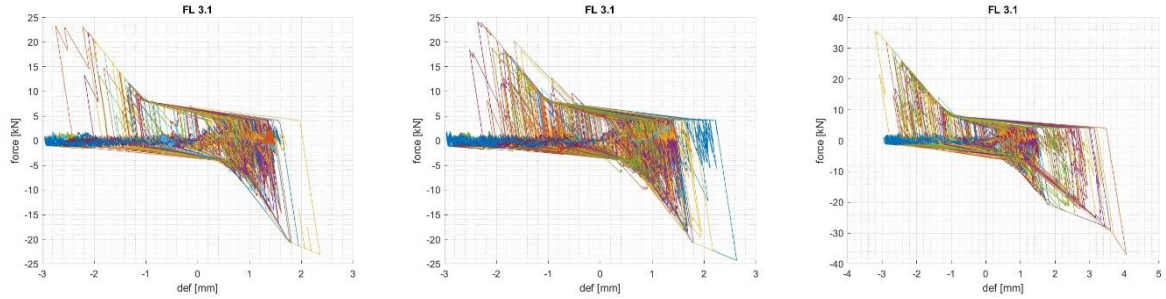

a) b) c)

Figure 3.42. Results on fusible links of the asymmetric configuration equipped with Detail 3145 from analyses performed with a) Accelerogram 1, b) Accelerogram 2 and c) Accelerogram 3.

Table 23. Forces obtained on fusible links in comparison with the detail capacity.

Symmetric configuration				
Component	Accelerogram 1	Accelerogram 2	Accelerogram 3	Capacity
Detail 3.1	24.00 kN	24.00 kN	36.00 kN	115.00 kN
Detail 4	3.54 kN	5.40 kN	4.84 kN	26.30 kN
Detail 5	4.28 kN	5.59 kN	3.91 kN	50.50 kN
Asymmetric configuration				
Component	Accelerogram 1	Accelerogram 2	Accelerogram 3	Capacity
Detail 3.1	23.00 kN	24.00 kN	37.00 kN	115.00 kN
Detail 4	5.00 kN	6.50 kN	5.00 kN	26.30 kN
Detail 5	4.80 kN	6.00 kN	4.50 kN	50.50 kN

From the results reported in the table above, a general low level of stress in the fusible links can be highlighted. The similarity of periods between the symmetric and asymmetric configuration of the structures did not introduced differences of results, as expected. From Figure 3.41 and Figure 3.42, two series of results can be observed: i) the cycles with a well-defined pinching shape were obtained from the fusible links connected to the portal frames columns, while ii) the results with similar displacements but less forces are representative of the fusible links on the additional columns located between the portal frames. In both configurations the maximum values are under the details' capacities derived from the experimental tests.

With regard to the configurations equipped with Detail 3245, in terms of local outputs on the fusible links, hereafter the main results obtained on Detail 3.2 from the three accelerograms in Figure 3.43 and in Figure 3.44 are reported, while in Table 24 the results regarding all the components involved in the model and explained in Section 3.1.2, can be read.

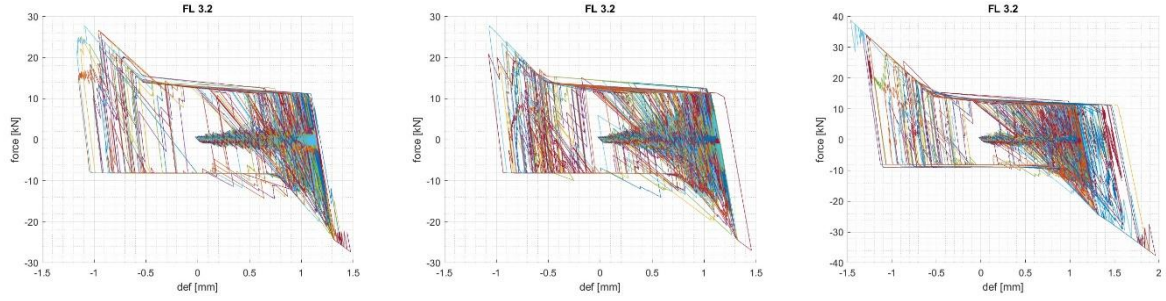

a) b) c)

Figure 3.43. Results on fusible links of CS3_SO equipped with Detail 3245 from analyses performed with a) Accelerogram 1, b) Accelerogram 2 and c) Accelerogram 3.

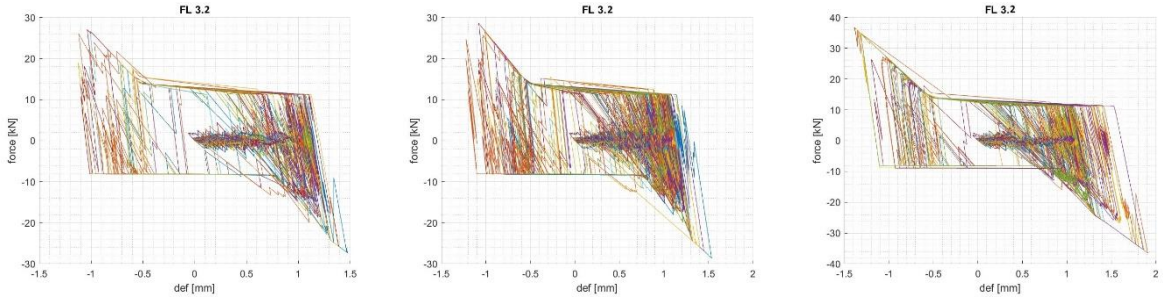

a) b) c)

Figure 3.44. Results on fusible links of CS3_AO equipped with Detail 3245 from analyses performed with a) Accelerogram 1, b) Accelerogram 2 and c) Accelerogram 3.

Table 24. Forces obtained on fusible links in comparison with the detail capacity.

Symmetric configuration				
Component	Accelerogram 1	Accelerogram 2	Accelerogram 3	Capacity
Detail 3.2	28.00 kN	27.00 kN	39.00 kN	115.00 kN
Detail 4	4.00 kN	5.60 kN	5.40 kN	26.30 kN
Detail 5	4.80 kN	5.60 kN	6.40 kN	50.50 kN
Asymmetric configuration				
Component	Accelerogram 1	Accelerogram 2	Accelerogram 3	Capacity
Detail 3.2	27.00 kN	29.00 kN	37.00 kN	115.00 kN
Detail 4	13.00 kN	14.00 kN	9.00 kN	26.30 kN
Detail 5	13.08 kN	14.00 kN	9.00 kN	50.50 kN

Considering the similarities between Detail 3145 and Detail 3245, similar findings were obtained. Indeed, the same level of forces was recorded on the details in the two configurations analysed. Figure 3.43 and Figure 3.44 presents, again, two series of results, one with well-defined pinching shape cycles obtained from the fusible links connected to the portal frames columns, and results with significantly lower forces representatives of the fusible links on the additional columns located between the portal frames. None of the component overcome the maximum capacity measured during the experimental tests.

3.3.2.2.2 Configuration with the firewall parallel to the portal frames

As reported in Table 20, the last two details presented were involved also in the models with the wall parallel to the portal frames. Figure 3.45 reports the global outputs obtained in both configurations, symmetric and asymmetric in comparison.

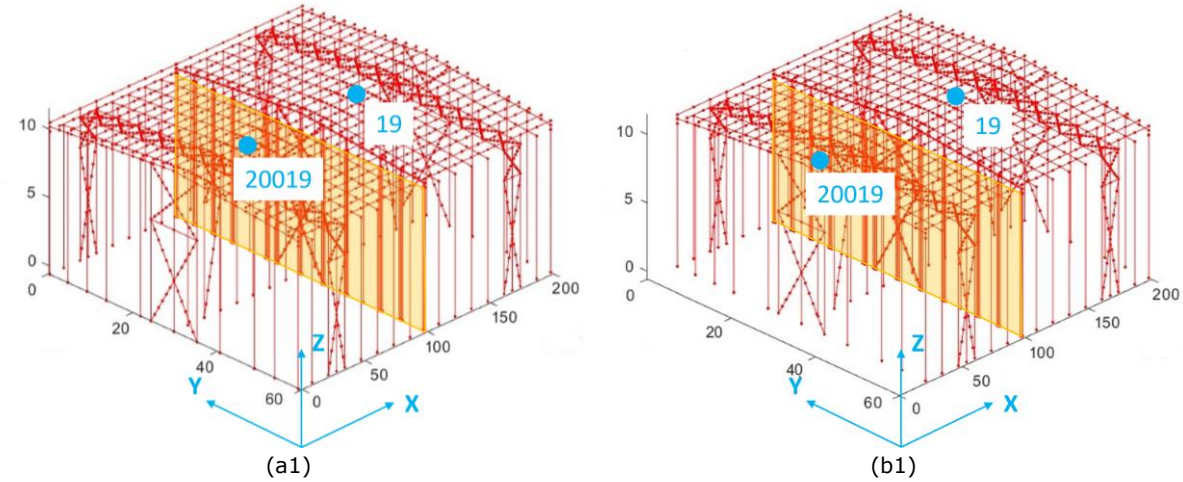

(a1) (b1)

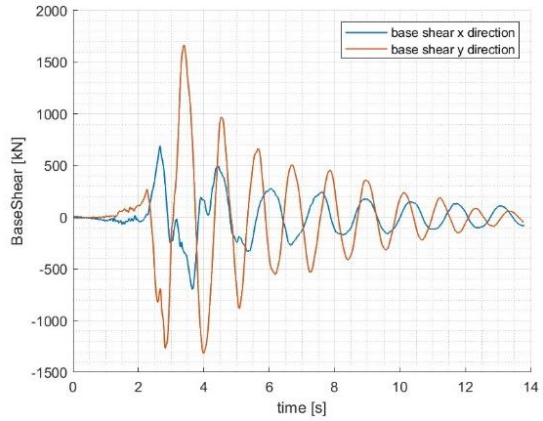

(a2)

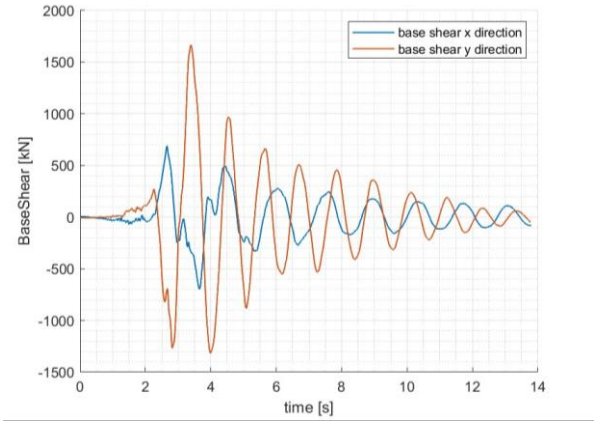

(b2)

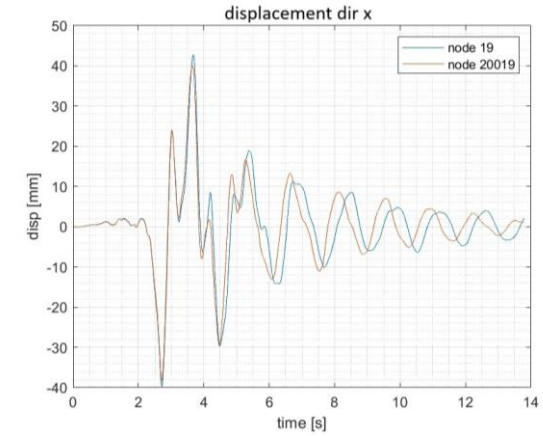

(a3)

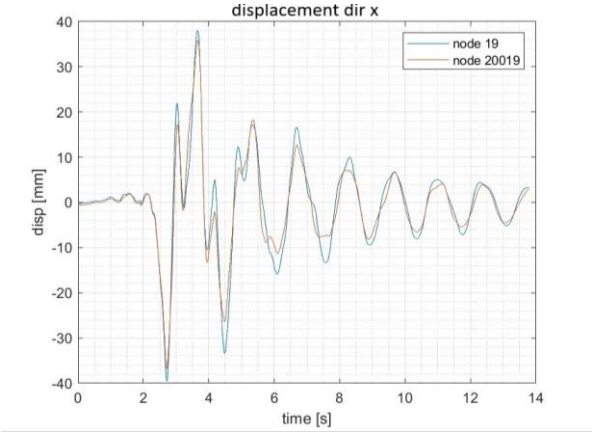

(b3)

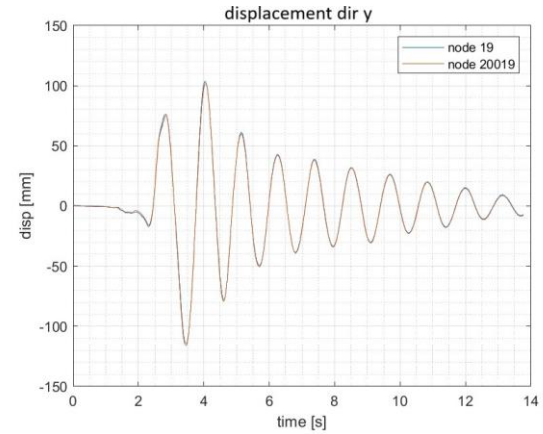

(a4)

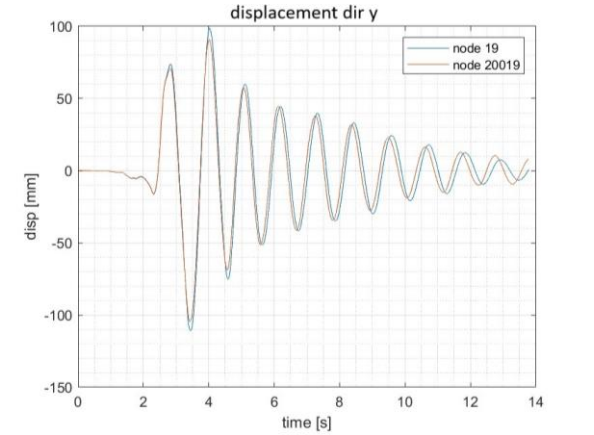

(b4)

Figure 3.45. Case study 3 global outputs (a) symmetric model with firewall parallel to the portal frames and (b) asymmetric model with firewall parallel to the portal frames.

The outputs reported in Figure 3.45 are consistent with the global outputs observed for the orthogonal firewall location: between the two configurations, as expected, an increase of forces can be read in terms of base shear on the direction orthogonal to the portal frames, where the mass was reduced but the resisting system given by the facades was kept unchanged. With respect to the global displacement, a general symmetric behaviour can be observed between the two configurations.

In terms of local outputs on the fusible links, hereafter the main results obtained on Detail 3.1 from the three accelerograms are reported and in Table 25 the results regarding all the components involved in the model and explained in 3.1.3.1, can be read.

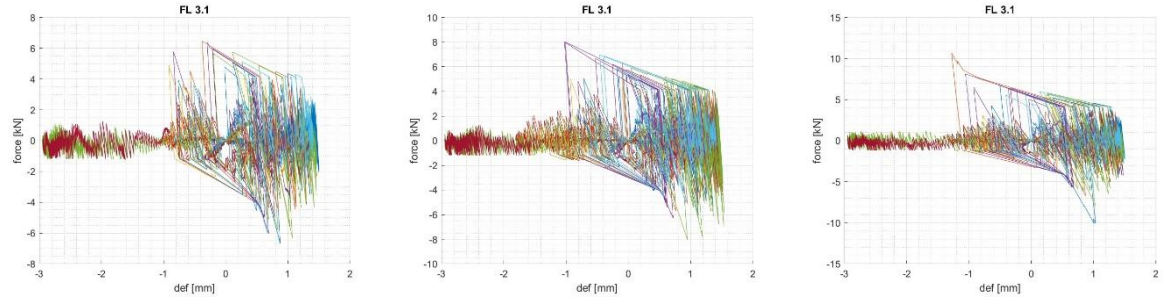

a) b) c)

Figure 3.46. Results on fusible links of the symmetric configuration equipped with Detail 3145 from analyses performed with a) Accelerogram 1, b) Accelerogram 2 and c) Accelerogram 3.

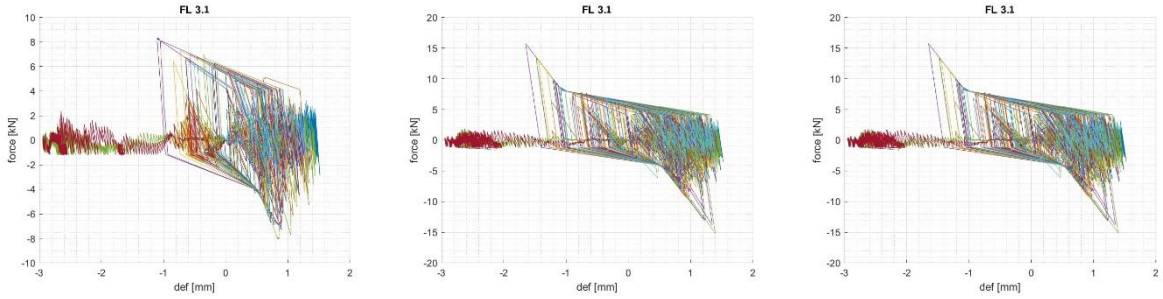

a) b) c)

Figure 3.47. Results on fusible links of asymmetric configuration equipped with Detail 3145 from analyses performed with a) Accelerogram 1, b) Accelerogram 2 and c) Accelerogram 3.

Table 25. Forces obtained on fusible links in comparison with the detail capacity.

Symmetric configuration				
Component	Accelerogram 1	Accelerogram 2	Accelerogram 3	Capacity
Detail 3.1	6.50 kN	8.00 kN	11.00 kN	115.00 kN
Detail 4	2.30 kN	2.40 kN	1.80 kN	26.30 kN
Detail 5	2.30 kN	2.50 kN	1.90 kN	50.50 kN
Asymmetric configuration				
Component	Accelerogram 1	Accelerogram 2	Accelerogram 3	Capacity
Detail 3.1	8.00 kN	16.00 kN	16.00 kN	115.00 kN
Detail 4	2.30 kN	2.00 kN	2.00 kN	26.30 kN
Detail 5	2.00 kN	2.00 kN	2.30 kN	50.50 kN

With regards to the values obtained in the fusible links in the above table, all the forces are under the details' capacities. Moreover, despite the moderate seismicity accelerograms given as input to the time-history analyses, the forces recorded in the fusible links are very low. This is due to the high number of columns present on the building façades, see Figure 3.45(a and b), and small differential displacement between the fusible link system and the steel structures. In fact, a higher number of fusible links was linked to main structure, with respect to the orthogonal configuration, and the global load was distributed on more elements. Only two couple of columns spanned more than 5m and, thus, only two additional columns were added. The stress on the fusible links located on them is, once again, represented by the curves with the lowest forces and higher displacement in Figure 3.46 and in Figure 3.47. Differently from the orthogonal configuration, an increase of forces was observed between the symmetric and asymmetric models.

With respect to Detail 3245, similar evaluations in terms of local outputs on the fusible links can be provided. The main results obtained on Detail 3.2 from the three accelerograms are reported in Figure 3.48 and in Figure 3.49 and in Table 26 the results regarding all the component involved in the model and explained in 3.1.3.2, can be read.

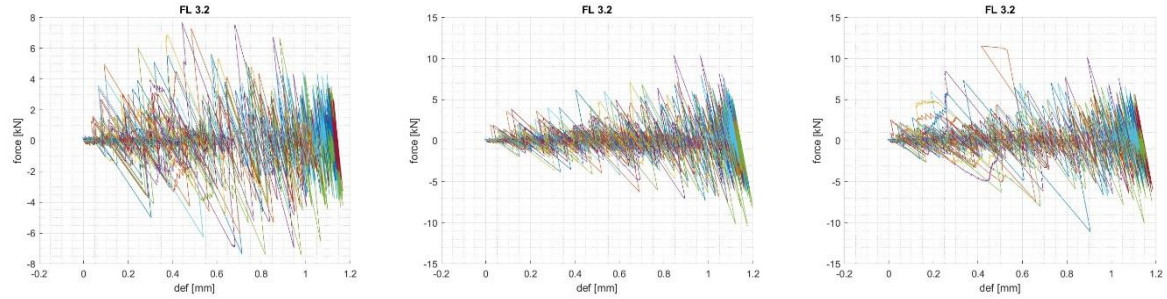

a) b) c)

Figure 3.48. Results on fusible links of the symmetric configuration equipped with Detail 3245 from analyses performed with a) Accelerogram 1, b) Accelerogram 2 and c) Accelerogram 3.

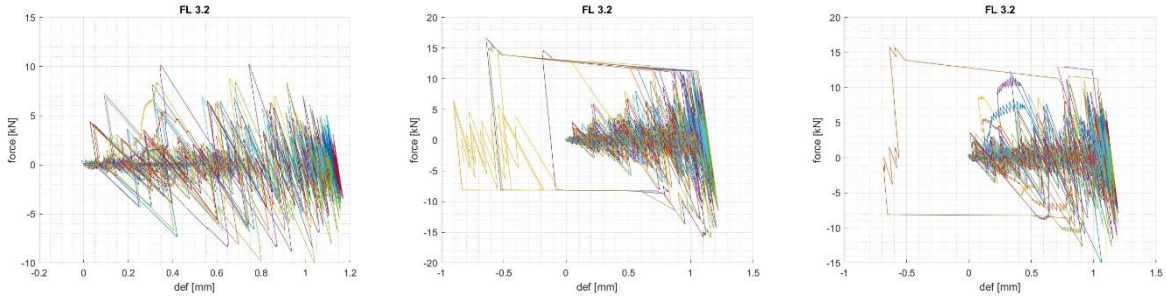

a) b) c)

Figure 3.49. Results on fusible links of the asymmetric configuration equipped with Detail 3245 from analyses performed with a) Accelerogram 1, b) Accelerogram 2 and c) Accelerogram 3.

Table 26. Forces obtained on fusible links in comparison with the detail capacity.

Symmetric configuration				
Component	Accelerogram 1	Accelerogram 2	Accelerogram 3	Capacity
Detail 3.1	7.50 kN	10.00 kN	11.00 kN	115.00 kN
Detail 4	4.80 kN	5.00 kN	4.00 kN	26.30 kN
Detail 5	5.00 kN	5.00 kN	4.00 kN	50.50 kN
Asymmetric configuration				
Component	Accelerogram 1	Accelerogram 2	Accelerogram 3	Capacity
Detail 3.1	10.00 kN	16.00 kN	16.00 kN	115.00 kN
Detail 4	4.80 kN	4.20 kN	3.60 kN	26.30 kN
Detail 5	4.00 kN	4.00 kN	4.60 kN	50.50 kN

The maximum values obtained in both configurations did not overcome the details' capacities. In addition, the values obtained are very low, in agreement with the results obtained with Detail 3145 models. An increase of forces in the fusible links can observed from the symmetric to the asymmetric configuration.

3.3.3 Case study 4: Bressuire

In this section, the results of the time-history analyses carried out on Case study 4 are presented. Considering the configurations presented in Section 3.1.2, Table 27 depicts all the numerical analyses that were performed on case study 4, while Figure 3.50 illustrates the different building configurations.

Table 27. Case study 4 analyses

Wall position / building configuration	Low seismicity (Design PGA=0.04g	Moderate seismicity (Design PGA=0.12g)		
Orthogonal/ Symmetric	Detail 1	Detail 2	Detail 3145	Detail 3245
Orthogonal /Asymmetric	Detail 1	Detail 2	Detail 3145	Detail 3245
Parallel /Symmetric	-	-	Detail 3145	Detail 3245
Parallel /Asymmetric	-	-	Detail 3145	Detail 3245

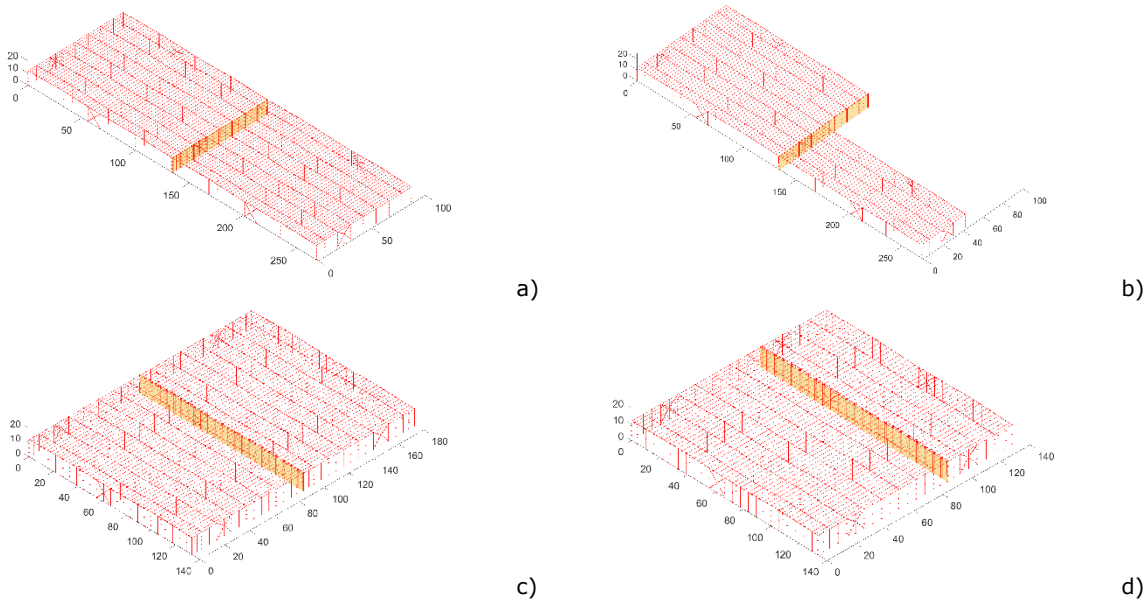

a) b) c) d)

Figure 3.50. Case study 4 structure configurations: a) Orthogonal – Symmetric; b) Orthogonal – Asymmetric; c) Parallel – Symmetric; d) Parallel – Asymmetric. Dimensions in m

3.3.3.1 Low seismicity

In this section, the outcomes of the time-history analyses performed on Case study 4 subjected to low seismicity ground motions, previously modified by means of the Arias Intensity function, are presented. For completeness, in addition to the results on the fusible links details, some global outcomes are reported as well. As reported in Table 27, Detail 1 was tested only in orthogonal models, in both symmetric and asymmetric configuration. The results, both global and local are presented as a comparison between the configurations.

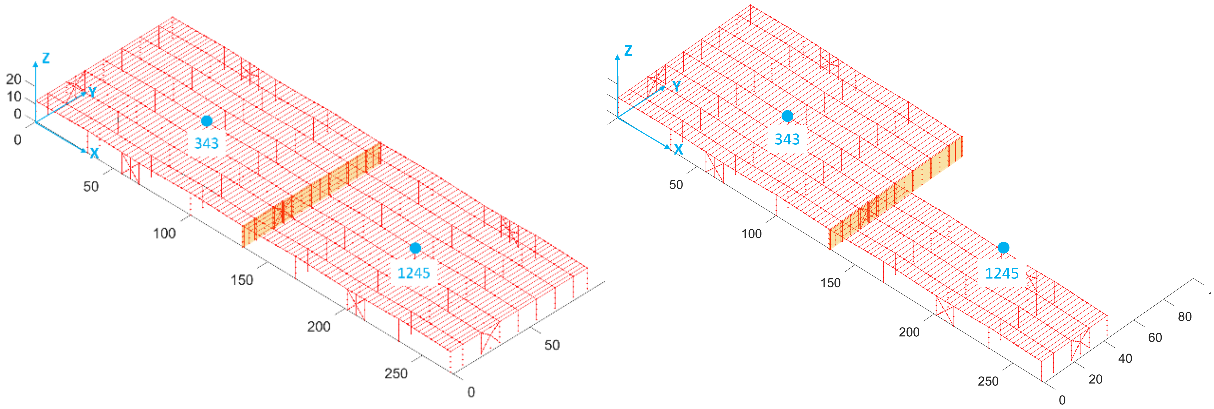

(a1) (b1)

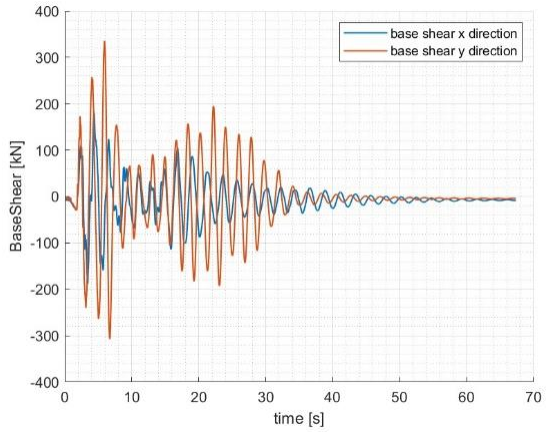

(a2)

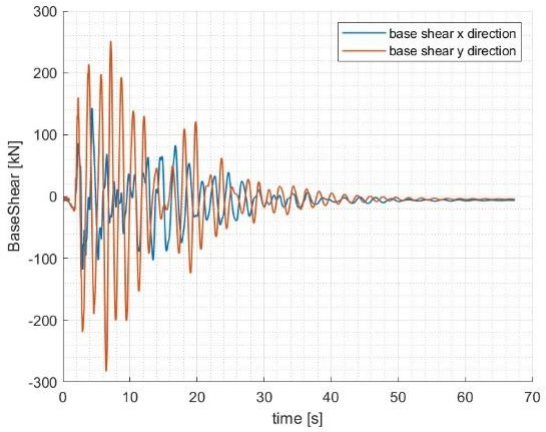

(b2)

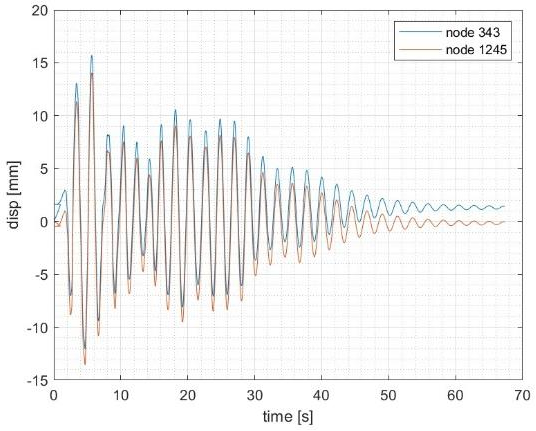

(a3)

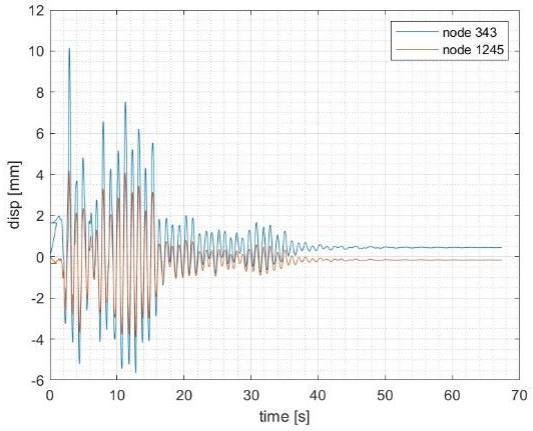

(b3)

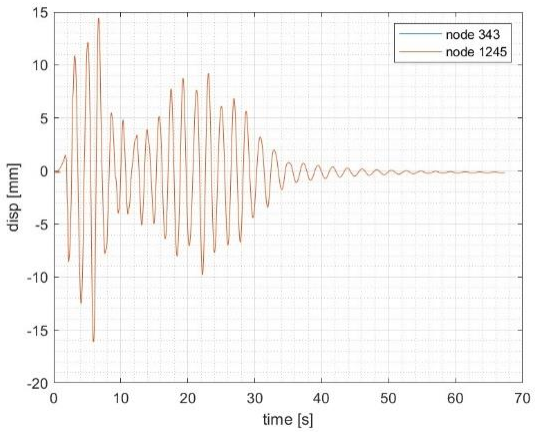

(a4)

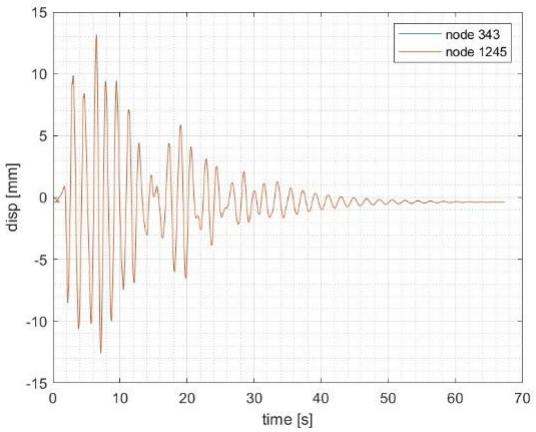

(b4)

Figure 3.51. Case study 4 global outputs (a) symmetric model with firewall orthogonal to the portal frames and (b) asymmetric model with firewall orthogonal to the portal frames.

The global outputs in terms of base shear and displacement on Case study 4 are illustrated in Figure 3.51. The base shear curves highlighted in both configuration a stiffer behaviour of the bracing system with respect to the portal frame system, emphasized by the constraints applied to represent the roof bracing system. In terms of global displacement, despite the asymmetry introduced, on the direction orthogonal to the portal frames, the two structures behaved symmetrically, whilst on the other one, a more asymmetric behaviour can be observed.

In terms of local outputs, the maximum forces recorded in the fusible links characterized by the Detail 1 numerical model are shown in Figure 3.52 and in Figure 3.53, while Table 28 reports the forces also in Detail 3145 that were used on the additional columns between the portal frames.

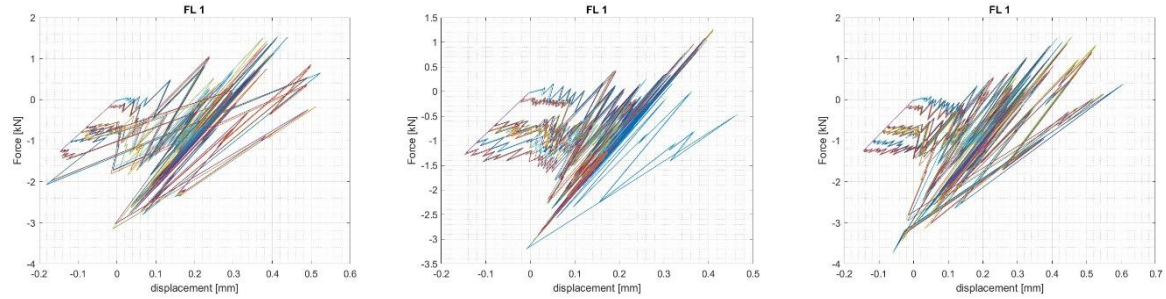

a) b) c)

Figure 3.52. Results on fusible links of the symmetric configuration equipped with Detail 1 from analyses performed with a) Accelerogram 1, b) Accelerogram 2 and c) Accelerogram 3.

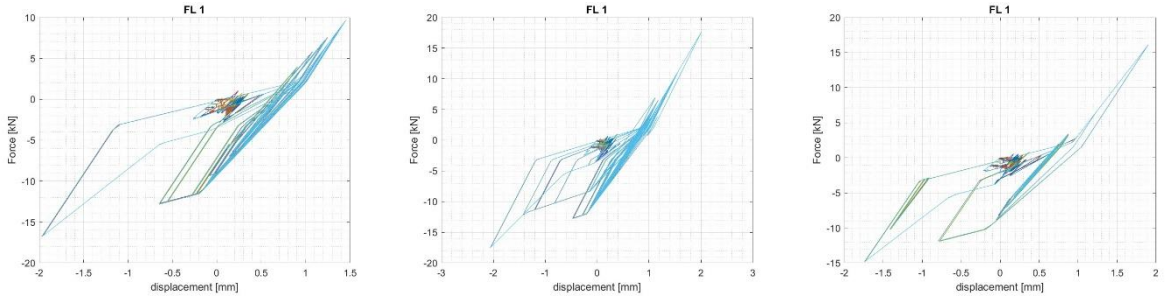

a) b) c)

Figure 3.53. Results on fusible links of the asymmetric configuration equipped with Detail 1 obtained from analyses performed with a) Accelerogram 1, b) Accelerogram 2 and c) Accelerogram 3.

Table 28. Forces obtained on fusible links in comparison with the detail capacity.

Symmetric configuration				
Component	Accelerogram 1	Accelerogram 2	Accelerogram 3	Capacity
Detail 1	3.20 kN	3.20 kN	3.70 kN	22.00 kN
Detail 3.2	0.50 kN	0.36 kN	0.53 kN	57.50 kN
Detail 4	0.17 kN	0.20 kN	0.17 kN	26.30 kN
Detail 5	0.17 kN	0.20 kN	0.17 kN	50.50 kN
Asymmetric configuration				
Component	Accelerogram 1	Accelerogram 2	Accelerogram 3	Capacity
Detail 1	17.00 kN	17.00 kN	16.00 kN	22.00 kN
Detail 3.2	0.50 kN	0.36 kN	0.53 kN	57.50 kN
Detail 4	0.17 kN	0.20 kN	0.17 kN	26.30 kN
Detail 5	0.17 kN	0.20 kN	0.17 kN	50.50 kN

The results obtained showed that under low seismicity accelerograms, the details involved did not overcome their maximum capacity. However, introducing the asymmetry, an increase of forces in the fusible links directly connected to the main structure, i.e. Detail 1, was observed because of a reduction of columns and thus of elements, while the other component was hardly at all stressed.

3.3.3.2 Moderate seismicity

Detail 2, Detail 3145 and Detail 3245 were designed and tested for a seismicity level characterised by PGA = 0.12g. The moderate seismicity accelerograms presented in section 3.2.3, and modified by means of the Arias Intensity function, were used in the time-history analyses. For the sake of completeness, in addition to the results on the fusible links details, some global outcomes are reported as well. As reported in Table 27, Detail 2 was tested only in orthogonal models, in both symmetric and asymmetric configuration, while Detail 3145 and Detail 3245 were tested with the firewall in both positions, orthogonal and parallel to the portal frames. Eventually, despite that two different set of accelerograms were selected for the symmetric and asymmetric configuration, the results, both global and local are yet presented as a comparison of configurations.

3.3.3.2.1 Configuration with the firewall orthogonal to the portal frames

Figure 3.54 reports the global results in the orthogonal symmetric and asymmetric configurations equipped with one of three details covered in this section.

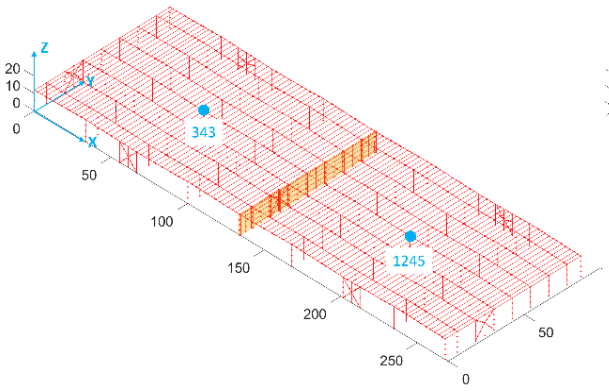

(a1)

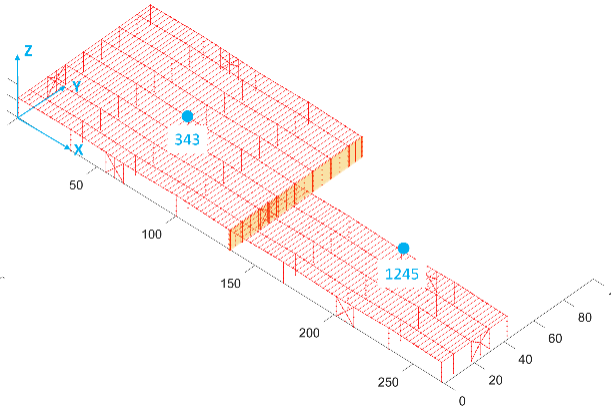

(b1)

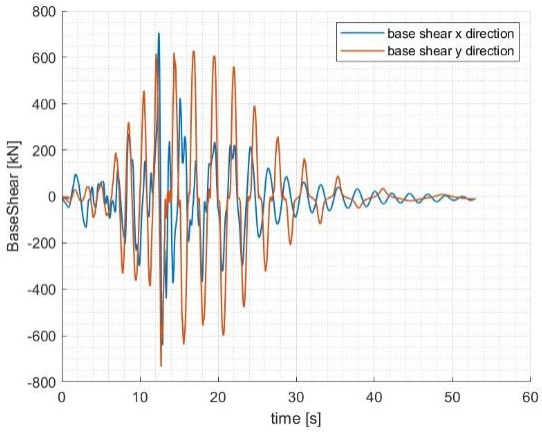

(a2)

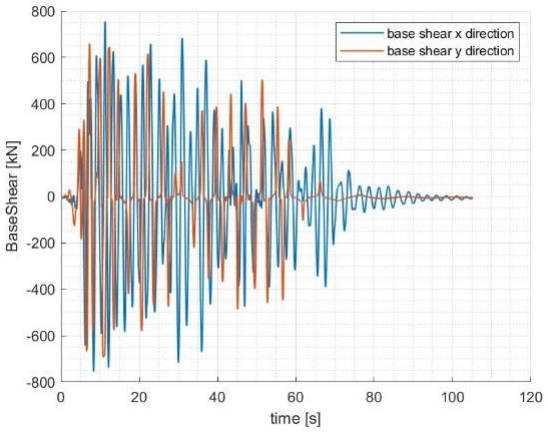

(b2)

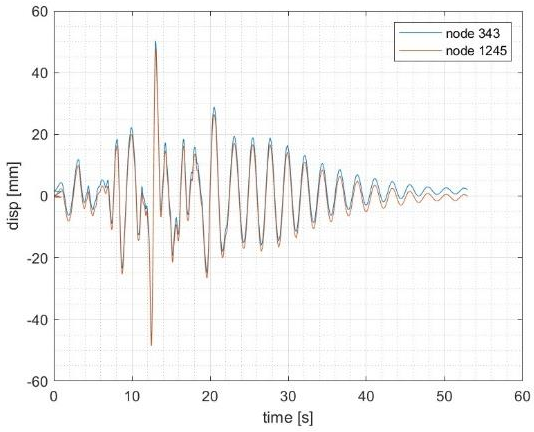

(a3)

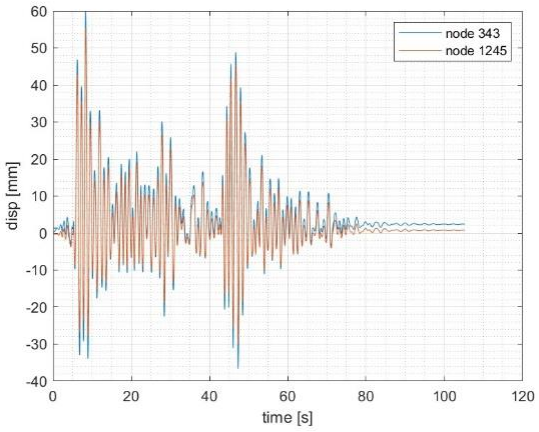

(b3)

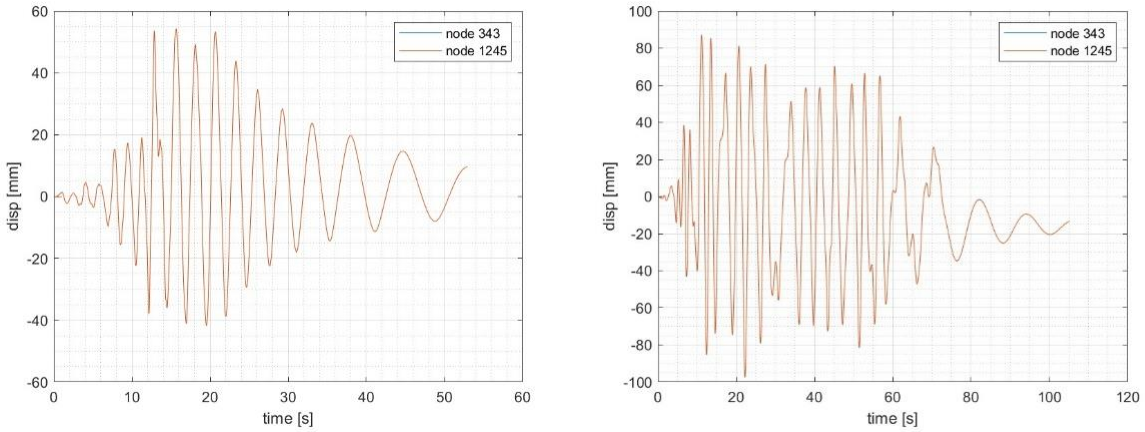

(a4) (b4)

Figure 3.54. Case study 4 global outputs (a) symmetric model with firewall orthogonal to the portal frames and (b) asymmetric model with firewall orthogonal to the portal frames

The global outputs of the two structures are reported in Figure 3.54. In terms of base shear, a consistent level of forces was obtained within the two configurations and the two different accelerograms. It is interesting to observe that, with respect to the global displacement, the asymmetry introduces induced only a slight difference in the direction parallel to the portal frames.

In terms of local outputs, the results obtained on Detail 2 are depicted in Figure 3.55 and in Figure 3.56, while in Table 29 the results concerning also Detail 3145 that are involved in the columns between the portal frames are reported.

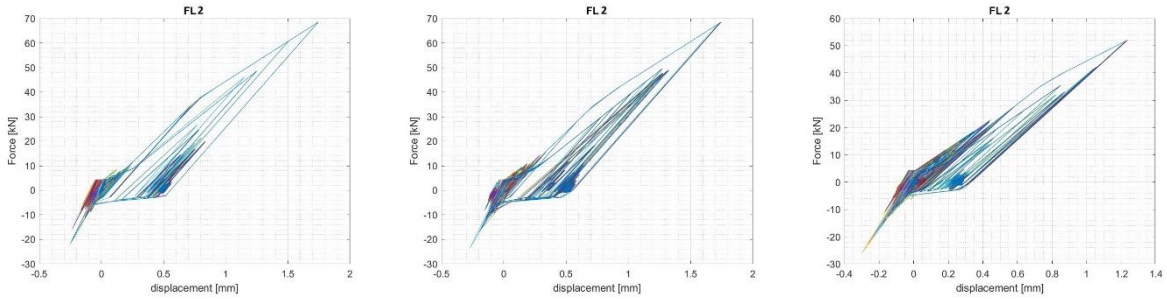

a) b) c)

Figure 3.55. Results on fusible links of the symmetric configuration equipped with Detail 2 from analyses performed with a) Accelerogram 1, b) Accelerogram 2 and c) Accelerogram 3.

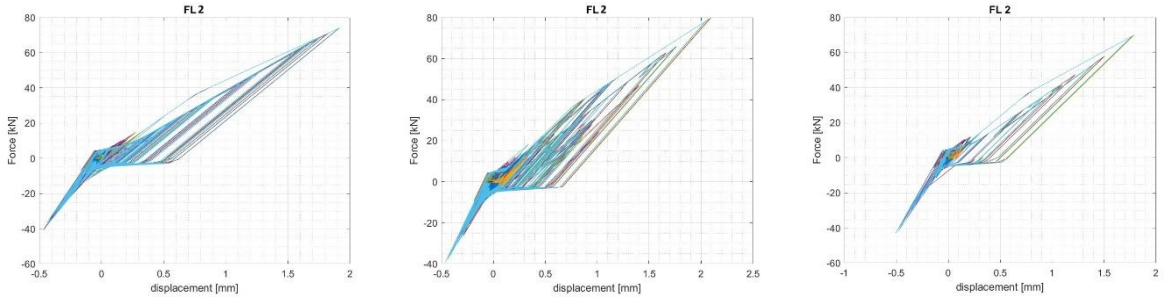

a) b) c)

Figure 3.56. Results on fusible links of the asymmetric configuration equipped with Detail 2 from analyses performed with a) Accelerogram 1, b) Accelerogram 2 and c) Accelerogram 3.

Table 29. Forces obtained on fusible links in comparison with the detail capacity.

Symmetric configuration				
Component	Accelerogram 1	Accelerogram 2	Accelerogram 3	Capacity
Detail 2	68.00 kN	68.00 kN	52.00 kN	110.00 kN
Detail 3.1	1.70 kN	1.40 kN	1.30 kN	115.00 kN
Detail 4	0.10 kN	0.50 kN	1.07 kN	26.30 kN
Detail 5	0.40 kN	0.85 kN	0.17 kN	50.50 kN
Asymmetric configuration				
Component	Accelerogram 1	Accelerogram 2	Accelerogram 3	Capacity
Detail 2	75.00 kN	80.00 kN	70.00 kN	110.00 kN
Detail 3.1	1.25 kN	1.50 kN	0.50 kN	115.00 kN
Detail 4	0.60 kN	1.20 kN	0.05 kN	26.30 kN
Detail 5	0.90 kN	1.20 kN	0.18 kN	50.50 kN

The results abovementioned highlighted an increase of forces in the fusible links from the symmetric to the asymmetric configuration. This is mainly because in the asymmetric model provided for the reduction of the building's columns and consequently the number of the fusible links, therefore, the global stress is shared between less elements. Once again, the action on the fusible links located on the additional columns between the portal frames resulted very low. Finally, none of the detail failed during the analyses conducted.

With respect to the results obtained on the configuration with Detail 3145, the curves obtained for Detail 3.1 are illustrated in Figure 3.57 and in Figure 3.58, while the forces recorded in the component of the whole fusible link system can be read in Table 30.

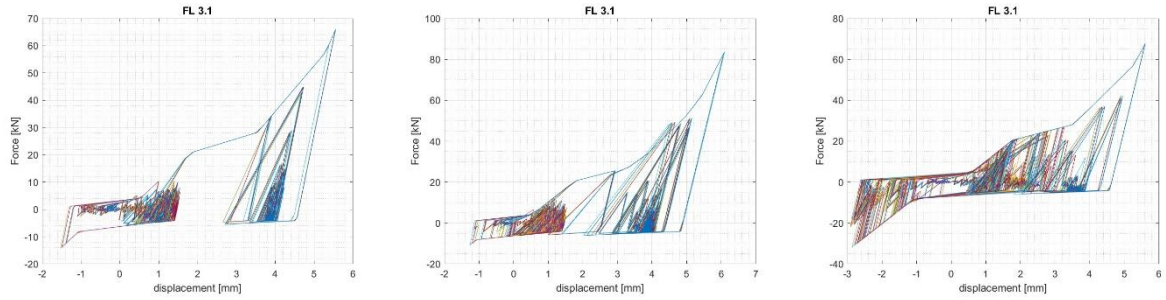

a) b) c)

Figure 3.57. Results on fusible links of the symmetric configuration equipped with Detail 3145 from analyses performed with a) Accelerogram 1, b) Accelerogram 2 and c) Accelerogram 3.

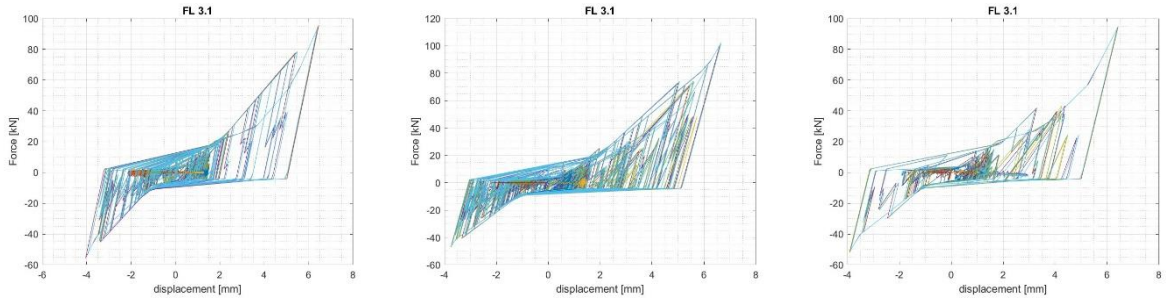

a) b) c)

Figure 3.58. Results on fusible links of the asymmetric configuration equipped with Detail 3145 from analyses performed with a) Accelerogram 1, b) Accelerogram 2 and c) Accelerogram 3.

Table 30. Maximum values obtained on fusible links in comparison with the detail capacity.

Symmetric configuration				
Component	Accelerogram 1	Accelerogram 2	Accelerogram 3	Capacity
Detail 3.1	66.00 kN	85.00 kN	70.00 kN	115.00 kN
Detail 4	1.60 kN	1.50 kN	3.50 kN	26.30 kN
Detail 5	1.50 kN	2.00 kN	3.50 kN	50.50 kN
Asymmetric configuration				
Component	Accelerogram 1	Accelerogram 2	Accelerogram 3	Capacity
Detail 3.1	95.00 kN	100.00 kN	95.00 kN	115.00 kN
Detail 4	16.00 kN	16.00 kN	14.00 kN	26.30 kN
Detail 5	14.00 kN	13.00 kN	11.00 kN	50.50 kN

On the premises outlined on Detail 2 outputs, similar considerations can be envisaged. Indeed, higher forces were recorded on the asymmetric model, and, a significant increase was observed on the Detail 4 and Detail 5, which is in line with the decrease of the number of fusible links and with a distribution on the stress on less elements.

Detail 3245 curves are reported in Figure 3.59 and in Figure 3.60, while the values obtained on the fusible links are reported in Table 31.

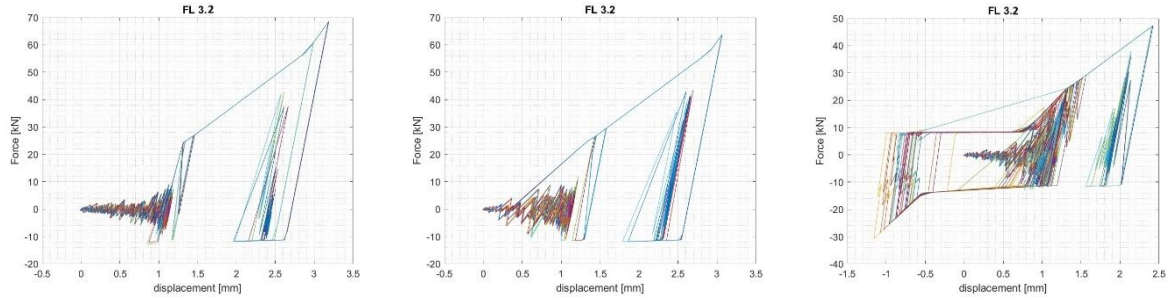

a) b) c)

Figure 3.59. Results on fusible links of the symmetric configuration equipped with Detail 3245 from analyses performed with a) Accelerogram 1, b) Accelerogram 2 and c) Accelerogram 3.

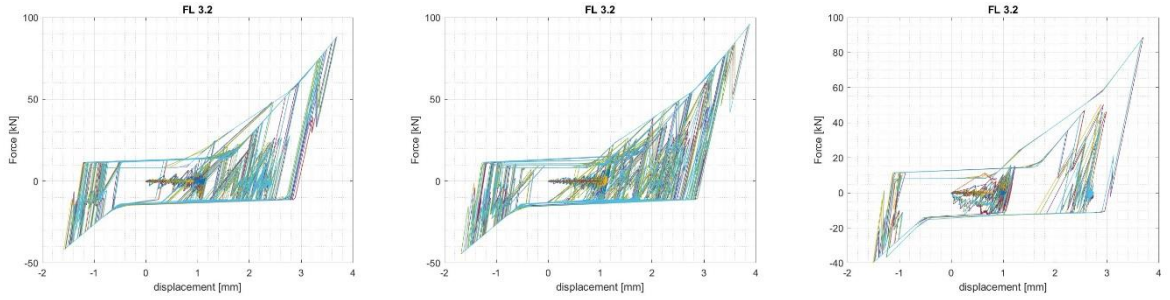

a) b) c)

Figure 3.60. Results on fusible links of the asymmetric configuration equipped with Detail 3245 from analyses performed with a) Accelerogram 1, b) Accelerogram 2 and c) Accelerogram 3.

Table 31. Maximum values obtained on fusible links in comparison with the detail capacity.

Symmetric configuration				
Component	Accelerogram 1	Accelerogram 2	Accelerogram 3	Capacity
Detail 3.2	68.00 kN	65.00 kN	47.00 kN	115.00 kN
Detail 4	2.00 kN	2.00 kN	3.20 kN	26.30 kN
Detail 5	1.70 kN	1.50 kN	3.20 kN	50.50 kN
Asymmetric configuration				
Component	Accelerogram 1	Accelerogram 2	Accelerogram 3	Capacity

Detail 3.2	88.00 kN	95.00 kN	90.00 kN	115.00 kN
Detail 4	17.00 kN	15.00 kN	14.00 kN	26.30 kN
Detail 5	15.00 kN	14.00 kN	11.00 kN	50.50 kN

3.3.3.2.2 Configuration with the firewall parallel to the portal frames

As reported in

Table 27, Detail 3145 and Detail 3245 were involved also in the models with the wall parallel to the portal frames. reports the global outputs obtained in both configurations, symmetric and asymmetric in comparison.

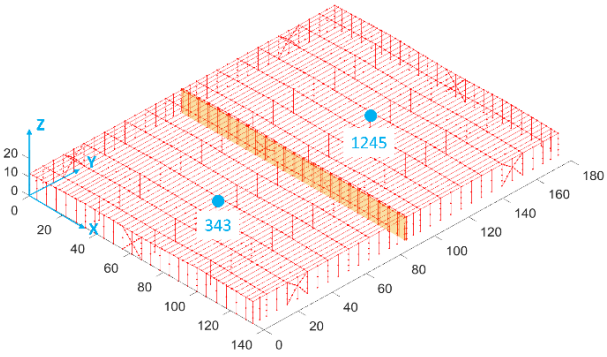

(a1)

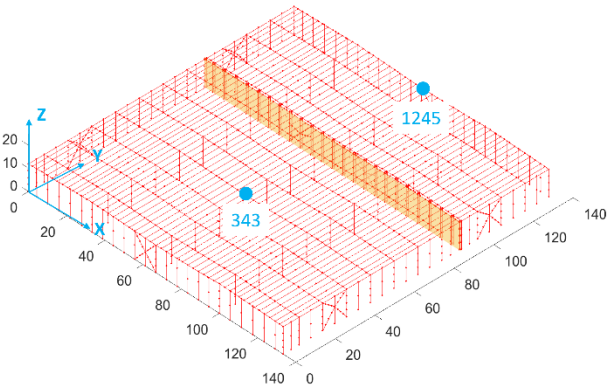

(a)

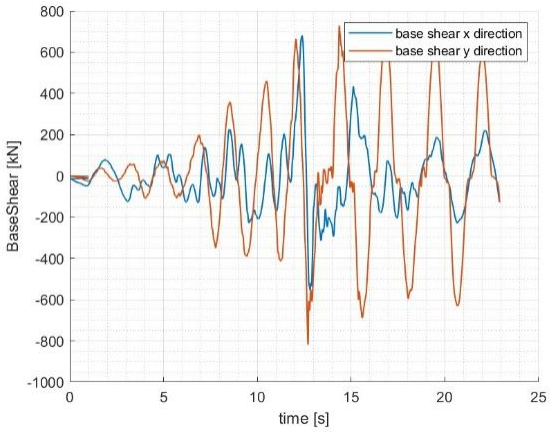

(a2)

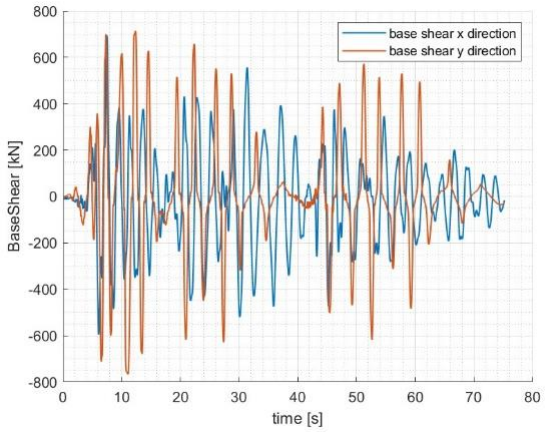

(b)

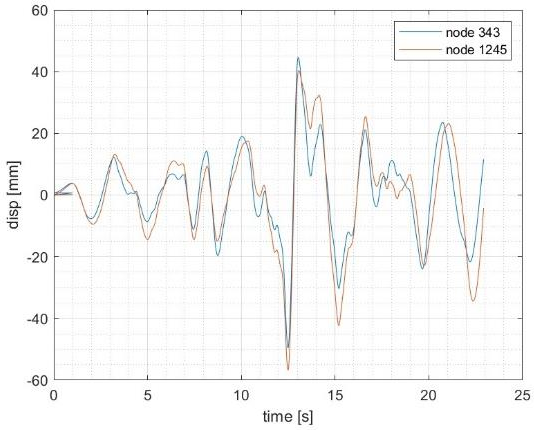

(a3)

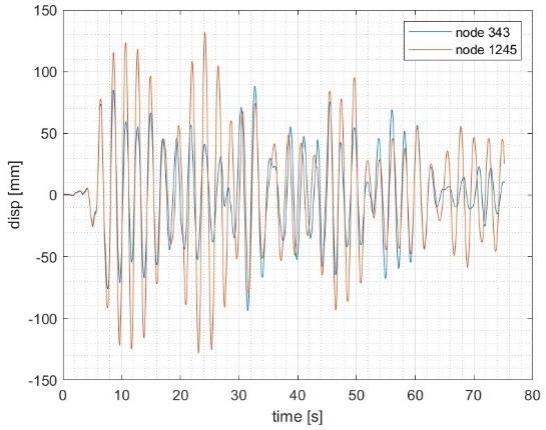

(c)

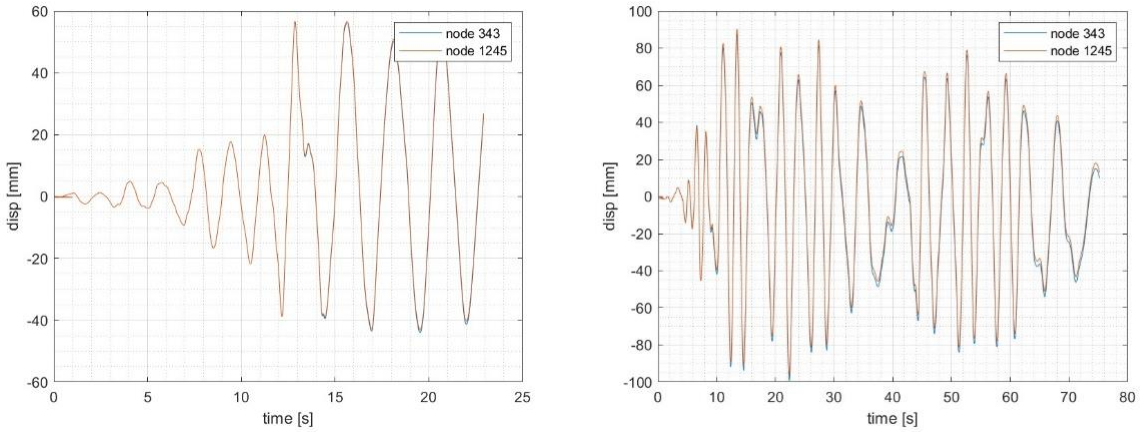

(a4) (d)

Figure 3.61. Case study 4 global outputs (a) symmetric model with firewall orthogonal to the portal frames and (b) asymmetric model with firewall orthogonal to the portal frames.

The local output of this configuration on Detail 3145 and hereafter illustrated. Figure 3.62 and in reported the curved detected on Detail 3.1 while the maximum values recorded in all the components in comparison with their capacities are reported in Table 32.

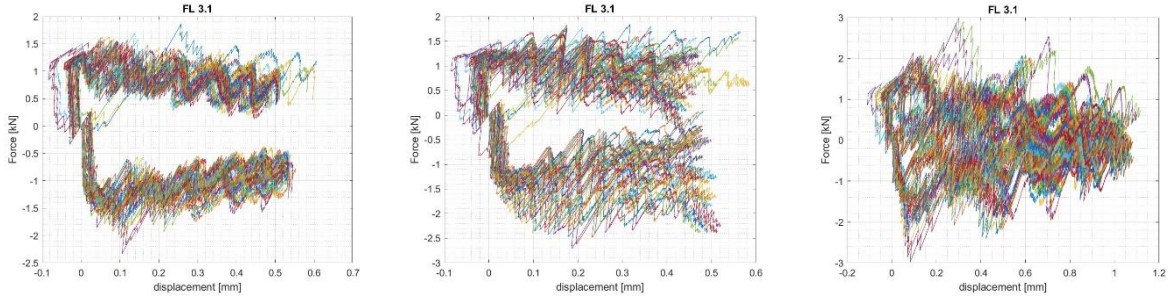

a) b) c)

Figure 3.62. Results on fusible links of the symmetric configuration equipped with Detail 3145 from analyses performed with a) Accelerogram 1, b) Accelerogram 2 and c) Accelerogram 3.

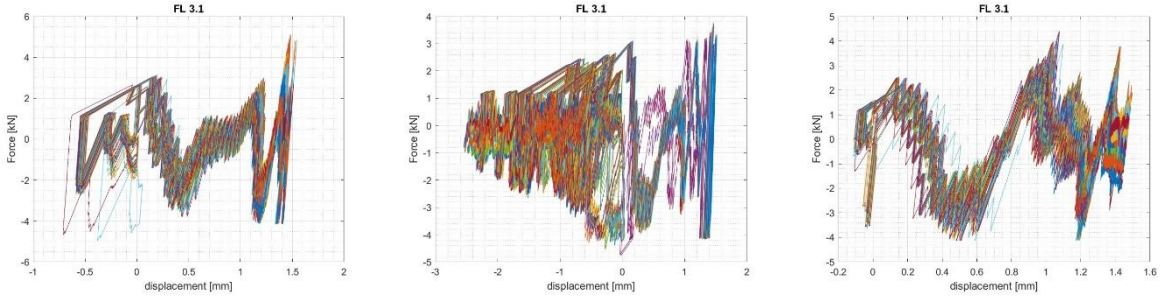

a) b) c)

Figure 3.63. Results on fusible links of the asymmetric configuration equipped with Detail 3145 from analyses performed with a) Accelerogram 1, b) Accelerogram 2 and c) Accelerogram 3.

Table 32. Maximum values obtained on fusible links in comparison with the detail capacity.

Symmetric configuration				
Component	Accelerogram 1	Accelerogram 2	Accelerogram 3	Capacity
Detail 3.1	2.40 kN	2.50 kN	3.00 kN	115.00
Detail 4	3.00 kN	3.50 kN	2.20 kN	26.30
Detail 5	3.50 kN	3.50 kN	2.70 kN	50.50
Asymmetric configuration				
Component	Accelerogram 1	Accelerogram 2	Accelerogram 3	Capacity
Detail 3.1	5.00 kN	4.80 kN	4.50 kN	115.00 kN
Detail 4	0.50 kN	2.20 kN	3.50 kN	26.30 kN

Detail 5	1.50 kN	3.00 kN	4.50 kN	50.50 kN

Despite the difference set of accelerograms applied to the two configurations, the magnitude of the results is quite similar, indeed they are both characterized by very small displacements This is due to the asymmetry, that did not influence directly the fusible links, as occurred on the orthogonal position of the firewall. The very low magnitude of the results is also to be ascribed to the high number of columns present of the building facades, see Figure 3.61a1 and Figure 3.61b1. For each of them a fusible link detail is linked to the firewall, therefore, the shear stress is distributed on many more elements than the orthogonal configuration.

Detail 3245 outcomes are reported in Figure 3.64 and in , while in Table 33 the maximum forces extracted for each component are reported.

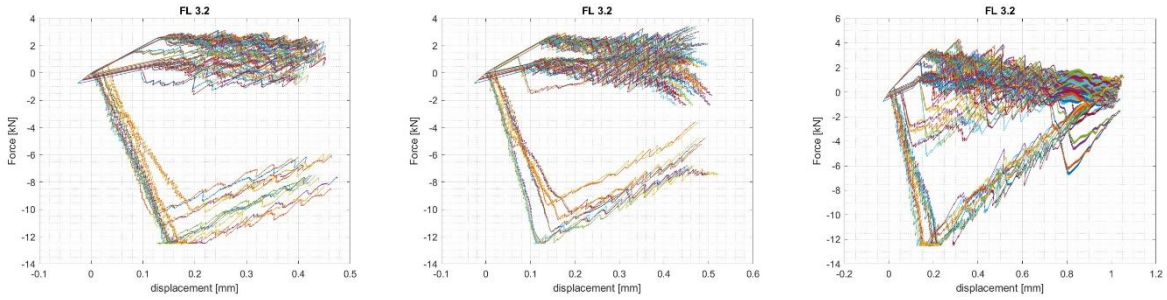

a) b) c)

Figure 3.64. Results on fusible links of the symmetric configuration equipped with Detail 3245 from analyses performed with a) Accelerogram 1, b) Accelerogram 2 and c) Accelerogram 3.

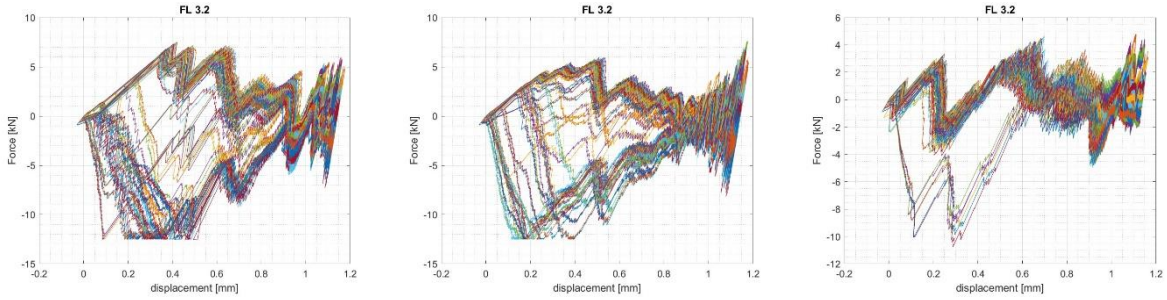

a) b) c)

Figure 3.65. Results on fusible links of the asymmetric configuration equipped with Detail 3245 from analyses performed with a) Accelerogram 1, b) Accelerogram 2 and c) Accelerogram 3.

Table 33. Maximum values obtained on fusible links in comparison with the detail capacity.

Symmetric configuration				
Component	Accelerogram 1	Accelerogram 2	Accelerogram 3	Capacity
Detail 3.2	12.50 kN	12.50 kN	12.50 kN	115.00 kN
Detail 4	3.00 kN	3.50 kN	2.40 kN	26.30 kN
Detail 5	3.50 kN	3.50 kN	2.80 kN	50.50 kN
Asymmetric configuration				
Component	Accelerogram 1	Accelerogram 2	Accelerogram 3	Capacity
Detail 3.2	12.50 kN	12.50 kN	11.00 kN	115.00 kN
Detail 4	1.40 kN	2.20 kN	3.00 kN	26.30 kN
Detail 5	1.50 kN	2.20 kN	2.00 kN	50.50 kN

With respect to the outputs obtained on Detail 3245, the same evaluations derived for Detail 3145 are applicable.

4 DEVELOPMENT OF FRAGILITY FUNCTIONS

As anticipated in the Introduction, the second part of this report is devoted to the presentation of the fragility functions development. The fragility functions of a new structural typology or a component, as it is the case, are essential for risk assessment and/or a probabilistic Performance-Based Earthquake Engineering application. A fragility curve can express the probability of exceedance of an engineering demand parameter (EDP) given an intensity measure (IM). The computation of seismic fragility functions requires several numerical simulations. In this case, the multiple stripes analysis (MSA) technique was employed and was applied to nonlinear FE models built in OpenSees. In this respect, a suite of representative ground motion records was selected based on the Conditional Mean Spectrum (CMS) and then scaled to various intensity levels. The selected intensity measure was the spectral acceleration at the first mode of vibration period ($Sa(T_1)$). The EDPs considered were, at a local level, the fusible link capacity, and, at a global level, the peak interstorey drift. This procedure was conducted on Case study 4, that is located in a moderate level of seismicity area, and it is seismically designed in accordance with the French prescriptions [20]. The case study was analysed in the asymmetric configuration shown in Section 3.3.3, because larger forces on the fusible link systems were observed. Both firewall positions, orthogonal and parallel to the portal frames were analysed, as depicted in Figure 4.1.

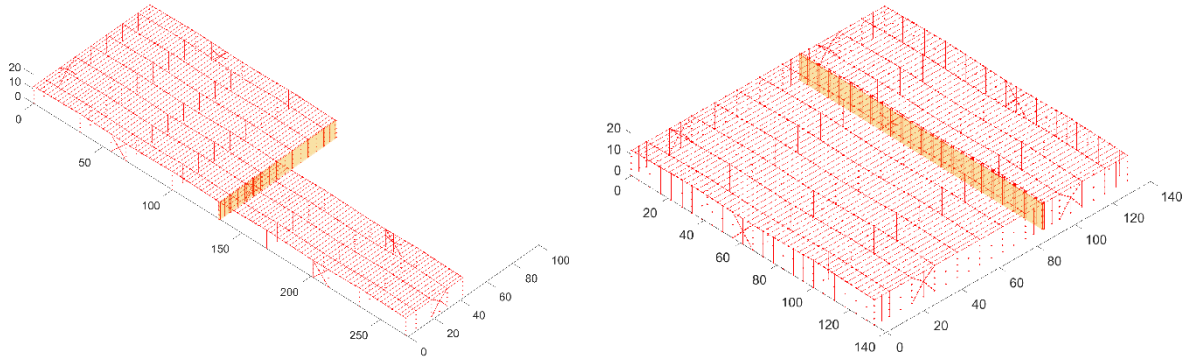

(a) (b)

Figure 4.1. Case study 4, (a) asymmetric model with firewall orthogonal to the portal frames and (b) asymmetric model with firewall parallel to the portal frames.

The firewall was equipped with two of the 4 details presented in Section 3.1.3. Considering the outputs of both the experimental campaign and the time histories analyses, Detail 2 and Detail 3145 were selected. The columns added between the portal frames were, in both cases, equipped with Detail 3145, as explained in Sections 3.1.3.1 and in Section 3.1.3.4.
Eventually, three configurations were analysed:

- asymmetric model with firewall orthogonal to the portal frames equipped with Detail 2 (OA - DET2);
- asymmetric model with firewall orthogonal to the portal frames equipped with Detail 3145 (OA - DET3145);
- asymmetric model with firewall parallel to the portal frames equipped with Detail 3145 (PA - DET3145).

For each of the three models, a modal analysis was performed to derive the most significant periods of the structures characterised by large modal masses, that are reported in Table 5.1, Table 5.2 and Table 5.3.

Table 5.1. Dynamic properties of OA - DET2 model.

Mode	T [s]	Ux [%]	Uy [%]	Rz [%]
1°	2.42	25.66	0.00	3.63
3°	2.06	0.00	98.08	0.22
4°	2.02	40.07	0.00	2.24

Table 5.2. Dynamic properties of OA - DET3145.

Mode	T [s]	Ux [%]	Uy [%]	Rz [%]
1°	2.48	25.47	0.00	3.66
3°	2.16	39.88	0.00	2.18
4°	1.98	0.64	82.98	0.12

Table 5.3. Dynamic properties of PA - DET3145.

Mode	T [s]	Ux [%]	Uy [%]	Rz [%]
1°	2.59	29.81	0.00	0.47
3°	2.31	18.74	0.00	10.14
4°	2.21	13.74	0.00	3.62
8°	1.88	0.00	98.22	0.16

Based on these results, a Conditional Mean Spectrum (CMS) was derived from each structure. As described by Baker [6], the main goal of dynamic structural analyses is to predict the structure response to a set of ground motions derived from a spectral acceleration at a given period. The ground motions selected usually match a target response spectrum that allows large-amplitude spectral values at all periods within a single ground motion. The above-mentioned CMS provide the target response spectrum conditioned on the occurrence of a target spectral acceleration at a period of interest. A target spectrum, based on the Eurocode 8, was derived to obtain a target spectral acceleration at first period and 4% of damping ratio. Therefore, the CMS conditioned on that spectral acceleration was used to define the set of ground motion. The spectrum target was derived at a Life Safety limit state with an A type soil classification, as it is the actual location of the building representing Case study 4 and a damping ratio of 4%. Since significant modal masses are distributed among different modes that characterize the translational first mode along the x-direction (see Table 5.1-Table 5.3), it was decided to select as the representative period for the CMS, the weighted mean of the first modes along x. In particular for OA-DET2 and OA-DET3145 models, two modes were selected, whereas for the PA-DET3145 model three modes were considered. The resulting periods are reported in Table 5.4.

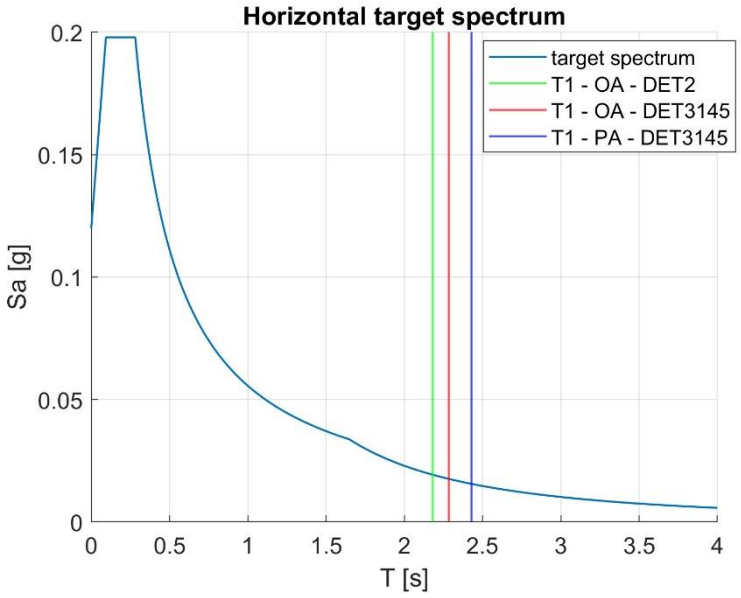

Figure 4.2. Target spectrum of Case study 4.

The Sa(T_1)s at which the CMSs were calculated are reported in Table 5.4.

Table 5.4. Target Sa(T_1)

	T_1	Sa(T_1)
OA - DET2	2.18 s	0.0198 g
OA - DET3145	2.29 s	0.0182 g
PA – DET3145	2.43 s	0.0164 g

The three conditional mean spectra calculated for the three structures are hereinafter reported in Figure 4.3.

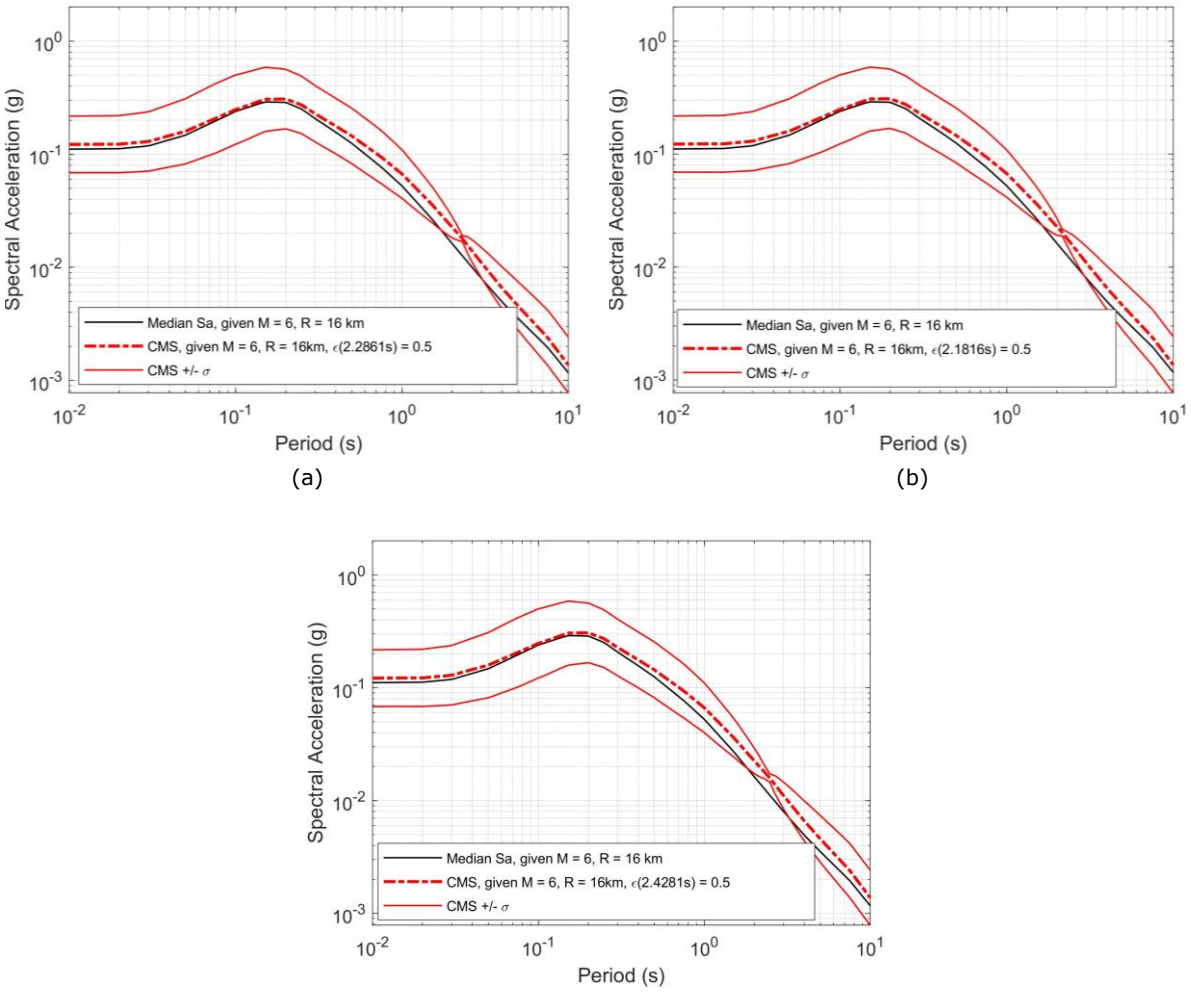

Figure 4.3. CMS of the three investigated configurations: a) OA - DET2, b) OA - DET3145 and c) PA – DET3145.

4.1 Selection of ground motions

In order to find the events that better fitted the CMSs of the investigated structures, a large set of ground motions was considered from the European database ESM [13]. The selection included far-field accelerograms with a Joyner-Boore distance (Rjb) of more than 20 km, a site category A was selected for the analyses, in agreement with the target spectrum, and magnitude range of 5.5 and 6.5 was determined to be consistent with the moderate seismicity level design of the details used. The efficient ground-motion selection algorithm proposed by Jayaram et al. [7] was used to scale each of the available ground motions in the database created so that their Sa(T_1) matched the target mean spectrum Sa(T_1). Consequently, the selected 20 ground motions are reported in Table 34.

Table 34. Selected time histories.

Number	Event ID/Station code	Case study	Mw	Rjb [km]	PGA [g]
1	INT-20210927_0000049/ HL.IACM	All	6.0	21.7	0.09
2	INT-20211012_0000090/ HL.KARP	All	6.4	86.1	0.02
3	EMSC-20161026_0000095/ IT.ACC	All	5.9	25.2	0.08
4	EMSC-20161026_0000095/ IT.ASS	All	5.9	47.4	0.04
5	IT-1997-0006/IT.ASS	All	5.7	21.6	0.18
6	EMSC-20160824_0000006 /IT.MNF	All	6.0	40.3	0.07
7	IT-1984-0004/ IT.ORT	All	5.9	33.6	0.08
8	EMSC-20170118_0000034 / IT.RTQ	All	5.5	28.2	0.12
9	EMSC-20160824_0000006/ IT.SPM	All	6.0	39.6	0.06
10	EMSC-20161026_0000095/ IT.SPM	All	5.9	38.0	0.07
11	IT-1997-0137/ IT.SPM	All	5.6	27.1	0.04
12	EMSC-20161026_0000095/ IV.FIU1	All	5.9	35.3	0.08
13	EMSC-20160824_0000006/ IV.MDAR	All	6.0	55.4	0.05
14	EMSC-20161026_0000095/ IV.MDAR	All	5.9	31.4	0.13
15	EMSC-20161026_0000095/ IV.MMUR	All	5.9	60.2	0.10
16	EMSC-20161026_0000095/ IV.T1215	All	5.9	25.3	0.02
17	EMSC-20161026_0000095/IV.T1218	All	5.9	26.8	0.08
18	EMSC-20161026_0000095/IV.TERO	All	5.9	49.6	0.04
19	IT-2009-0009/IT.ANT	OA - DET2 PA – DET3145	6.1	26.2	0.02
20	EMSC-20160824_0000006/ IV. FEMA	OA - DET2 OA – DET3145	6.0	32.9	0.25
21	EMSC-20160824_0000006/ IT.ASS	OA - DET3145 PA – DET3145	6.0	66.3	0.04

As said, the ground motions were scaled to fit the $Sa(T_1)$. In Figure 4.4 the response spectra of the ground motions and the mean value for each structure is reported and in Table 5.5 the scale factor applied are shown.

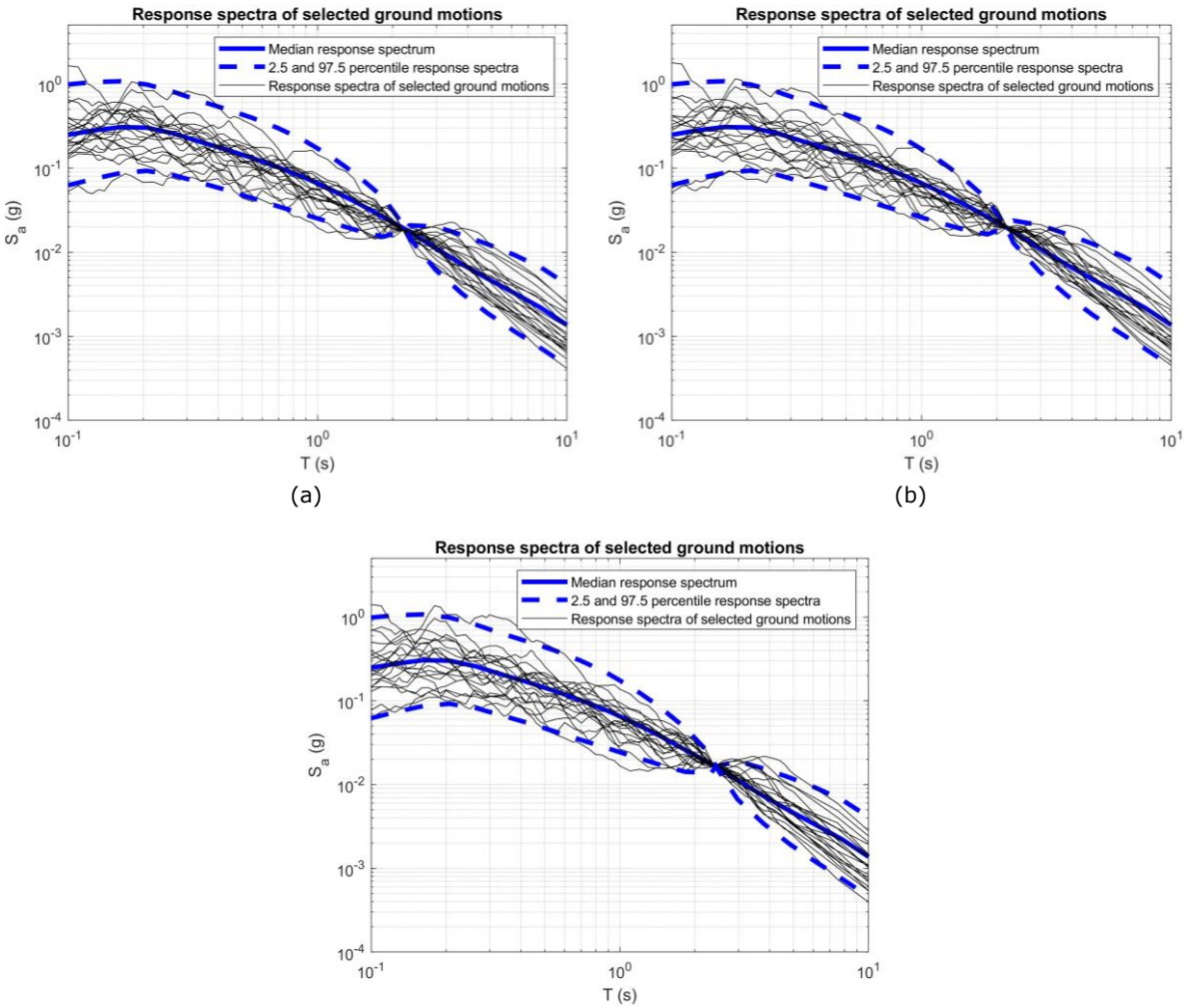

Figure 4.4. Response spectra of the selected records.

Table 5.5. Scale factors applied to the common ground motions.

Number	Event ID/Station code	OA - DET2	OA - DET3145	PA – DET3145
1	INT-20210927_0000049/HL.IACM	0.88	0.82	0.78
2	INT-20211012_0000090/L.KARP	1.82	1.68	2.47
3	EMSC-20161026_0000095/IT.ACC	0.95	0.88	0.88
4	EMSC-20161026_0000095/IT.ASS	3.78	3.489	3.48
5	IT-1997-0006/IT.ASS	1.526	1.40	1.80
6	EMSC-20160824_0000006/IT.MNF	1.745	1.61	1.45
7	IT-1984-0004/IT.ORT	2.57	2.33	2.77
8	EMSC-20170118_0000034 /IT.RTQ	2.14	1.97	1.69
9	EMSC-20161026_0000095/ IT.SPM	1.948	1.79	1.94
10	IT-1997-0137/ IT.SPM	2.143	1.98	1.88
11	EMSC-20160824_0000006/ IV. FEMA	0.40	0.37	3.66
12	EMSC-20161026_0000095/IV.FIU1	2.94	2.71	3.07
13	EMSC-20160824_0000006/IV.MDAR	1.72	1.59	1.58
14	EMSC-20161026_0000095/IV.MDAR	0.81	0.75	0.86
15	EMSC-20161026_0000095/IV.MMUR	2.66	2.46	2.68
16	EMSC-20161026_0000095/IV.T1215	3.31	3.05	3.08

17	EMSC-20161026_0000095/IV.T1218	1.81	1.67	1.72
18	EMSC-20161026_0000095/IV.TERO	3.28	3.02	3.03
19	IT-2009-0009/IT.ANT	1.79	-	2.17
20	EMSC-20160824_0000006/ IV. FEMA	0.41	0.37	-
21	EMSC-20160824_0000006/IT.ASS	-	3.82	3.66

4.2 Seismic performance and fragility functions

In order to assess the structural response, two significant EDPs were identified in terms of global and local quantities. In particular, the Peak Interstorey Drift Ratio (PIDR) was considered as global measure, whilst the fusible link detail capacity was taken as local measure. To define the exceedance of the collapse limit state, for PIDR, the thresholds were considered in accordance with FEMA356 provisions [19]. Considering that the structures are characterized by two different lateral-resisting systems in the two horizontal directions, the following values were taken:

- 5.0%, that is conventionally defined as the Near Collapse (NC) limit state threshold for the moment resisting frame system;
- 2.0%, that is conventionally defined as the Near Collapse (NC) limit state threshold for the braced system.

In order to assess the local EDP, the maximum fusible link detail capacities are derived from the experimental campaign and widely described in Deliverable 4.1 [11]. The values are reported in Table 35.

Table 35. Local EDP capacities.

	Detail 2	Detail 3.1	Detail 4	Detail 5
Capacity	110.00 kN	115.00 kN	26.30 kN	50.50 kN

4.2.1 Formulation of fragility functions

Using the results from the MSAs, fragility curves were developed for the EDP levels aligned with predefined limit states. In accordance with the method outlined by Baker [9], the probability P that a ground motion with intensity measure, in this work defined as the spectral acceleration at the first period, IM = x will cause the exceedance of a given limit state, e.g. collapse, is modelled as a lognormal cumulative distributed.

$$P(C|IM = x) = \Phi\left(\frac{\ln(x/\theta)}{\beta}\right) \quad (1)$$

where Φ () is the standard normal cumulative distribution function (CDF), θ is the median of the fragility function and β is the standard deviation of ln(IM). The equation implies that the IMs applied to the selected ground motions that caused the collapse of the structure, are lognormally distributed. Differently to other analyses method, such as incremental dynamic analyses (IDAs), the MSAs results provide the fraction of ground motions at each IM that causes the collapse. Indeed, at each IM, the structural analyses produce only some number of collapses out of the total number of ground motions selected. The observation of collapse or of no-collapse from each ground motion is independent from the other ground motions, and the probability of observing z_j collapses out of n_j ground motions with IM = x_j is given by a binomial distribution:

$$P(z_j \text{ collapses in } n_j \text{ ground motions} = \binom{n_j}{z_j} p_j^{z_j}(1-p_j)^{n_j-z_j} \quad (2)$$

where p_j identifies the probability that an IM = x_j applied to a ground motion will cause the collapse of the structure. In order to evaluate the fragility function that will predict p_j, the maximum likelihood approach is suitable to identify the fragility curve that maximizes the probability of observing the collapse data obtained from structural analysis. As frequently occurs, multiple IM levels are employed, therefore, Baker suggests considering the product of the binomial probabilities at each IM level to obtain the likelihood of the whole data set.

$$Likelihood = \prod_{j=1}^{m} \binom{n_j}{z_j} p_j^{z_j}(1-p_j)^{n_j-z_j} \quad (3)$$

where *m* is the number of intensity measure levels and ∏ identifies a product on all the levels. Substituting the probability estimated in (1) in p_j position of (3), the fragility functions parameters, θ and β, are explicit.

$$Likelihood = \prod_{j=1}^{m} \binom{n_j}{z_j} \Phi\left(\frac{\ln\left(x/\theta\right)}{\beta}\right)^{z_j} \left(1 - \Phi\left(\frac{\ln\left(x/\theta\right)}{\beta}\right)\right)^{n_j - z_j} \quad (4)$$

the parameters θ and β can be estimated by maximizing the likelihood function, which is equivalent of maximizing the logarithm of the likelihood function procedure. Therefore, the estimation of the fragility function parameters is obtained by finding the couple of parameters that maximize the logarithm of the likelihood function:

$$\{\hat{\theta}, \hat{\beta}\} = \underset{\theta,\beta}{\operatorname{argmax}} \sum_{j=1}^{m} \left\{ \ln\binom{n_j}{z_j} + z_j \ln \Phi\left(\frac{\ln x_j/\theta}{\beta}\right) + \left(n_j - z_j\right) \ln\left(1 - \Phi\left(\left(\frac{\ln x_j/\theta}{\beta}\right)\right)\right) \right\} \quad (5)$$

Eventually, a fragility function can be represented by a lognormal distribution whose parameters are $\hat{\theta}$ and $\hat{\beta}$.

The results of the MSAs performed with respect to the first period spectral acceleration on the investigated structures are hereafter reported. The scale factors applied to the $Sa(T_1)$, illustrated in Table 5.4, are [1, 1.5, 2, 2.5, 4, 6, 8, 10].

4.2.1.1 Asymmetric configuration with firewall orthogonal to the portal frames equipped with Detail 2 (OA - DET2).

The IM-EDP results in terms of global EDP are shown in Figure 4.5 where it can be observed that the NC limit states in the two building principal directions are never exceeded, with the exception of one isolated accelerogram associated with spectral acceleration equal to 0.198g.

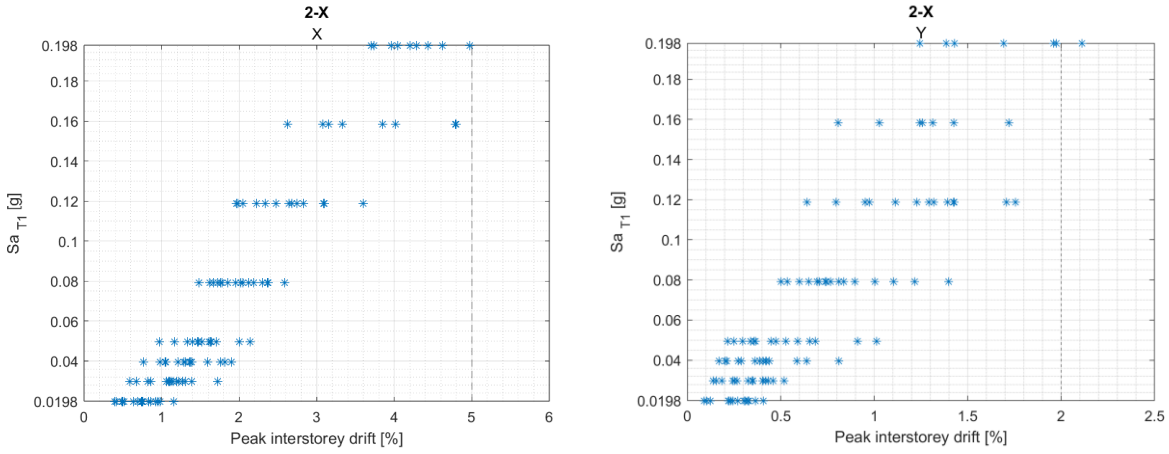

(a) (b)

Figure 4.5. MSAs results with global EDP of OA – DET2 model: a) direction parallel to the portal frames - MRF b) direction orthogonal to the portal frames – lateral bracing system.

In terms of local EDP, which is the fusible link detail capacity, the MSAs results are hereafter shown in Figure 4.6. Considering Detail 2, the one linked to the portal frame columns, several collapses were observed from IM scaled up to 2 to 10, where in all the analyses the detail capacity was overcome (see Figure 4.6a). With respect to Detail 3.1 some failures were observed without a well-defined pattern. Regarding Details 4 and 5 located on the additional columns, they were less stressed than Detail 2, and consistently with the outcomes of the parametric analyses, did not report any failure. On these premises, the fragility functions related to Detail 2 was derived and illustrated in Figure 4.7, where the target $Sa(T_1)$ is also reported consistent with table 5.4 for Detail 2. It has to be noted that the number of failures is low, in particular on the low values of IM, that causes fairly large dispersion. The median probability of exceedance is given for spectral accelerations equal to about 0.065g, whereas the 80% probability of exceedance the fusible link capacity is given for IM = 0.09g. Finally, consistently with the parametric analyses, for low to moderate seismic intensity, the fusible link capacity is not exceeded and to observe failure of the fusible link system large scale factors must be applied to the ground motions.

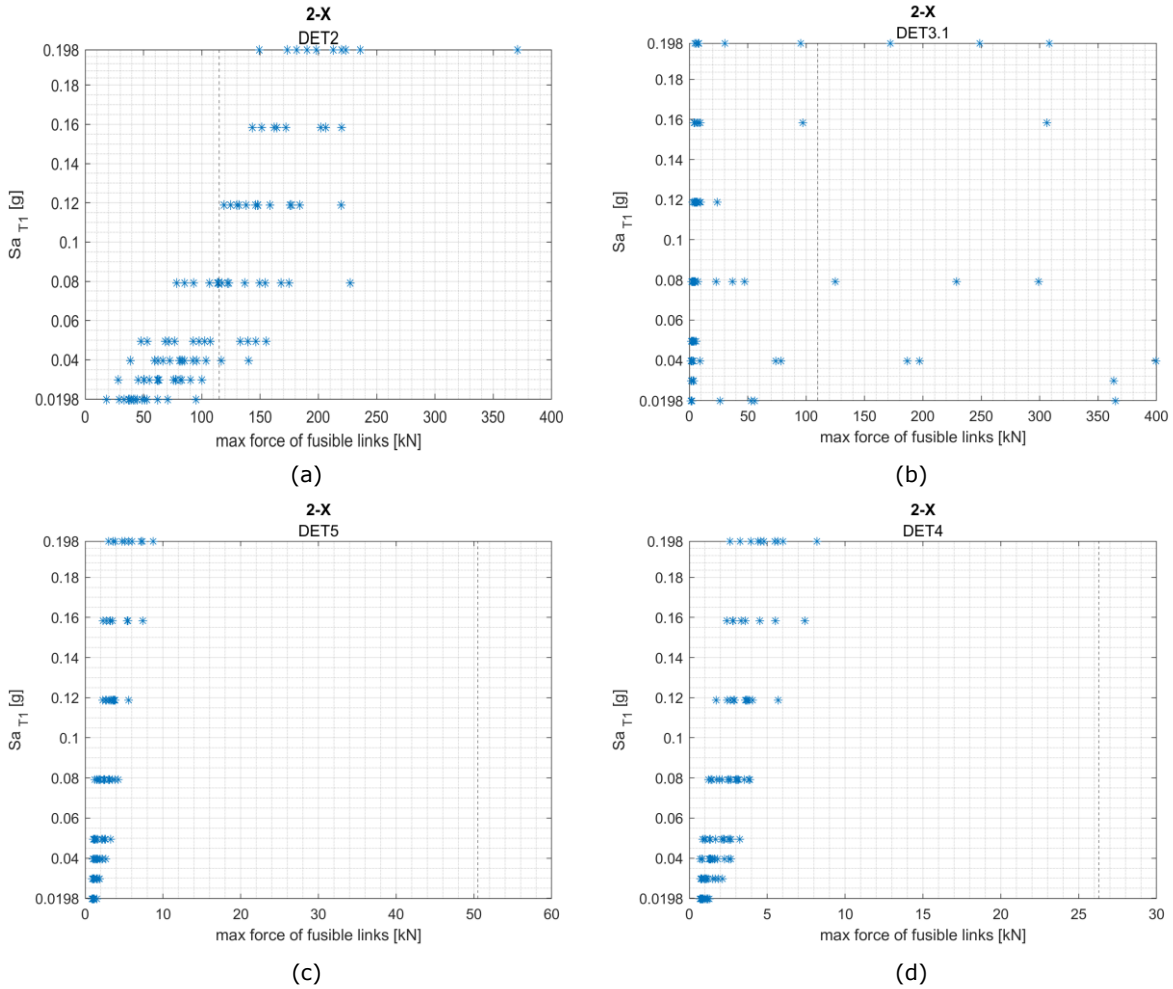

Figure 4.6. MSAs results with local EDP of OA - DET2 model.

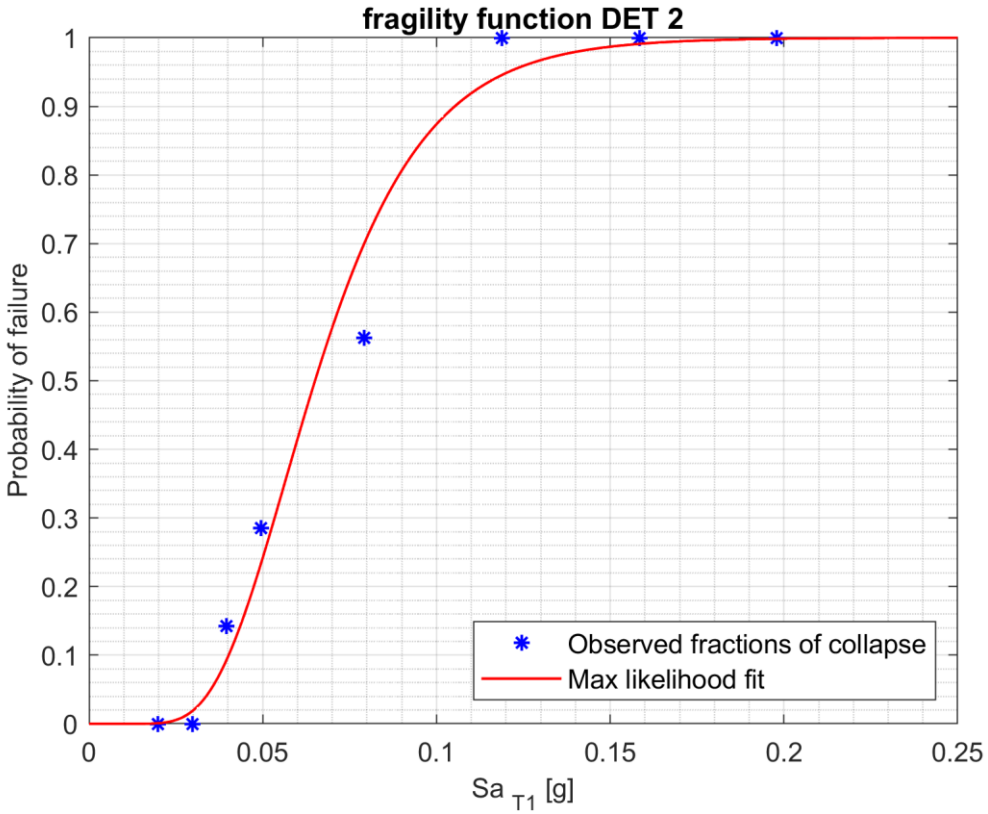

Figure 4.7. Fragility curve for the local EDP of Detail 2.

4.2.1.2 Asymmetric configuration with firewall orthogonal to the portal frames equipped with Detail 3145 (OA – DET3145).

The results in terms of global EDP are shown in Figure 4.8, where it can be observed that the NC limit states in the two building principal directions are never exceeded, with the exception of two analyses at an IM equal to scale factor equal to 8.

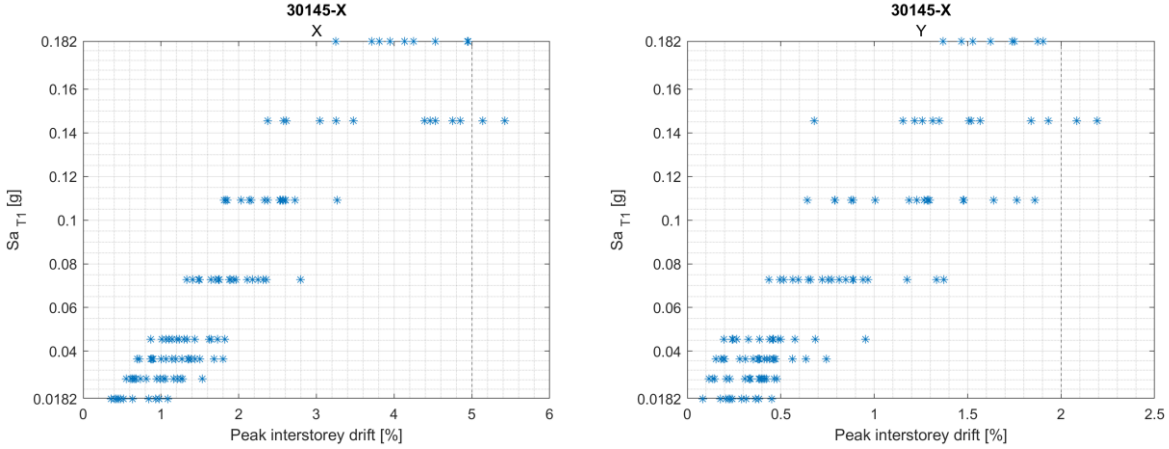

(a) (b)

Figure 4.8. MSAs results with global EDP of OA – DET3145 model: a) direction parallel to the portal frames - MRF b) direction orthogonal to the portal frames – lateral bracing system.

In terms of the fusible link detail capacity, the MSAs results are hereafter shown in Figure 4.9, where the target $Sa(T_1)$ is also reported consistent with Table 5.4 for Detail 3145. As observed for the global EDP, also in terms of local EDP, in general, most of the analyses did not record any failures. However, considering Detail 3.1, an increasing number of exceedances of the detail capacity was recorded from IM equal to $1.5Sa(T_1)$ to the maximum IM considered, i.e. $10Sa(T_1)$, where in all the analyses the detail capacity exceedance was observed.

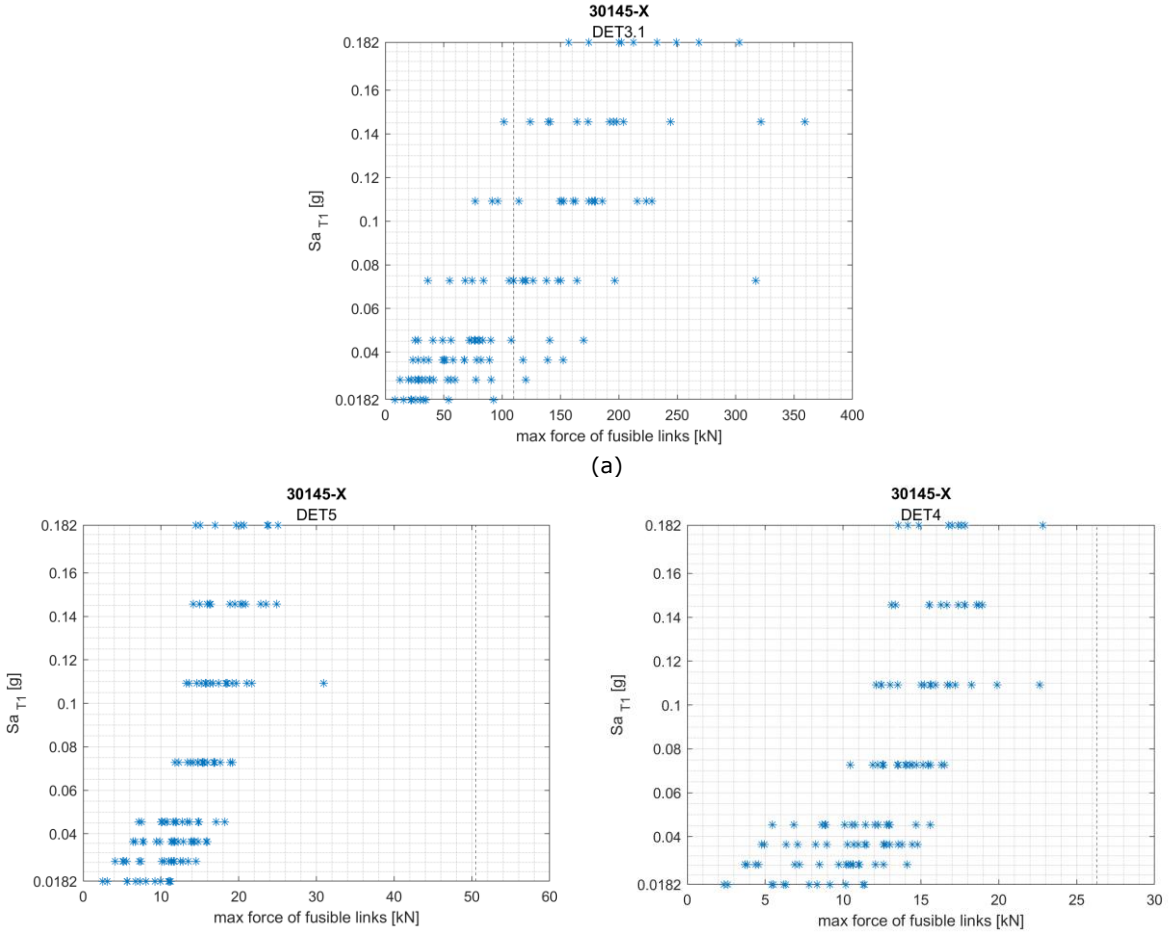

(a)

(b) (c)

Figure 4.9. MSAs results with local EDP of OA – DET3145 model.

The fragility curve related for Detail 3.1 is illustrated in Figure 4.10. As observed for Detail 2, it has to be noted that the number of failures is low for the IM from $Sa(T_1)$ to $2.5Sa(T_1)$, while they are more consistent for the higher levels of IM. Larger dispersion than the case equipped with Detail 2 is observed. The median probability of exceedance is given for IM = 0.068g, whilst the 80% probability of exceedance the fusible link capacity is given for IM = 0.11g. As previously described, consistently with the parametric analyses, for low to moderate seismic intensity, the fusible link capacity is not exceeded and to observe failure of the fusible link system large scale factors must be applied to the ground motions.

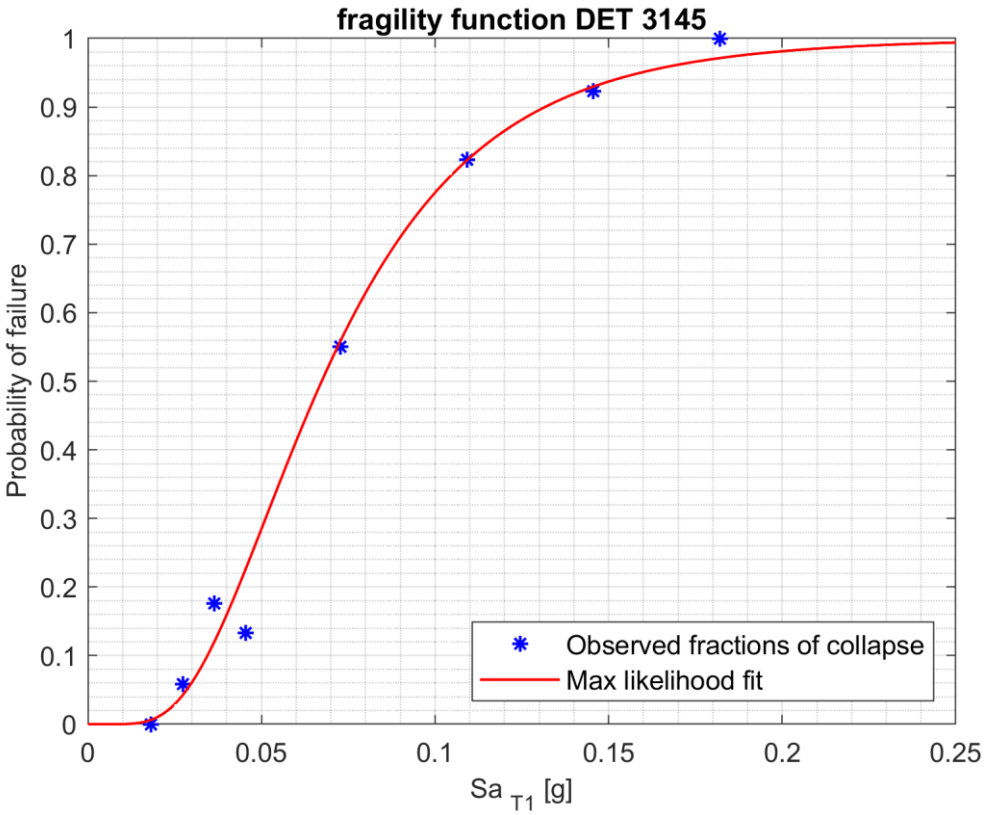

Figure 4.10. Fragility curve for the local EDP of Detail 3.145.

4.2.1.3 Asymmetric model with firewall parallel to the portal frames equipped with Detail 3145 (PA – DET3145).

Figure 4.11 reports the results of the MSAs performed on the PA - DET3145 model. As occurred for the previous models, the IM-EDP results in terms of global EDPs, highlight that the NC limit states in the two principal building directions are reached only for isolated analyses.

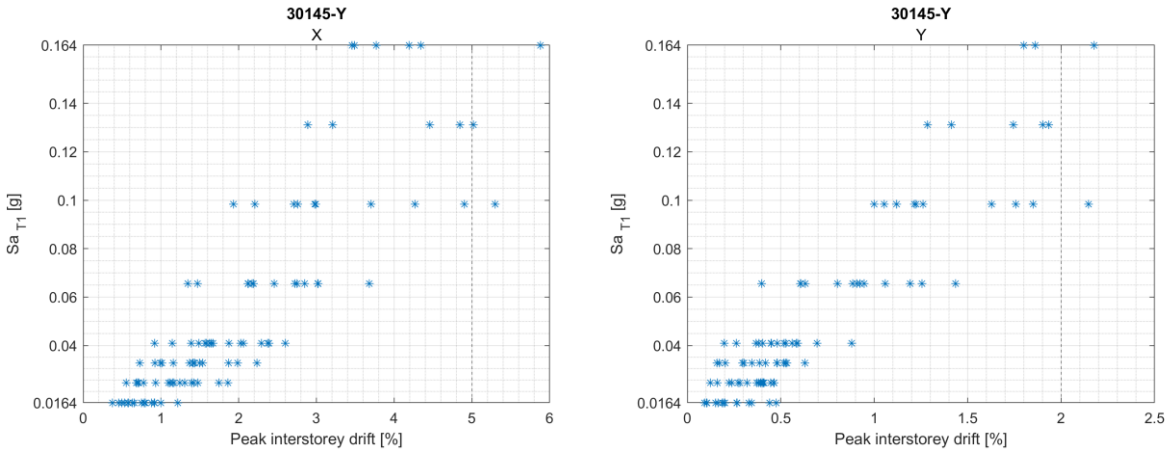

(a) (b)

Figure 4.11. MSAs results with global EDP of PA – DET3145 model: a) direction parallel to the portal frames - MRF b) direction orthogonal to the portal frames – lateral bracing system.

In terms of local EDP, the fusible link detail capacity, the MSAs results are hereafter shown in Figure 4.12. As can be seen, fusible link details did not reach their maximum capacity at any level of IM. The forces observed on the elements are significantly low. This is consistent with the results observed from the parametric nonlinear analyses performed on the same case study and configurations. Indeed, due to the elevated number of columns on the structure façades and therefore, the high number of fusible links, the stress induced on them was distributed in more elements and the final single effort was low. For this reason, the fragility curves were not meaningful.

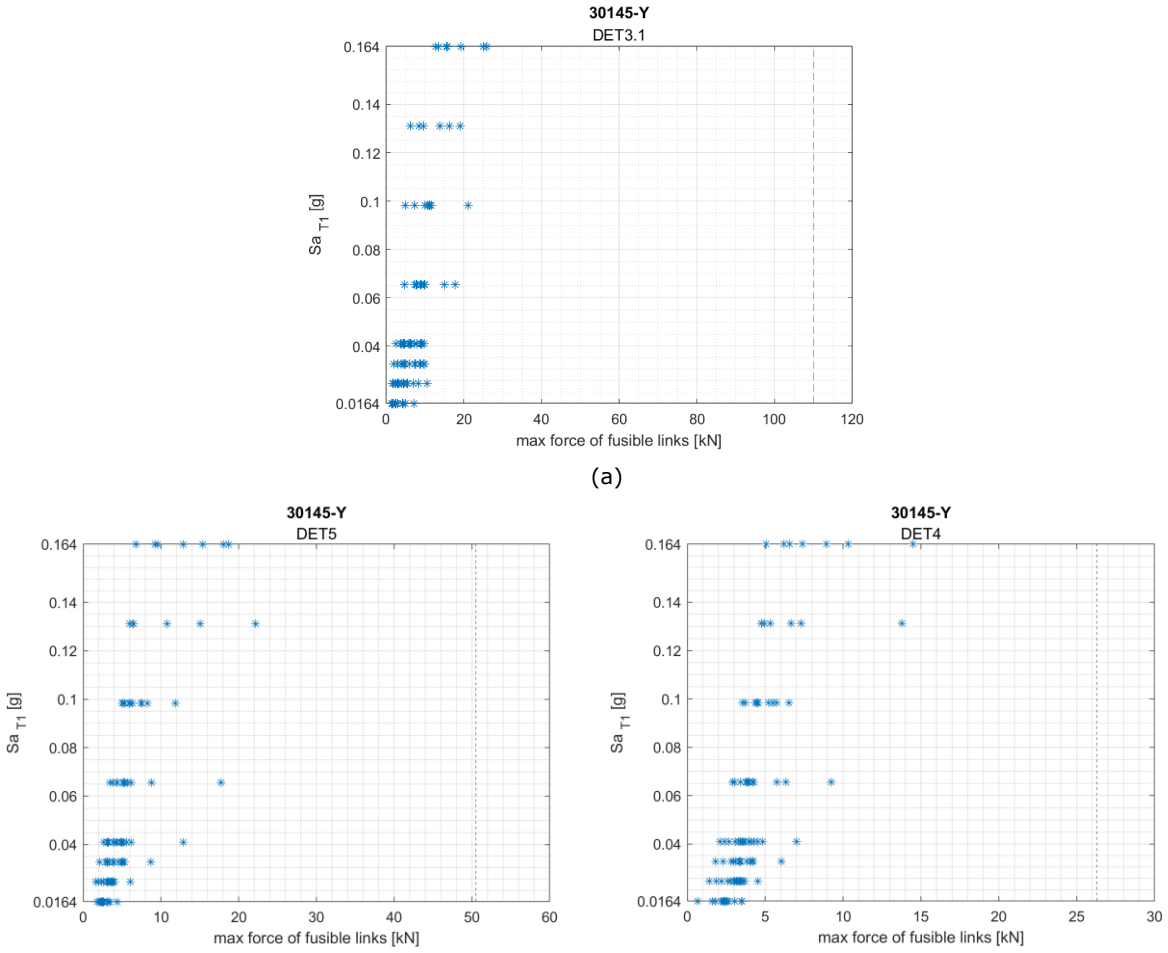

Figure 4.12. MSAs results with local EDP of PA – DET3145 model.

5 CONCLUSIONS

In this report, the parametric nonlinear time-history analyses carried out on the most relevant case studies, designed for 0.04g and 0.12g PGA values, were presented. Orientation of the fire wall, seismic intensity, type of fusible link detail and soil classification of the ground motions were changed to investigate the global response of the buildings and, in particular, of the fusible link system. Moreover, symmetric and asymmetric building configurations were considered to emphasize the effect of the variation of the dynamic properties. Thus, the most insightful results were presented for Case study 1, Case study 3 and Case study 4 in terms of comparison between symmetric and asymmetric configuration outcomes. In this respect, a set of three spectrum-compatible accelerograms was selected and 108 analyses were performed.

One main finding, common to all analyses, concerns the fact that no detail exceeded its maximum capacity for the considered seismic intensity levels, highlighting that no specific seismic recommendations are needed for such a fusible link system. Thus, the design can follow the provisions given in the EN 1998, EN 1993 and EN 1999. Moreover, the response of the fusible links was not highly affected by the asymmetry of the structure, mainly because of the similar dynamic properties of the two buildings. The configuration with the wall parallel to the portal frames recorded lower level of stress in the fusible links with respect to the orthogonal orientation of the fire wall to the portal frames because the firewall was located between the building facades, characterized by many columns. A common evaluation can be provided regarding the magnitude of forces in the fusible links directly connected to the portal frames, rather than the one located on the columns added between the portal frames when spanned more the 5m; the latter was significantly less stressed, due to the flexible connection to the main structure.

Considering the probabilistic seismic demand analysis, the development of the fragility functions by means of Multiple Stripes Analysis was carried out. This procedure was performed on Case study 4, equipped with Detail 2 and Detail 3145. Only the asymmetric configuration of the structure was considered with the firewall position both orthogonal and parallel to the portal frames. A total of three models were consequently analysed and the selection of the set of accelerograms was done according to the Conditional Mean Spectrum. The IM selected was the spectral acceleration at the first period, $Sa(T_1)$, while two different EDPs where monitored: at the local level, the fusible link capacity, whereas the peak interstorey drift was chosen at a global level and it was compared with NC limits of FEMA365. At the global level only isolated collapses were recorded at the highest level of IMs considered, while a few were observed in terms of maximum force on the fusible link. Additional analyses were performed, up to IM = $10Sa(T_1)$, that recorded a trend of failures on the fusible links and very few collapses on the PIDR. Consistently with the parametric analyses, for low to moderate seismic intensity, the fusible link capacity is not exceeded and to observe failure of the fusible link system large scale factors must be applied to ground motion.

Finally, 3D numerical analyses were carried out on the fusible link solution consisting of a steel profile assembled with aluminium bolts to a steel channel spanning between the columns of the building steel structure. The findings confirmed that both link configurations with an L-shaped or a T-shaped profile, designed with comparable dimensions, are equally suitable and can withstand a design force of either 40 kN or 90 kN.

6 REFERENCES

[1] Deliverable D1.3: Analysis of seismic behaviour of single-storey buildings, RFSC project FISHWALL, 2020.

[2] Deliverable D4.2: Development and validation of FE numerical models, RFSC project FISHWALL, 2020.

[3] McKenna, F., Fenves, G. L, and Scott, M. H. (2000) Open System for Earthquake Engineering Simulation. University of California, Berkeley, http://opensees.berkeley.edu.

[4] Mazzoni, S., McKenna, F., Scott, M. H., and Fenves, G. L. (2006) OpenSees Command Language Manual. University of California, Berkeley, http://opensees.berkeley.edu/manuals/usermanual.

[5] CEN, Eurocode 8: Design of structures for earthquake resistance. Part 1-1: General rules, seismic actions and rules for building, 2005.

[6] Baker, J. W., 2011. The conditional mean spectrum: A tool for ground motion selection, ASCE Journal of Structural Engineering 137, 322–331.

[7] Jayaram N, Lin T, Baker JW. A Computationally Efficient Ground-Motion Selection Algorithm for Matching a Target Response Spectrum Mean and Variance. Earthquake Spectra. 2011;27(3):797-815.

[8] Vamvatsikos, Dimitrios & Cornell, C. (2002). Incremental Dynamic Analysis. Earthquake Engineering & Structural Dynamics. 31. 491 - 514. 10.1002/eqe.141.

[9] Baker, J. W. (2015). "Efficient analytical fragility function fitting using dynamic structural analysis." Earthquake Spectra, 31(1), 579-599.

[10] Computer and Structures Inc., CSI Analysis Reference Manual, SAP2000: https://www.csiamerica.com/products/sap2000

[11] Deliverable D4.1: Full seismic test report including all detailed experimental data gathered during the seismic tests, RFSC project FISHWALL, 2020.

[12] Luzi L., Lanzano G., Felicetta C., D'Amico M. C., Russo E., Sgobba S., Pacor, F., & ORFEUS Working Group 5 (2020). Engineering Strong Motion Database (ESM) (Version 2.0). Istituto Nazionale di Geofisica e Vulcanologia (INGV). https://doi.org/10.13127/ESM.2

[13] Felicetta C., Russo E., D'Amico M., Sgobba S., Lanzano G., Mascandola C., Pacor F., Luzi L. (2023) Italian Accelerometric Archive v4.0 - Istituto Nazionale di Geofisica e Vulcanologia, Dipartimento della Protezione Civile Nazionale, doi: 10.13127/itaca.4.0.

[14] CEN, Eurocode 8: Design of structures for earthquake resistance. Part 1-1: General rules, seismic actions and rules for building, annex C, 2018.

[15] CSLP, NTC 2018, Norme tecniche per le costruzioni, Ministero delle Infrastrutture e dei Trasporti, Roma, 2018.

[16] Lowes LN, Mitra N, Altoontash A. A beam-column joint model for simulating the earthquake response of reinforced concrete frames, Pacific Earthquake Engineering Research Center, PEER. Report n. 2003/10.

[17] Deliverable D3.1: Material test on aluminium bolts, RFCS project FISHWALL, 2020

[18] https://itaca.mi.ingv.it/itaca40ws/rexel-disaggregation-values/1/query-options.html;

[19] FEDERAL EMERGENCY. Prestandard and commentary for the seismic rehabilitation of buildings - FEMA 356, volume 356. 2000.

[20] Arrêté du 25 octobre 2012 modifiant l'arrêté du 22 octobre 2010 relatif à la classification et aux règles de construction parasismique applicables aux bâtiments de la classe dite « à risque normal ».